APPLICATION OF PARAMETRIC OPTIMIZATION AND CONTROL IN THE SMART MANUFACTURING OF HYDROGEN SYSTEMS

A Dissertation

by

GERALD SOMEKELECHUKWU OGUMEREM

Submitted to the Office of Graduate and Professional Studies of
Texas A&M University
in partial fulfillment of the requirements for the degree of

DOCTOR OF PHILOSOPHY

Chair of Committee,	Efstratios Pistikopoulos
Committee Members,	Hong-Cai Zhou
	Mahmoud El-Halwagi
	Faruque Hasan
Head of Department,	Arul Jayaraman

December 2019

Major Subject: Chemical Engineering

ABSTRACT

The main objective of this dissertation is to develop and deploy and test explicit model predictive control feedback strategy on hydrogen systems using the PARametric Optimization and Control framework (PAROC). In line with the Smart Manufacturing initiative, our endeavor explores a new model based embedded control architecture that can enable the flexibility and adaptability of hydrogen process system to artificial intelligent algorithms. First a hydrogen supply chain model is developed to identify sustainable hydrogen technologies and then explicit model predictive control is developed using the PAROC framework. Both *in silico* and laboratory implementations are considered towards a smart prototype system application and demonstration. *In silico* PAROC considerations include the development and validation of high-fidelity models based on which the application of the multi-parametric programming techniques results in the derivation of explicit optimal feedback design strategy through the solution of a receding horizon optimization problem formulation. The derived explicit parametric control strategy is validated first *in silico* and then in real-time. Thus, laboratory scale experimental prototypes have been designed and built. The prototypes include: (i) a metal hydride hydrogen storage system (MHSS) and (ii) a PEM Water Electrolysis (PEMWE). The MHSS is designed to replicate the refueling process of a Fuel Cell Electric Vehicle (FCEV) in a hydrogen gas station while the PEMWE is designed as a module in a large scale modular hydrogen production process. Integration of the explicit MPC feedback control strategy and the online implementation on the prototype systems create smart hydrogen energy technologies. Both prototypes are tested using the explicit model predictive control strategies developed and the results obtained from the real-time implementation of the explicit feedback strategy demonstrates the potential of the proposed strategy and effective control design that meets the desired control objectives.

DEDICATION

Dedicated To my parents; Nrakanshi and Nchedo, my siblings; Chiwenwa, Chukwunomso and Chukwudubem and my uncle Augustine

ACKNOWLEDGMENTS

My deepest gratitude goes to my supervisor and mentor, Prof. Stratos Pistikopoulos for believing in me even when I couldn't believe in myself. His support and guidance has made all the difference. Obviously "nobody was born knowing it", but coming from him, these words changed my perspective about learning and persistent effort. I am also grateful to the late Professor Chris Floudas for accepting and welcoming me into the Energy institute. I would also like to thank my committee members Prof. Mahmoud El-Halwagi Prof. Hong-Cai Zhou, Dr. Faruque Hasan and late Prof. Sam Mannan for the very helpful feedback and support that they offered.

I extend many thanks to chemical engineering and Texas A&M Energy Institute staff members Mrs. Lisa Groce, Mrs. Vickie Gracia, Mrs. Ashely Henley, Mrs. Robyn Pearson, Mr. Jeff Sammons, Mrs. Terah Copper for there help when I needed to order supplies for our Energy Systems Laboratory.

I am grateful to Nikos Diangelakis, Richard Oberdieck, Ioana Nascu, Amit manthanwar and Maria Papathanasiou for welcoming me to the group and helping me get acquainted with advanced process optimization and control and some of the software tools needed for my research.

Many thanks to my colleagues: Styliani Avraamidou, Baris Burnak, Justin Katz, Alex Niziolek, Onur and Melis Onel, Burcu Beykal, Doga Demirhan, Will Tso, Yuhe Tian and Iosif Pappas for the times we shared, they made a difference.

I am also grateful to my family who stood and still stands by my side and to my friends and roommate Sam Agabi, Emmanuel Nwoye, Isaac Oti, thank you for being there.

CONTRIBUTORS AND FUNDING SOURCES

This work was supported by a dissertation committee consisting of Professor Efstratios Pistikopoulos (advisor), Professor Mahmoud El-Halwagi (member), Dr. Faruque Hasan (member) and late Prof. Sam Mannan of the Department of Chemical Engineering and Professor Hong-Cai Zhou of the Department of Chemistry.

All other work conducted for the dissertation was completed by the student independently.

Funding Sources

Graduate study was supported by funding from Texas A&M University, Texas A&M Energy Institute, Shell, and Clean Energy Smart Manufacturing Innovation Institute (CESMII).

NOMENCLATURE

PAROC	PARmetric Optimization and Control
SM	Smart Manufacturing
MHSS	Metal Hydride Storage System
SMHRS	Smart Metal Hydride Refueling System
PEMWE	Proton Exchange Membrane Water Electrolysis(zer)
PEM	Proton Exchange Membrane
MPC	Model Predictive Control
eMPC	explicit Model Predictive Control
mpMPC	multi-parametric Model Predictive Control
FCEV	Fuel Cell Electric Vehicle
DOE	Department of Energy
PLC	Programmable logic Control
AI	Artificial Intelligence
ASCPM	Advanced Sensors Control Platform and Model
IT	Information Technology
MI	Manufacturing Intelligence
SMLC	Smart Manufacturing Leadership Coalition
CESMII	Clean Energy Smart Manufacturing Innovation Institute
IIoT	industrial Internet of things
ERP	Enterprise resource planning
MES	Manufacturing execution systems
DIR SOFC	Direct Internal Reformed Solid Oxide Fuel Cell (DIR SOFC)

mpP	multi-parametric programming
MEA	Membrane Electrode Assembly
SOC	State of Charge
MH	Metal Hydride
mpQP	multi-parametric quadratic programming problem
SOWE	Solid Oxide Water Electrolysis
AWE	alkaline water electrolysis

TABLE OF CONTENTS

Page

LIST OF FIGURES

FIGURE Page

LIST OF TABLES

TABLE Page

1. INTRODUCTION

1.1 Overview

The primary aim of this thesis is to develop and apply explicit model predictive control feedback design strategy on hydrogen systems using the PARametric Optimization and Control framework. One logical question will be, why is it important to develop and apply explicit model predictive control laws? Camacho et al. [2] highlights some of the needs for automation and control in the process manufacturing industry. While model based control, such as Model Predictive Control (MPC) have become very popular due to its ability to incorporate constraints among other benefits, explicit MPC is known to be more suitable for the following scenarios; (i) when avoiding the cumbersome optimization at every time step is advantageous for the system (ii) when insights about the control strategy are needed for further analysis and (iii) when a complete map of solution of a lower-level problem is needed for solving an upper level problem. Explicit MPC is also suitable for an embedded model-based control architecture and can play a major role in the on going industrial revolution, termed Smart Manufacturing in the US.

The incremental development of advanced computing power has enabled the development of more sophisticated analytical and optimization techniques. Also Manufacturing assets or equipment are becoming more computerized and fitted with sensors which makes them smarter assets capable of changing the manufacturing landscape [3, 4, 5]. Also as the proliferation of these smart asset creates better asset monitoring, a consolidated and intelligent manufacturing ecosystem necessitates a seamless integration of these smart assets into an enterprise wide network to provide manufacturing intelligence for decision making and unlocking an innovation trajectory [5]. This paradigm shift is characterized by the term “Smart Manufacturing" (SM) which will be discussed in details in the next chapter. The integration of these key components enables enterprise wide connectivity which provides the ability to leverage advanced technologies for AI for innovations to effectively transform manufacturing data to manufacturing intelligence [6]. Despite the fact that

manufacturing asset are becoming smart, most of the process equipments, are still embedded with Programmable Logic Control (PLC) which are unaware of the process dynamics or the chemical interactions of the system. Replacing the PLC in a these system with an embedded model-based control strategy or a hybrid of both increases the system's flexibility and its adaptability to an artificially intelligent (AI) network or Cyber-Physical System (CPS) . These proposition coupled with the manufacturing intelligences generated from the manufacturing data provide an unprecedented insight to make better decisions and improve the competitiveness of the manufacturing enterprise.

Another logical question will be: why hydrogen system? The global energy demand is projected to increase by 30% in 2040 and CO_2 emission will follow the same trend if drastic actions are not taken. In addition, variable Renewable energy has increased tremendously within the last decade, with at least 1800% increase in solar energy and about 300% increase in wind energy [7]. As renewable energies gain more traction due to improving efficiencies and decreasing cost, there is an expected gradual transition away from the dependence on fossil fuels toward the deployment of more environmentally friendly energy technologies. Hydrogen is an energy vector or carrier that can facilitate transition hydrogen, which has enormous potential as a fuel for vehicle mobility and electricity generation [8, 9]. However, its integration into the energy and or manufacturing landscape is currently strained by the dearth of enabling infrastructure.

Developing these infrastructure given different short-term and long-term technological, environmental, and economical actualizations can be challenging. The question some researchers in seeks to answer is "what are the most energy efficient, environmentally benign, and cost effective pathways to deliver hydrogen to the consumer considering prevalent uncertainties?"[10]. Answering this question will equip policy makers, investors and the general public with relevant information and decision tools for the development of hydrogen infrastructures. To address this challenges, several researchers have studied various aspect of the hydrogen supply chain [11, 12, 13, 14, 15, 16, 17, 18, 19] and the steam methane reform process is the main technology for the production of hydrogen because of its relative low cost of hydrogen production. However, these studies did not consider oxygen (which is a valuable by-product of electrolysis) as a revenue

generating option. Chapter 3 details a study we conducted showing that when oxygen is considered as a revenue generating option, water electrolysis is not only environmentally friendly but also cost effective [20]. Electrolysis is an energy intensive process and to maintain its sustainability, it is imperative that a renewable source is adopted. Researchers have identified and modeled some controllable but complex interactions in the electrolysis process that have the potential to reduce its energy intensity [21, 22, 23, 24, 25, 26, 27, 28, 29]. Others have also observed that the system integration associated with the balance of plant (BOP) of hydrogen system can be challenging [30].

Energy Storage is another important hydrogen infrastructure challenge that continues to plague the integration of variable renewable energy into the energy landscape. Energy storage as hydrogen has attracted a lot of research interest mainly because it can be easily integrated with variable renewable energy through the electrolysis or onboard a Fuel Cell Electric Vehicle (FCEV). Hydrogen can be stored in its gaseous form (compressed), in a solid form (absorbed or adsorbed), in its liquid form (cryo-cooled). Compressed hydrogen is the most common hydrogen storage option and hydrogen storage in solid form is not fully developed yet. Several studies have been dedicated to developing materials that can store large amounts of hydrogen. While some other studies have focused on modeling the prevalent interactions in the hydrogen storage process. Temperature control which is directly related to absorption and desorption of hydrogen in metal hydrides has been a major set back in the adoption of metal hydrides storage option. This challenge is partly associated with the physiochemical property of the material [31], the design of the housing, and the control design of the desorption and adsorption process. In Chapter 4 - 6, we developed a thermal management operating strategy for the safe operation of storing hydrogen in metal hydrides.

Since its inception, the process system engineering community has been leading the research and development of tools and techniques that are pivotal to smart manufacturing in the process industry. These techniques include the integration of detailed modeling, design and operational optimization, controller design and scheduling/planning policies. The advancement and diversification of real-time and life-cycle modeling is indispensable to smart manufacturing. it is a common component in process system engineering techniques. Model based control methods have become

a popular and highly sought-after control design method for the process manufacturing industry [32]. While modeling is becoming common practice in the process manufacturing industry, there is a need for tools and techniques that simplify and cost-effectively build, deploy, and maintain models across large heterogeneous systems. Pistikopoulos et al. [33] proposed PARmeteric Optimization and control (PAROC) framework which enables the representation and solution of demanding model-based operational optimization and control problems following an integrated procedure featuring high-fidelity modeling, approximation techniques and optimization-based strategies, including multi-parametric programming. The PAROC framework is a platform that integrates the various technology in Advanced Sensor Control Platform and Model (ASCPM) which makes it appropriate for developing SM systems. In this paper we will demonstrate how PAROC integrates aspect of ASCPM in the design and optimal operation of a smart metal hydride hydrogen storage/refueling system.

1.2 Scope and Objective

1.2.1 Objectives

As stated earlier, the primary objective is to develop and deploy an explicit model predictive control feedback law on hydrogen systems using the PARametric Optimization and Control framework. Below are four research questions that this thesis seeks to address.

Q1 What are the most energy efficient, environmentally benign, and cost effective pathways to meet the hydrogen demand amid prevalent uncertainties? Section 1.2.2.1 elaborates on this.

Q2 Can we facilitate our understanding of the behavior, and predictability of hydrogen energy system without actually testing the system in the real world? Section A.8 elaborates on this.

Q3 Can we design and maintain optimal operating strategies given prevalent operating constraints that can guarantee fast response, and efficient operation of hydrogen energy systems? Section 1.2.2.3 elaborates on this.

Q4 Can we improve the easy and flexibility of deploying optimal control algorithms or operating

strategies for smart chemical processes? Section 1.2.2.4 elaborates on this.

1.2.2 Scope

1.2.2.1 Hydrogen Supply Network

The scope for the hydrogen supply network research project is the development of a super-structure based mathematical programming model. The model is used to design a multi-objective hydrogen supply chain network formulated as an MINLP model to simultaneously (i) maximize the NPV and (ii) minimize the GHG emission. The model is applied, using Texas and California as case studies. The solutions from this higher level modeling creates the basis for choosing what hydrogen based system is further analyzed. The hydrogen energy systems considered in the study are the proton exchange membrane water electrolysis (PEMWE) and the Metal Hydride (MH) Hydrogen Storage. More details are presented in Chapter 3

1.2.2.2 Development of High Fidelity System Models

- The scope of this research includes developing high fidelity dynamic and steady-state models for hydrogen based energy system. The physics based or semi-empirical models of the hydrogen energy systems and integrated balance of plant components are aimed to capture complex interactions and phenomenon in the system that are pivotal to the performance, cost and durability of the system. Chapter 4 discusses the development of *in silico* models for three different systems: (i) the direct internal reform solid oxide fuel cell, (ii) the metal hydride hydrogen storage system and (iii) the proton exchange membrane water electrolysis.

- Also within the main scope of this research is developing two prominent experimental test platforms: (1) A lab-scale metal hydride hydrogen storage facility and (2) A lab scale proton exchange membrane water electrolysis facility. These platforms will enable the validation of the high fidelity models, and implement or test new efficient and robust control policies for hydrogen system operation. Chapter 5 discusses the design and fabrication of two laboratory scale experimental setup used for validating the high fidelity models.

1.2.2.3 Development of Controllers

Next goal is to design online and offline model-based predictive controllers for the integrated system using multiparametric programming techniques. The governing piecewise affine optimal control policy can then be enforced on-line as a sequence of simple function evaluations. This administration of parametric predictive control is aimed to achieve the robust stability, feasibility and performance under uncertainty scenarios. The control strategies are developed using the PAROC framework in Chapter 4

1.2.2.4 Deployment of MPC-on-a-Chip

This research also aims to develop the hardware platform and software framework that can be easily adapted for efficient operation of hydrogen systems. The closed-loop MPC-on-chip control policies designed can be rigorously tested and validated on any of the experimental facilities that are developed as a part of this research work. This will enable us demonstrate the automation architecture and embedded MPC-on-a-chip strategy as an option for making smarter hydrogen systems and decisions that foster reliably operations and further improve its competitive advantage. Chapter 6 discusses the deploying and implementing the control strategies into the lab-scale prototypes developed in Chapter 5

2. SMART MANUFACTURING - A BRIEF OVERVIEW

2.1 Synopsis

Smart manufacturing encapsulates a new revolution in the manufacturing industry. It is envisioned to leverage network technologies such as the industrial Internet of things, big data analytics, smart assets (machinery or equipment) and highly skilled workforce to create a new manufacturing ecosystem that will make available the right data in the right form, the right people with the right knowledge, the right technology and the right operations, whenever and wherever needed. This new manufacturing ecosystem will enable technology innovation, economic health and resources for an agile, safe and sustainable manufacturing industry. Towards rapid development and deployment of smart manufacturing, a number of technologies are prioritized for accelerated research and development. These technology areas include; (1) advances sensing, control, platform, and modeling (ASCPM), (2) Visualization, informatics, and Digital Manufacturing (VIDM), and (3) Advanced Material Manufacturing (AMM). The onboard hydrogen gas storage in a metal hydride system is presented as an example of a smart manufacturing application in energy systems.

2.2 Introduction

The invention of transistors and integrated circuit in the 1980's harbingered the information technology (IT) age and the ubiquity of digital systems such as computers, automated systems and industrial robots etc. These technology innovations enabled embedding computer technology into a range of object including large machinery. Currently most factory floors and chemical plants are lined with automated and sophisticated machinery. Over the years these technologies have been continually updated to improve productivity and profitability. However, in most cases these upgrades were increased and may not be sufficient for companies to stay competitive thus, there is a need for a radical new approach to developing and deploying technologies and business models. Smart manufacturing is a terminology that characterizes such a paradigm shift in the manufacturing industry.

Smart manufacturing generally involves making available the right data in the right form, the right people with the right knowledge, the right technology and the right operations, whenever and wherever needed throughout the manufacturing enterprise. The manufacturing industry generates enormous amount of data but are wanting in knowledge or manufacturing intelligence. Manufacturing intelligence (MI) is an integral aspect of smart manufacturing. It is simply the information or knowledge gathered from the manufacturing data. Forging MI involves any combination of the following; data aggregation, structuring the data, data analytics, data visualization and data propagation. The essence is to derive knowledge from manufacturing data. In a publication by Davis et al [5] Smart Manufacturing was defined as the intensified application of manufacturing intelligence throughout the manufacturing enterprise. It leverages the aggregation of cutting-edge technologies and manufacturing intelligence for effective and accurate engineering decision making in real time.

Economies around the world are developing and implementing strategies that are expected to improve their competitive advantage in the manufacturing industry. In 2013, Germany initiated Industry 4.0 [34] which is aimed at creating intelligent factories where manufacturing technologies are transform by cyber-physical systems and other technologies. Consequently, in 2015 China initiated Made-in-China 2025 [35], which is a 10 years plan that focuses on improving the quality

of products made in China, building a solid manufacturing capability by developing cutting-edge advanced technologies, researching new materials, and producing key parts and components of major products. Similarly, the US has instituted various industry-government partnership to advance the manufacturing industry and in 2016, Smart Manufacturing Leadership Coalition (SMLC) was selected to lead the new Smart Manufacturing Innovation Institute, in partnership with the US Department of Energy [36]. The focus is on accelerating the development and adoption of advanced sensors, data analytics, and controls in manufacturing, while reducing the cost of these technologies by half and radically improving the energy efficiency of U.S. manufacturing industry.

Recently, the Clean Energy Smart Manufacturing Innovation Institute (CESMII) was established [4]. CESMII focuses on research activities and developments that improve energy efficiency and advance the aggregation of smart manufacturing technologies such as advanced real-time sensors, monitoring, data analytics, and digital controls in U.S. manufacturing operations. Industry 4.0, Made-in-China 2025 and Smart Manufacturing, all have some commonality of interest which include; (1) achieving a competitive edge, (2) digitalization - which involves developing smart assets like machines equipment and sensors or embedding the digital systems into these assets to increase the level of automation and (3) connectivity - which involves asset interaction through the Industrial Internet of things (IIoT).

2.3 Goals of Smart Manufacturing

The goals of smart manufacturing can be distilled to the following [37]

- Seamless interoperation of manufacturing automation equipment from different vendors allowing plug and-play configurations
- Energy use and waste streams per unit output from manufacturing plants are reduced by 20% to 50%
- Deployment cost of sensors fall by an order of magnitude
- Real-time optimization and control to adapt to changes in feedstock, market demands and

plant performance

The overarching outcomes of smart manufacturing can be summarized as follows [6];

- **Technology Innovation and Economic Health:** An integrated system with standards and an enabling atmosphere to foster technology innovations that are pivotal to the economic growth and stability.
- **Agility:** An optimized enterprise-wide platform connecting end user that is flexible and situation-aware, which enables rapid response to uncertainties such as in customer demands, price fluctuations.
- **Resource Efficiency:** Ready access to manufacturing intelligence (data, R&D solutions), labor, energy, feedstock, water etc.
- **Next Generation Workforce:** foster advanced skilled workforce to optimize the use of manufacturing intelligence.
- **Safety and Sustainability:** Improved occupational, safety, process safety, sustainability and minimized environmental impacts.

The manufacturing industry can be categorized into process and discrete manufacturing. Products from process manufacturing are mostly continuous fluid or solid streams with fluid-like properties while those of discrete are mostly parts or an assembly of multiple parts. The challenges encountered in the two industries will differ so are some of the technologies required to make them smart. The process and energy system engineering community has been leading the research and development of tools and techniques for facilitating integrated design and operation in process manufacturing. Tool with simulation and optimization capabilities already exist [38, 39, 40, 41] and are constantly being updated with new algorithms. Plant-wide optimization techniques [42] are also used in some process manufacturing industries to improves resource integration which maximizes profitability and reduces environmental impact.

2.4 Elements of Smart Manufacturing

There are five key elements of smart manufacturing; network, data, smart asset, workforce and products/materials. Smart manufacturing requires the seamless integration or interoperability of the physical elements; smart machine/equipment, workforce and Product/materials using the network to facilitate the transformation of data to intelligence for better decision making [43]. The strategies that will enable smart manufacturing will simultaneously advance these elements

2.4.1 Smart Assets

Smart assets are IIoT-enabled machines or equipments which have an embedded digital system that allows it to receive data, process data, perform certain task(s) and transmit data. As shown in figure it is integral to the manufacturing enterprise and an important aspect of the smart asset is automation. In a smart factory, smart assets have to be able to communicate with each other and also be integrated into the cyber-physical system through the industrial Internet of things. Some important benefits of smart asset include, improved productivity, remote operation, safety of workers etc. Smart assets also enable system simulation, application of a advanced control, real-time optimization, proper asset monitoring and increased operational profitability. Sensors are key to enabling a smart system since they not only create better monitoring system but they can also generate data used to validate and periodical update the mathematical model of the system.

2.4.2 Asset Autonomy

Asset autonomy is an important concept in SM and its pivotal to the development of cyber-physical systems. It involves the automation of a manufacturing asset such that a greater part of the primary function of the asset can be performed without an operator. It enables the decentralization of some elements of the control infrastructure in the manufacturing system. Asset autonomy is easily adapted in the discreet manufacturing industry because of its inherent nature where parts are made or assembled as they travel through different sections or assets with primary functions. In the process manufacturing industries, the operations involve blending and or chemical reactions and the products are not easily taken apart. From a control standpoint, the process manufacturing

tends to be an aggregation of regulatory control loops. For instance, in a distillation column, there are several control loops that are synchronized through the Supervisory Control And Data Acquisition (SCADA). Figure 2.1 shows a typical control framework for the implementation of advanced process control in the process manufacturing industry. The decision at the scheduling or planning level is implemented through the Advanced Process Control (APC) and or Real-Time Optimization (RTO) setup such that optimal or efficient setpoints are sent to the PID loops. This control architecture has been improved over time through incremental upgrades.

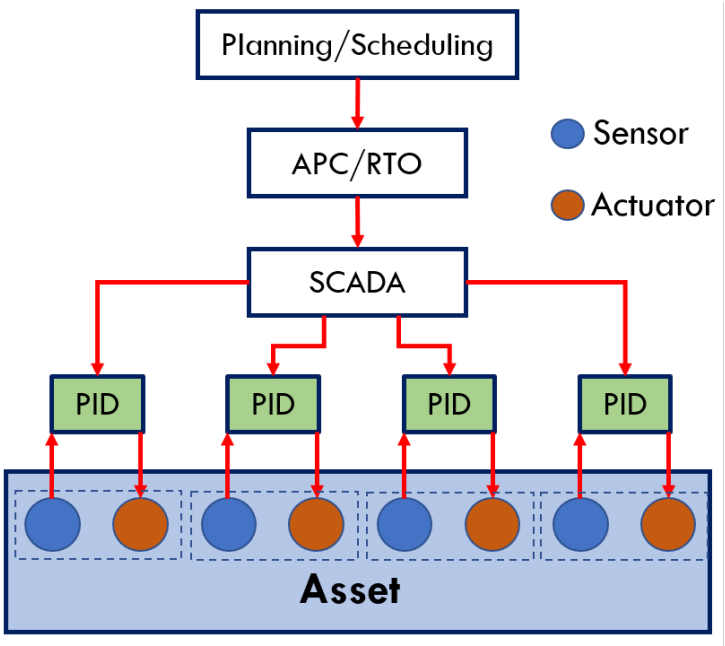

Figure 2.1: Schematic of a typical process control architecture in a process manufacturing plant

As we tend towards more modularized and intensified process manufacturing industry, there is a need to develop hardware and computational frameworks that will aid asset autonomy. The concept of asset autonomy in the process manufacturing industry is such that a model-based optimal operating strategy of a manufacturing asset is embedded in the asset at the programmable logic control (PLC) level. The optimal strategy will be an integration of the PLC, digital twin (for implementing measurable and unmeasurable boundaries of the operation), and optimal operating

algorithm (derived from the digital twin or high-fidelity model). Figure 2.2 shows a conceptual framework for implementing advanced process control on a modular autonomous system. In the framework, the optimal operating strategy is embedded in the manufacturing asset. Just like in the traditional control framework illustrated in figure 2.3, the system described in figure 2.4 requires a synchronized connection between autonomous assets. For instance, the operating strategy in the reactor is synchronized with that of the distillation column following it.

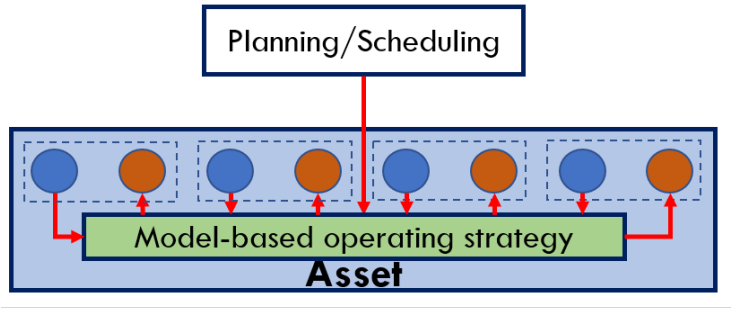

Figure 2.2: Schematic diagram of a conceptual control architecture with autonomous process units

2.4.3 Workforce

The manufacturing workforce is essential to smart manufacturing. Though asset automation has tremendous economic and in some case health and safety benefits there is always the question of, how much automation is needed in an asset? The benefits of automation plateaus after a certain level and over automation can result in inefficiency. The future manufacturing workforce will have the ability to leverage advance technology and manufacturing intelligence in decision making. The workforce will also manage uncertainties that automation is not able to handle.

2.4.4 Materials and Product

Products and materials are centric to smart manufacturing. A focus of smart manufacturing is product customization. The manufacturing industry needs to evolution, into making the products

that are needed, when they are needed, and in the quantities in which they are needed [5]. This involves the active participation of the costumers. Smart Manufacturing enables a more flexible production of variable volumes of products, with information driven operations. Robust data system will enable accurate record of each product - unique identification, procedure, specification, observational data, quality and product characteristics, safety data sheet, suppliers, etc. The data can be used to estimate the carbon footprint of the product.

2.4.5 Data Infrastructure

The data generated in a typical manufacturing environment is large and multifaceted. However even with sophisticated modeling and control technology, there still exist lack of intelligence from the data. Managing data effectively is critical for smart manufacturing. It involves data abstraction, storage, processing, transmission and analysis. Data systems will also need to be interoperable and exchangeable across diverse platforms and uses. Big data techniques can be deployed for effective transformation of data to intelligence. Other data related activities include using data for real-time optimization, supply chain.

2.4.5.1 Data Analytics

The senors and monitoring system in the manufacturing operation have advanced and they generate real-time data used by operators to make necessary changes. The data generated by modern manufacturing industry are enormous, however, the modern manufacturing industry is still plagued by the dearth of Manufacturing Intelligence (MI). Computation of data analytics techniques is an integral component in the conversion of raw manufacturing data from sensors or monitoring systems to manufacturing intelligence. The data analytic tools or techniques used to develop MI can be categorized into three groups [44]:

- **Descriptive analytics** The main objective is to clearly present the state of the system such that is easily articulated. The primary questions that the analytical techniques try to answer are "what happened?", "what is happening (real-time)?", etc.

- **Predictive analytics** The main objective of the methods deployed here is are to predict what

will happen based on current or passed indicators. This usually involves models of the system.

- **Prescriptive analytics** here based on the current state of the system or a projected state of the system the primary objective of the analytics deployed is to suggest possible actions

As the manufacturing industry fight for smart operation, there needs to be a combination of the three groups of analytics or intelligence. Until recently the prescriptive intelligence has been attached to the role of highly skilled employees but the recent developments in big data analytics, optimization, machine learning, deep learning, etc. are enabling algorithms to provide prescriptive intelligence. This creates a level of autonomy in the system.

2.4.6 Network

Communication is key to smart manufacturing and it is enabled by a robust network. Some industries have an existing fragmented network infrastructure. Figure 2.3 shows different levels of the manufacturing enterprise. The levels may have existing network infrastructure and in some cases a connection with adjacent network level. In smart manufacturing, fragmented operational network structures give way to the full horizontal integration at various levels and a vertical integration of various levels in the manufacturing enterprise. Enterprise resource planning (ERP) allows organization to use integrated applications to manage the entire manufacturing business. Manufacturing Execution Systems (MES) are applications used to track and document the transformation of raw materials to finished goods.

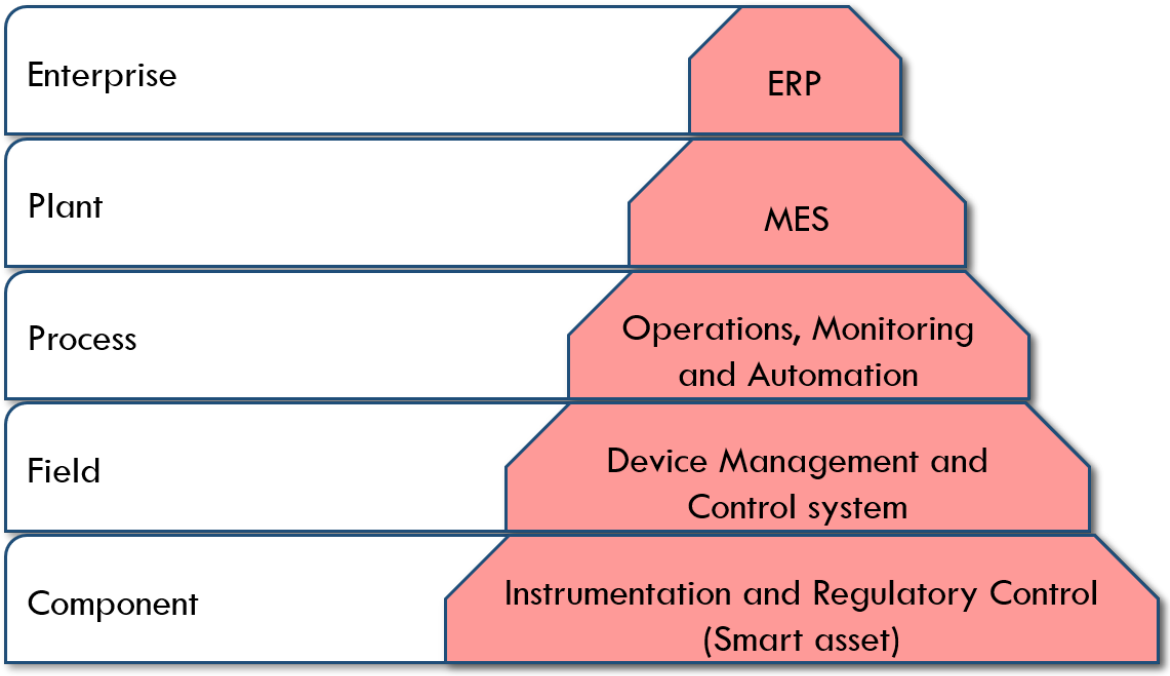

Figure 2.3: Enterprise application architecture for smart manufacturing.

2.5 Smart Manufacturing Technology Focus Areas

The Advanced Manufacturing Partnership (AMP) is an Industry-academia-Government Partnership saddled with revitalizing the United State manufacturing industry. A report published by [45] in 2011 identified three Manufacturing Technology Areas of high national priority. These areas are: Advanced Sensing, Controls, Platforms, and Modeling for Manufacturing (ASCPM); Visualization, Informatics and Digital Manufacturing (VIDM); and Advanced Materials Manufacturing (AMM) [45].

2.5.1 Advanced Sensing Controls Platforms and Modeling

ASCPM is expected to enable cross connection of diverse data, process control applications, and decision workflow using advanced sensors and a network-based, open architecture, plug-and-play platform. ASCPM is championed by CESMII and they are expected to establish manufacturing technology testbeds to demonstrate the use of new technologies [46].

2.5.1.1 Advanced Sensing

Advanced sensing includes data-generating or monitoring nodes within the enterprise. They are fast noninvasive hard sensors/equipment or soft sensors (data-trained computer code). They are expected to be low cost, have the ability to evaluate sensor health, and continuously quantify measurement uncertainty. Network-integrated advanced sensors are used to improve reliability through asset monitoring, efficiency and productivity through monitoring the real-time management inputs like energy and materials through out the manufacturing ecosystem.

2.5.1.2 Control

This includes theories and algorithms for model-base control and optimization in the manufacturing enterprise. Digital control systems with embedded automated process controls can enable operation optimization, efficient energy consumption, and improve safety enterprise wide. The IIoT and cloud infrastructure can allow system-wide algorithms to operate each manufacturing component simultaneously to meet costumer demand.

2.5.1.3 Platform

Automation in the manufacturing industry relies primarily on single-vendor monolithic software architectures and device and vendor lock-in is a widely acknowledged barrier to innovation. Standardization and Service architecture approaches can enable multiple development environments, infrastructures that support composability, and cloud based orchestration allowing for plug-and-play interoperability in the platform. Appropriate cybersecurity considerations must be incorporated from the outset [46].

2.5.1.4 Model

Models are at the core of many ASCPM technology gaps. The advancement and diversification of real-time and life-cycle modeling is pivotal to smart manufacturing. Also are the tools and techniques to simplify and cost-effectively build, deploy, and maintain models across large heterogeneous systems. The synchronous interplay and model alignment is essential to advanced

manufacturing. For example, optimization models and control models should be able to iteratively exchange data such as updated constraints and new control setpoints [46].

2.5.2 Visualization Informatics and Digital Manufacturing

While ASCPM has a wider adoption in the chemical process industry, Visualization, Informatics and Digital Manufacturing (VIDM) has a wider adoption in the discrete manufacturing industry. VIDM is focused into three sub-areas (1) Digital Thread; (2) Integrated Information Systems; and (3) Manufacturing Big Data and Analytics [47]. Institutes like Digital Manufacturing and Design Innovation Institute (DMDII) and AIM Photonics are leading the development of innovative research in VIDM areas and they are expected to Create a manufacturing center of excellence, focused on basic research at earlier technology development levels [45].

2.5.2.1 Visualization

Visualization presents right information to right user in the right form at the right time. Visualization includes creating information that human can visualize and use for decision making. It involves an articulated display of information in the right context aggregation of information from multiple sources and sensors, and presenting it in a visual and comprehensible manner. Visualization turns data into information or graphics for human decision making.

2.5.2.2 Informatics

Informatics entails data mining, data analysis, and data processing before visualization. Informatics involves processing data and extracting intelligence.

2.5.2.3 Digital Manufacturing

Digital Manufacturing focuses on the use of integrated, computer-based systems comprised of simulation, three-dimensional visualization, analytics and various collaboration tools to create product and manufacturing process definitions simultaneously. Manufactured artifacts move seamlessly through conception, design modeling, analysis and manufacture. Digital Manufacturing objectives are concentrated on new products and shortened design to manufacturing life cycles

and new product changeovers [48].

2.5.3 Advanced Materials Manufacturing

AMM combines advanced computational methods with experimental methods for intelligent, focused development of improved materials for clean energy technologies and accelerates materials to market through a focus on process and end-use manufacturing. The focus is on structural material, optical materials, chemical materials, thermal materials and electronic materials.

2.6 Computational Framework in Smart Manufacturing

Computation in SM ranges from data analytics to model or framework development and implementation of operating strategies etc. In SM, a computational framework can be defined as a systematic combination of two or more analytical techniques to create manufacturing intelligence, unique solution or a new analytical technique or tool. It could be a computer application or platform.

One example of a computational framework for SM is the Open Process Automation (OPA) multi-ventor system developed by ExxonMobil. OPA is an integrated framework involving hardware and software architecture intended to make adding, upgrading, and swapping components easy. It is characterized by its: Portability, Open Standards, Modularity, and Interoperability. While the standards are been developed for hardware integration, such initiative should be adopted for computational framework or techniques especially in the development of models and efficient operating strategies.

Modeling is an integral part of the development of techniques and tool in the process systems engineering community. Model-based methods have become popular and highly sought-after in the process manufacturing industry. While modeling is becoming common practice there are multiple models for the same system for a different purpose; design, process synthesis, scheduling, control, etc. This modus operandi can lead to loss of information across the system, difficulty in integration and error in prediction. Thus, there is a need for systems or frameworks that simplify and cost-effectively build, deploy, and maintain models across large heterogeneous systems. One

approach is the vertical integration of the various computational operations such as planning, design, control, scheduling, etc. There have been major advances in the area of design and control [49, 50], scheduling and control [51, 52] and model-based advanced control [53, 54]. However, none of the aforementioned studies presented a framework or protocol or a software platform. In 2015 Pistikopoulos et al. proposed the PARmeteric Optimization and control (PAROC) framework which enables the representation and solution of demanding model-based operational optimization and control problems following an integrated procedure featuring high-fidelity modeling, modeling approximation techniques, and optimization-based strategies using multi-parametric programming techniques.

An integral component of PAROC is parametric programming. First implemented in 1952, by Orchard Hays, in switching the optimal basis as a function of the varying parameter [55, 56]. Since then, many researchers have made some key contributions to parametric and multi-parametric programming problems [57, 58, 59]. A detailed review on multi-parametric programming theory, algorithms and applications can be found in [60].

2.7 A Smart Manufacturing Application in an Energy System

2.7.1 Smart Metal Hydride Refuel for FCEV

The Fuel Cell Electric Vehicles (FCEV) market is expected to reach $16,248.23 million by 2026 growing at a CAGR of 34.5 % [61]. Fuel cell vehicle utilizes onboard stored hydrogen to produce onboard electricity to power the electric motor that turns the wheel. There are three main onboard hydrogen storage options; the compressed hydrogen gas storage, the liquid hydrogen storage, and the solid hydrogen storage. The compressed hydrogen gas storage is currently used in most fuel cell vehicles. Its easy to operate however, the storage canister is large and heavy because of the reinforcement needed to withstand high pressures [62]. Also, since the hydrogen is stored at high pressures (10,000psig), the onboard compressed hydrogen storage is inherently unsafe [63].

The solid hydrogen is a plausible option for on-board hydrogen storage especially for more compact sporty FCEV. it is basically a canister filled with metal alloys that react with hydrogen to

form metal hydride [64]. There are two main processes involved in the operation of hydrogen storage in metal Hydride: the filling of the metal hydride canister with hydrogen which is exothermic and the discharge of hydrogen from the metal hydride, which is endothermic. During the filling process the operating temperature increases and can lead to a runaway reaction if not managed properly. The Department of Energy (DOE) has set some targets for onboard hydrogen storage [65], which includes a limit on the operating temperature and refuel rate of the hydrogen storage system. In a metal hydride storage system, there is a trade-off between the operating temperature, pressure and the refuel rate. Smart manufacturing technologies can be adopted to address this operational challenge.

This case study shows how smart manufacturing technologies can be used to develop an optimal operating strategy for filling the metal canister that is not only fast but safe and within DOE targets. Figure 2.4 shows a schematic of the smart refueling system. When the hydrogen gas pump nozzle is plugged into the FCEV, real-time data is relayed to the pump for costumer monitoring. Some of the technologies employed are described below.

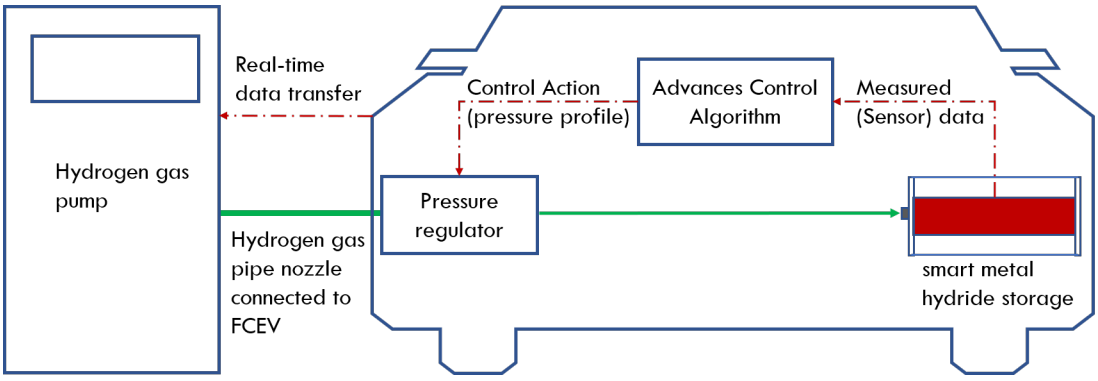

Figure 2.4: Schematic of metal hydride smart refueling system .

Several research studies have investigated and proposed advance control strategies for hydrogen discharge from the metal hydride canister [66, 67]. Parametric Optimization and Control (PAROC) framework (figure 2.5) is an integrated framework and software platform that enables

the use of model-based tools in design, operational optimization and advanced control studies [68]. PAROC provides a customized advanced control strategy that can be embedded into the FCEV without the sophistication of an embedded solver, making it easy to use.

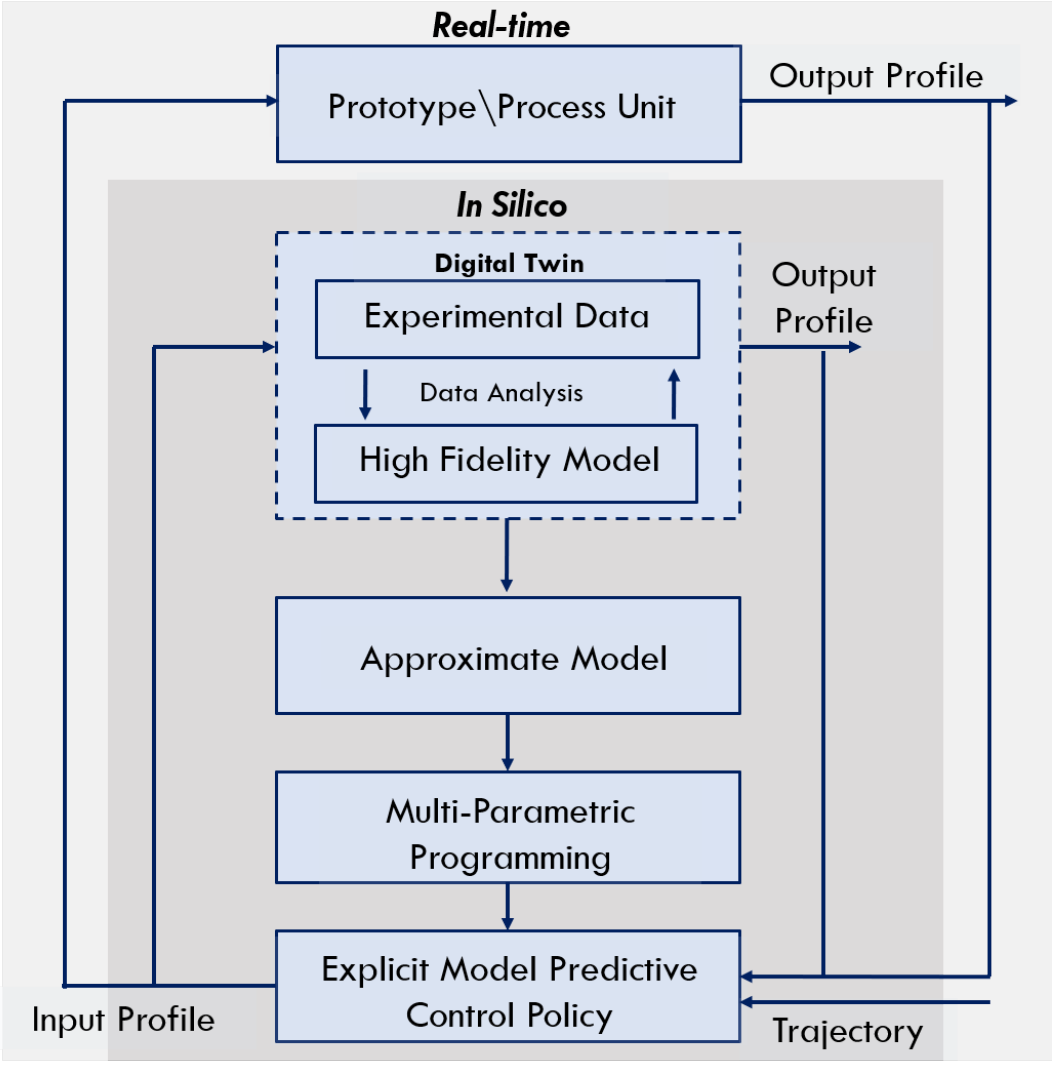

Figure 2.5: Schematic of the PAROC framework.

2.7.1.1 Design

A smart metal hydride canister will have smart sensor to enable accurate temperature and pressure reading. It will also have a temperature control mechanism. In the design stage a high-fidelity

multi-dimensional model is developed and a metal alloy is selected [67, 69, 70]. The model is used to determine an optimal aspect ratio or geometry of the canister that maximizes the removal of heat generated.

2.7.1.2 Modeling

The high-fidelity model used for design is validated with operation data to tailor the model to the specific metal alloy selected. The validated model is used to develop soft sensors for process variables,like the hydrogen content of the metal hydride canister, that cannot be measured by an instrument . If needed, a model reduction techniques is used to reduce the complexity of the model while maintaining its high fidelity.

2.7.1.3 Multi-parametric Programming

The reduced model is used to design a model predictive control (MPC) that maintains the temperature limits and maximizes the refueling rate [67]. The MPC is reformulated into a multi-parametric model predictive control (mpMPC) and solved using already established algorithms [68, 71]. The solution obtained are control policies which are affine function of the measured variable realized during the operation. The control policies are structured as look-up-table algorithms that can be embedded into a micro-controller. The micro-controller is connected to the unit to control the operation in the metal hydride.

2.7.1.4 Smart Refueling Protocol

. When the costumer plugs the hydrogen gas pump nozzle into the FCEV and starts refueling, the control algorithm controls the refuel process such that the operating temperature is maintained within the DOE limits and the refuel rate is maximized. Real-time process data is relayed to the pump display screen for the costumer to monitor the progress of the refuel operation.

2.8 Conclusion

The concept of smart manufacturing was introduced as a terminology characterizing the intensified application of manufacturing intelligence in the manufacturing enterprise. Economies

around the world have created various initiatives to develop and foster these trends of advancing technologies in the manufacturing industry. The general goals of Smart manufacturing are: to foster technological and economic health, build a costumer-aware agile platform, make resources available when the are needed, create the required workforce, improve safety and sustainability in the manufacturing industry. These goals can be achieved by simultaneously developing the key elements of smart manufacturing; smart assets, workforce, products, network and data. The Advanced manufacturing partnership (AMP) in the United States listed priority technology focus areas for the smart manufacturing initiative Advance sensing, control,platform and modeling (ASCPM); Visualization, Informatics, and digital manufacturing (VIDM); Advance Material Manufacturing (AMM). The smart metal hydride refueling system example demonstrates the implementation of SM in the hydrogen refueling system to address the challenges in the onboard hydrogen storage in metal hydride.

3. HYDROGEN SUPPLY CHAIN FOR TRANSPORTATION FUEL [1]

3.1 Synopsis

In this Chapter we present a multi-objective, multi-period, mixed integer, linear optimization formulation to analyze a hydrogen supply chain network. The objectives of the optimization problem are:(i) the maximization of the Net Present Value (NPV) and (ii)the minimization of the Greenhouse Gas (GHG) emissions, while determining: (i) the locations of the hydrogen facilities, (ii) the production technology, (iii) the size of each facility (iv) transportation unit and (v) the distribution route. The model was deployed for the state of Texas and two scenarios were investigated: (i) oxygen co-produced with hydrogen from electrolysis is discarded and (ii) oxygen co-produced form the electrolysis is further processed and sold to generate revenue. A Pareto curve of twenty efficient points is developed and the extreme points on the curve are used to test the aforementioned scenarios. We found that further processing of produced oxygen for sell instead of discarding it made electrolysis an economically viable technology option for the production of hydrogen.

[1]Reprinted with the permission from “Elsevier" G. S. Ogumerem, C. Kim, I. Kesisoglou, N. A. Diangelakis, and E. N. Pistikopoulos, “A multi-objective optimization for the design and operation of a hydrogen network for transportation fuel," Chemical Engineering Research and Design, vol. 131, pp. 279-292, 2018.

3.2 Introduction

As renewable energies gain more traction due to improving efficiencies and decreasing costs, there is expected to be a gradual transition away from dependence on fossil fuels toward the deployment of more environmentally friendly energy technologies. One such energy vector is hydrogen, which has enormous potential as a fuel for vehicle mobility and electricity generation. However, its integration into the energy landscape is currently strained by the dearth of enabling infrastructure. Several options exist for the production, storage, distribution and retailing of hydrogen to end users, but developing these infrastructure given different short- and long-term technological and economical actualizations can be challenging. Within the last decade, there has been increasing interest among researchers in hydrogen network development and the question most people ask is summarized as follows: “What are the most energy efficient, environmentally benign, and cost effective pathways to deliver hydrogen to the consumer considering prevalent uncertainties"?[14] Answering this question will equip policy makers, investors and the general public with relevant information and decision tools for the development of hydrogen infrastructures.

A hydrogen network is a supply chain required to produce, store and deliver hydrogen to the consumer, and it has been referred to as hydrogen supply chain (HSC) and hydrogen infrastructure (HI). In studying hydrogen network and that of other energy systems, parameters such as efficiency, size, safety, environmental impact which are pivotal to decision making are modeled/analyzed. An important consideration is the estimated hydrogen demand. Though saddled with uncertainties the demand of hydrogen is a major determining factor to establishing a hydrogen network. Currently most of the hydrogen produced is used in industrial processes for the production of other chemicals or products [1]. The amount of hydrogen infrastructures developed solely for transportation fuel to date is relatively small thus there is not enough data for the economic analysis of the various production technologies. However, the share of hydrogen used for fuel in transportation and electricity generation is rising. Figure 3.1 represents a study by Navigant which shows that hydrogen consumption for non-traditional applications will grow from 168 million kilograms (kg) in 2013 to nearly 3.5 billion kg in 2030 [1].

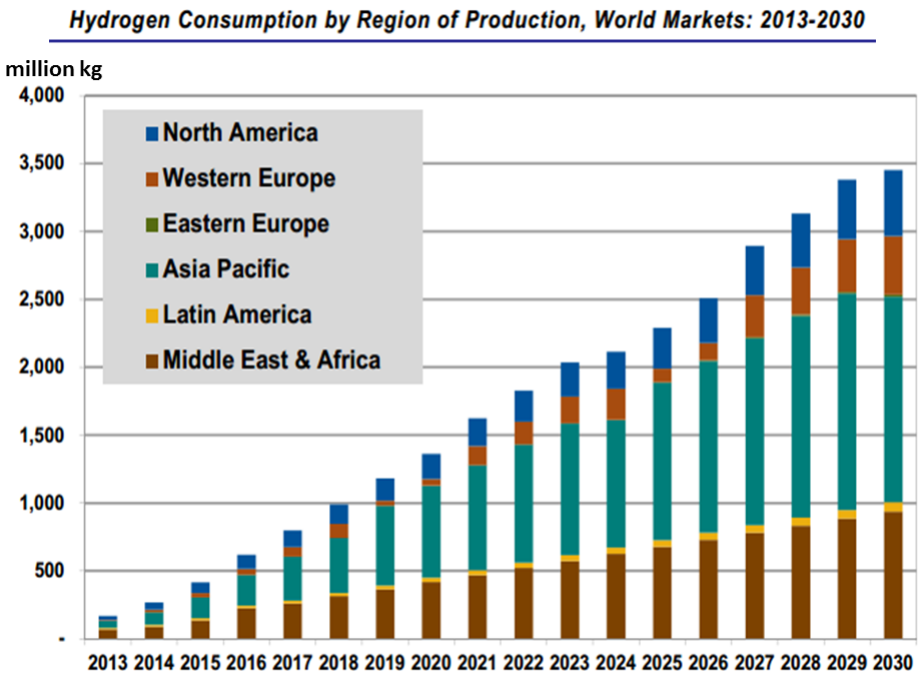

Figure 3.1: Hydrogen demand projection reprinted from [1].

Researchers in the hydrogen supply chain area, have adopted various approaches to analyze the breadth and depth of the hydrogen network in order to estimate parameters that are crucial to decision making. Several studies have been reported describing the design and optimization of a hydrogen network. Ogden et al [11] studied the development of hydrogen infrastructure and subsequently focused on the distribution network for hydrogen [12, 13]. Some of the studies conducted were approached as a single objective optimization [15, 17] while a few others adopted a multi-objective approach [19, 72, 73, 74, 75] Kim et al and Han et al [74, 73] used a generic optimization-based model with risk index to optimize monetary and safety criteria of a hydrogen network. Their Pareto optimal solutions showed a trade off between cost and safety levels. De-Leon et al. [19] focused on the design of a multi-criteria five-echelon hydrogen network, trading off cost, global warming potential and safety risk. Gonzalo et al., Hugo et al. and Liu et al traded off cost and greenhouse gas emission[14, 72]. Some researchers have considered a multi-period approach to demonstrate how changes in hydrogen demand affects the capacity of hydrogen production plants over a time period [14, 15, 16, 17, 18] . Some studies have also considered

uncertainty in various optimization instances [76, 77, 78].

None of of all the aforementioned studies considered electrolysis as a technology option for hydrogen production, evaluated the impact of oxygen as a valuable by-product. if oxygen is considered a revenue generating option, electrolysis can be a more cost effective option for producing hydrogen when compared to matured technologies, such as Steam Methane Reform (SMR) [79] . Kato et al. in their study, assessed the potential demand of oxygen for energy efficient industrial processes and concluded that there is an enormous demand of oxygen for various industrial processes and that the co-production of hydrogen and oxygen through electrolysis could cost-effectively meet the demand of oxygen[79].

In this Chapter, we develop a mixed-integer linear optimization formulation similar to that of Hugo et al., Liu et al. and Koltsaklis et al. [14, 80, 81] to analyze a hydrogen supply chain network. The formulation represents a multi period, plant location and capacity analysis problem with two conflicting optimization criteria: (i) the maximization of the net present value and (ii) the minimization of green house gas emissions. The model is structured as a multi objective programming problem, and a Pareto curve is created to show the efficient points for decision making. The model is deployed to analyze a hypothetical hydrogen network in Texas and California. Both case studies considers a forty years plan of adopting hydrogen as part of transportation energy mix (Texas) or as the only transportation energy source (California). Two scenarios are evaluated for both case studies: (i) when oxygen (by-product of hydrogen production from the electrolysis technologies) is vented into the atmosphere and (ii) when oxygen is collected, compressed and sold for revenue. Studies have shown SMR to be the most cost effective option for producing hydrogen [82]. However, the management and trading of co-produced oxygen has the potential to make electrolysis an economically viable option for the production of hydrogen.

3.3 Life Cycle Assessment

Given that the concept of hydrogen energy stems from the idea of a sustainable and environmentally benign alternative to fossil fuels, it is imperative that any study on the production of hydrogen for fuel includes an environmental impact assessment. Over the years there has been

an ongoing shift from the traditional end-of-pipe approach of waste management to a life cycle approach where the boundaries are expanded beyond a facility to include every stage in the life cycle of a product. Particularly, the emphasis is shifting from effluent concentrations to environmental impacts that contribute to an environmental issue [14]. The life cycle assessment approach advances waste minimization and pollution prevention.

In developing a hydrogen supply chain network and other facility location problems, environmental concerns are mostly formulated as constraints to an economic objective [83]. The set back to this approach is that it not only undermines the emphasis on the environmental impact of the network but also overlooks the possibility of trade off solutions. The environmental objective provides a measurement of the environmental behavior of a hydrogen network over its life time which comprises all primary types of emissions produced from both the plant operation and all the previous stages. The life cycle approach captures emissions associated with processing of the product as well as the emissions corresponding to the manufacturing (extraction) and supply of feedstock, equipment, energy and the use of the product. The Environmental Protection Agency (EPA) has published an emission inventory for various process and equipment and also the Global Warming Potential (GWP) of the greenhouse gases [84]. The GWP is a parameter that enables the comparison of the global warming impact of the GHG's with respect to CO_2. A cradle-to-gate GHG emissions indicator is established over the operating horizon, on a CO_2-equivalent basis. It comprises four parts:

- GHG emissions produced within the process during operation,
- GHG emissions produced throughout mining, extraction, and other preprocessing phases of the feedstock,
- GHG emissions produced during equipment production and plant construction and
- GHG emissions produced during the transportation of raw materials and finished products.

3.4 Model Formulation and Solution Strategy

Hydrogen infrastructural planning with mathematical programming and optimization techniques attempts to systematically obtain an optimum design from many potential alternatives. This provides a strategy to simultaneously incorporate decision variables at various stages of the planning horizon. A common approach is to develop a superstructure of all potential process routes with interconnections, as a mixed integer programming problem [85]. Optimization techniques are employed to simultaneously determine the optimal configuration of the network that maximizes profit and/or minimizes environmental impact. A typical hydrogen network is formulated to address the following concerns:

- capacity of each type of processes,
- timing and scale of capacity expansion or decommissioning,
- consumption rates of primary feedstocks over time and
- timing and scale of shift from one type of primary feedstock to another.

Here we develop a superstructure based Mixed-integer Linear Programing (MILP) model. The superstructure is designed to incorporate potential process route, feedstock, transportation modes and distribution route as shown in Figure 3.2. They MILP optimization model is similar to that of Hugo et al., Liu et al. and Koltsaklis et al. [14, 80, 81] for a hydrogen supply chain network. The model is multi period and has two conflicting optimization criteria: (i) the maximization of the net present value, (ii) the minimization of green house gas emissions (CO_2,CH_4,N_2O) and (iii) constraints that determines among other outcomes, (a) the location and (b) capacity of a proposed hydrogen plant at any time period, (c) the amount of hydrogen entering or leaving a plant, (d) the transportation mode and (e) the distribution route at any time period.The model is structured as a multi objective programming problem, and a Pareto curve is created to show the efficient points.

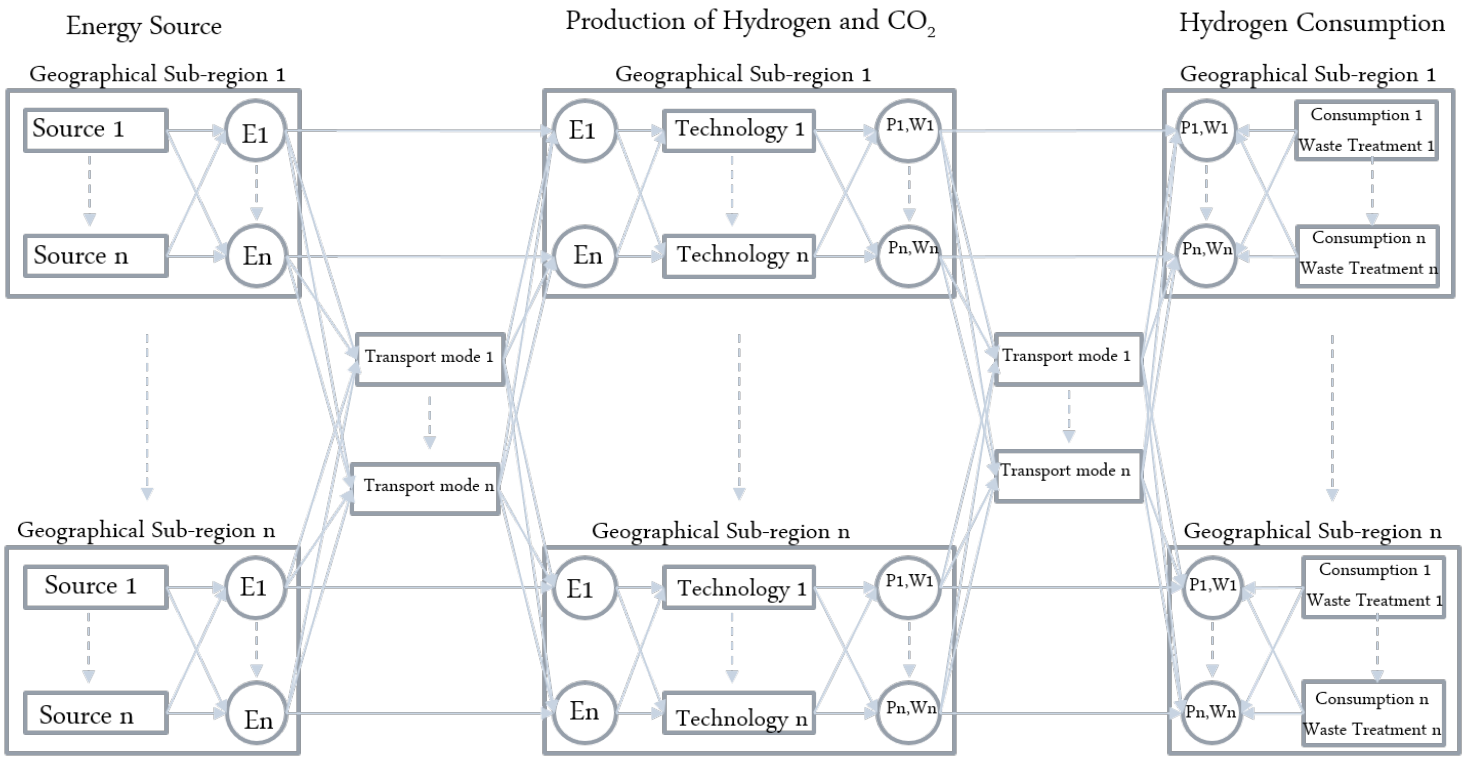

Figure 3.2: Hydrogen energy network superstructure

3.4.1 Problem Statement

The problem statement for the planning and design of hydrogen supply chain networks is stated as follows. Given:

- a set of markets distributors or customers and their demands for hydrogen and its by-products over a given time period and or planning horizon,
- a set of potential plants using known technologies to produce the hydrogen and
- the availabilities of the raw material and utility suppliers over the planning horizon

the task is to design the supply chain network of an integrated production facilities that would satisfy the demand over the entire planning horizon such that both:

- the net present value of the capital investment evaluated at the end of the planning horizon is maximized and
- the environment impact by way of greenhouse gas emission is minimized.

3.4.2 Hydrogen Production Technologies

Four hydrogen production technologies are considered in this case study. Each technology produces hydrogen at 30 bars and is compressed for transportation. Also, each hydrogen production method requires different raw material and different amount of electricity to produce the final product. The explanation of individual hydrogen production methods is described below. The operating conditions and other inputs for the four hydrogen production methods considered are taken from The Hydrogen Analysis (H2A) project of the U.S. Department of Energy [86]. The resource input require for all hydrogen producing technologies are given in table 3.1 some of the data used can be found in [86]

Table 3.1: Required resource input for per metric ton of hydrogen

Materials	SMR	CG	BG	Electrolysis
Biomass (ton)	0	0	13.49	0
Coal (ton)	0	8.508	0	0
Natural gas(ton)	3.86	0	0.146	0
Process Water (ton)	3.355	2.98	1.321	4.76
Electricity (Mwh)	2.146	2.167	1.240	56.393

3.4.2.1 Steam Methane Reform

The hydrogen produced from the SMR process accounts for more than 90% of all hydrogen produced till date however most of the hydrogen produced are used for sweetening or production other chemicals. The SMR technology uses natural gas or other hydrocarbons as a feedstock and the process consists of several different unit operations which include sulfur guard, steam reformer, water gas shift (WGS), carbon capture, pressure swing adsorption (PSA), and heat recovery steam generator (HRSG). Natural gas is fed into the system (with about 4ppm of sulfur), and it passes through a desulphurization unit where some of the hydrogen produced is used to remove sulfur as hydrogen sulphide (H_2S). The sweet natural gas is fed into the reformer where it reacts with steam in a catalytic reactor maintained at about 1273K and 30 bars. Syngas is produced from the reformer and it passes to a shift reactor where the ratio of hydrogen is increased. The shift reactor is maintained at a lower temperature and the effluent of the shift reactor is passed through a carbon capture technology where CO_2 is removed. Hydrogen is separated from other gases in a Pressure Swing Absorption (PSA) process. PSA offgas and some natural gas are used as fuel to produce steam and also generate heat for the reforming reaction. The SMR process flow diagram is shown in Figure 3.3.

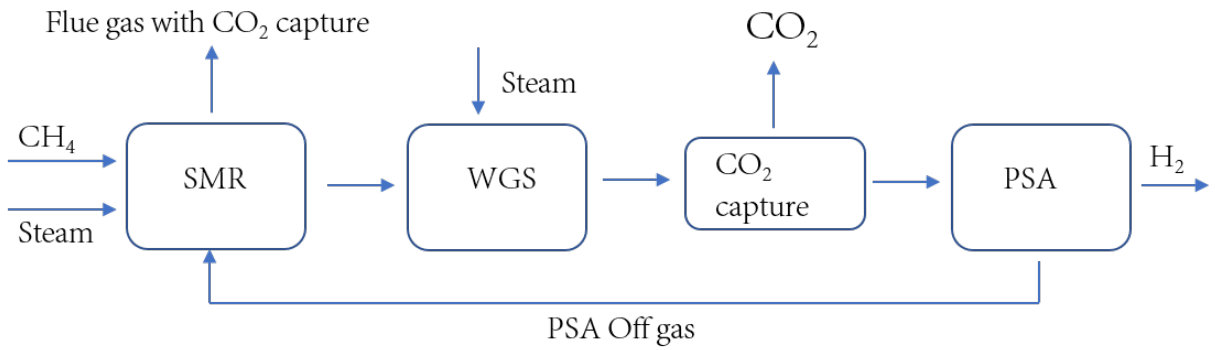

Figure 3.3: Steam methane reforming.

3.4.2.2 Electrolysis

Electrolysis is one of the promising hydrogen production methods benign to the environment[1] because it does not produce any GHG during hydrogen production. The process consists of water a management system, a power supply unit, an oxygen and hydrogen management unit, and the electrolyzer. When water and power is fed to the process, the electrolyzer splits water into hydrogen and oxygen. The electrolysis process can produce hydrogen 30 bars, saving part the required compression energy. Oxygen is considered a valuable b-product and for every metric ton of hydrogen produced about 8000 metric ton of oxygen is produced. The process flow diagram of the electrolysis technology is shown in Figure 3.4

3.4.2.3 Biomass Gasification

The process mainly consists of biomass drying, reforming, purification, steam cycle production, and a cooling water system. In this process, the biomass fed into the system, is dried by a rotary dryer. The dried mass reacts with steam in the gasifier unit and produces syngas. The produced syngas undergoes purification processes including scrubbing and catalytic treatment to remove sulfur components. The treated syngas is fed into the steam reformer and reacts with steam to produce hydrogen. Extra amount of hydrogen are produced from both high temperature shift

[1]Electrolysis requires electricity which can be provided by renewable energy resources thus making its operation GHG-free.

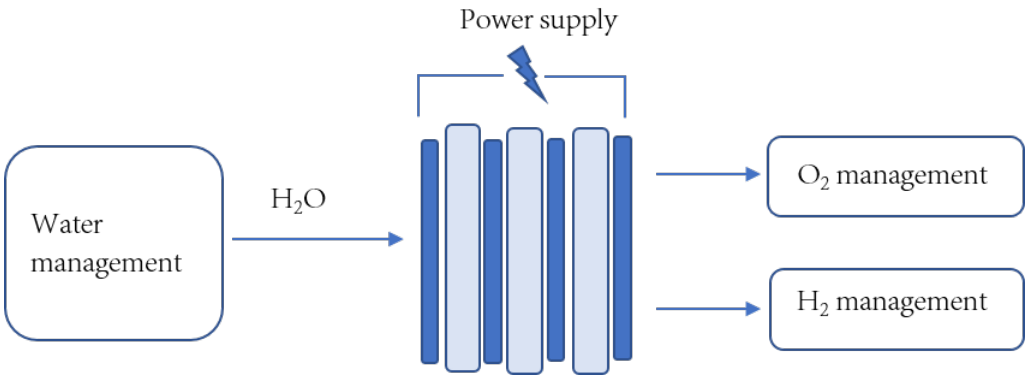

Figure 3.4: Electrolysis.

(HTS) and low temperature shift (LTS) processes. The produced hydrogen is purified in a PSA unit. The biomass used in this study is assumed to sequestrate 22kg of CO_2 per kg of biomass [87]. A generic process flow diagram of this technology and that of coal gasification is shown in Figure 3.5

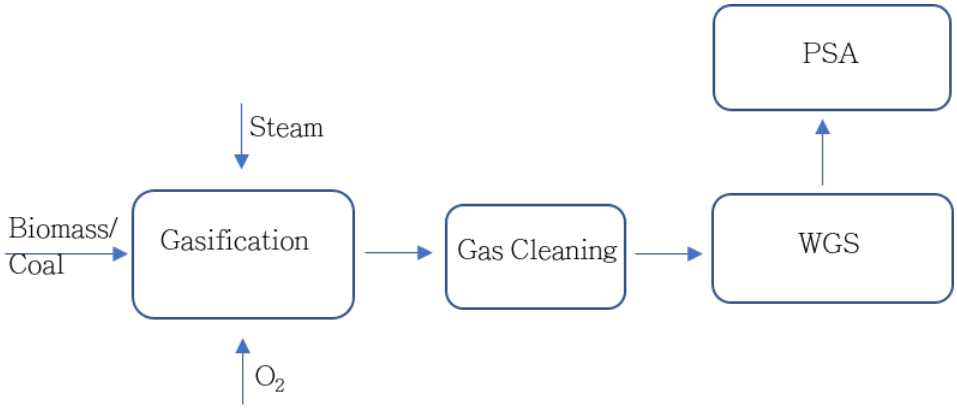

Figure 3.5: Schematic diagram of gasification process.

3.4.2.4 Coal Gasification

This Coal Gasification (CG) model used in this work was also taken from The H2A project of U.S. DOE. The hydrogen production process includes conventional gas cooling, commercial

shift conversion/acid gas cleanup, commercial sulfuric acid technology, and PSA. In this process, oxygen is first produced from air in an air separation unit (ASU) then it reacts with coal and water at coal gasifier unit. Then the produced gas reacts with high temperature steam again to enhance the hydrogen production ratio. Following shift reactor also contributes to producing extra amount of hydrogen. The produced syngas undergoes purification processes including a scrubber unit and a catalytic treatment to remove sulfur components. The sweet gas is sent to the PSA unit for further purification.

3.4.3 Distribution

As illustrated on the superstructure, transportation of raw materials and hydrogen occur between two geographical areas. There are two types of transportation units to transport both compressed hydrogen gas and raw materials, namely tube trailer for compressed hydrogen and truck trailer for biomass and coal. The natural gas utilization was restricted to areas with existing pipeline and Texas has an extensive natural gas pipeline network. The parameters for the two different transportation modes used for this case study are similar to those in Almansoori et al [88]. The distance between two regions has significant impact on the transportation cost. For this case study, the cities close to the center of each region are selected, and those cities are used to measure the distance between two regions. Google Maps was used to estimate distance in miles based on the zip code of those representative cities. The distances used for the 11 regions in this study can be found in the Appendix.

3.4.4 Solution Strategy

Based on the supply chain network described above, the primary problem is a mixed integer nonlinear programming problem. The nonlinearity stems from the capital investment and O&M cost constrains. To simplify the problem, the nonlinear constraints are linearized according to the methods described in Liu et al [89]. Consequently, the problem is posed as a multi-objective multi-period mixed-integer programming problem involving 23,775 discrete variables, 42,137 continuous variables, and 38,853 constraints. It is split into 20 single-objective optimization problems

using the ϵ-constraint method, and solved in GAMS [90] with CPLEX as the MIP solver. Before solving the problem, the variables and constraints are properly scaled to avoid issues associated with poorly scaled models [91].

3.5 Texas Case Study

Texas, the second largest state in the United States except for Alaska, has the biggest carbon dioxide emissions among the states in the US. From EIA database [92], The total carbon dioxide emissions from Texas was 642.0 million metric tons in 2014. This is mainly attributed to the large number of conventional power plants in the state and the heavy use of internal combustion engine vehicles for transportation. Such data triggers concerns related to global warming and accelerates the need for energy transition from fossil fuel to more sustainable energy. The following subsections describe some of the inputs that were used for the Texas case study.

3.5.1 Geographical Mapping

Texas has 254 counties. However, the geographical areas have been reduced to 11 regions through merging adjacent counties according to the Texas Department of State Health Service. Recasting the counties into 11 regions (shown in Figure 3.6) contributes to the size reduction of the problem without significantly affecting the accuracy of the problem statement . The population projection of each region has been estimated through the “Texas Population Projection by Migration Scenario Data". The data measures expected population of each region based on both 2000-2010 Texas migration ratio and natural phenomena, such as births and deaths. The projected population for each region over time periods can be found in appendix A.

3.5.2 Projected Hydrogen Demand In Texas

Hydrogen demand projection from 2015 to 2040 has been performed by the Energy Information Administration (EIA) [93]. The allocation of Texas hydrogen demand ratio is estimated by the ratio of registered vehicles in Texas to the number of registered vehicles in the United States [94]. Based on the EIA’s hydrogen demand projection, the Texas’ hydrogen demand until 2040 is estimated on the simplifying assumption that hydrogen demand at each period does not have a drastic change

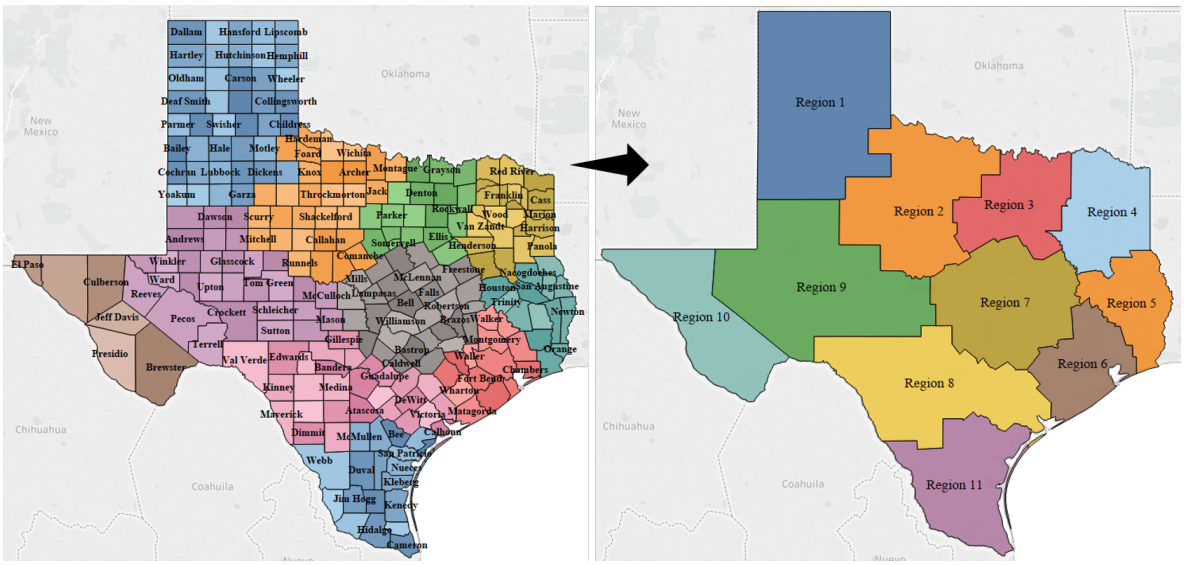

Figure 3.6: Assigned geographical areas for this case study. (according to the Texas Department of State Health Service)

for about five years. Regions with large population show faster hydrogen demand increase. Table 3.2 shows the hydrogen demand for each region over the planning horizon. Note that ton used in this study refers to metric ton.

3.5.3 Resource Availability

The hydrogen production technologies (discussed in the section) requires four primary feed-stock which are biomass, coal, Natural Gas (NG) and water. The maximum potentially extractable capacity of each raw material source in each region is the sum of all that is available in each of the counties assigned to the region. The parameters regard-9ing maximum raw material capacity are taken from U.S. EIA, as presented below in Table 3.3 [93], The capacities for process water are assumed to be unlimited (here it is a large numbers for computational purposes) [93].

3.6 Results and Discussion

The optimal results obtained from solving the single objective problems are used to generate the Pareto curve. This curve of efficient points separates the feasible and infeasible design space, as shown in Figure 3.7. The horizontal axis represents the difference between the upper bound of

Table 3.2: Projected hydrogen demand in each region in Texas (in ton)

regions	Period 1	Period 2	Period 3	Period 4	Period 5
i1	0.01636	0.36235	1.68881	2.70850	3.32391
i2	0.01062	0.22294	1.00229	1.54573	1.81976
i3	0.15060	3.17733	15.5781	26.4283	34.5121
i4	0.02233	0.47604	2.20852	3.52474	4.30781
i5	0.01481	0.32168	1.47556	2.32631	2.80466
i6	0.13107	2.91933	14.3286	24.1718	31.2190
i7	0.06242	1.44525	7.13155	12.0589	15.6100
i8	0.05257	1.21105	5.81648	9.55972	11.9314
i9	0.01077	0.24709	1.14802	1.83085	2.22956
i10	0.01606	0.37702	1.79600	2.91764	3.59896
i11	0.04490	0.98464	4.74307	7.79729	9.76208

Table 3.3: Daily extractable resource

Region	Biomass (ton)	Coal (ton)	Natural gas (ton)	Process water (ton)	Hydro (Mwh)	Solar (Mwh)	Wind (Mwh)
i1	158	0	0	10^7	0	10^7	10^7
i2	14	0	10^7	10^7	0	10^7	10^7
i3	96	0	10^7	10^7	1771	10^7	10^7
i4	106	1090	10^7	10^7	0	10^7	10^7
i5	151	0	10^7	10^7	2592	10^7	10^7
i6	154	0	10^7	10^7	0	10^7	10^7
i7	68	2151	10^7	10^7	7113	10^7	10^7
i8	45	177	0	10^7	1955	10^7	10^7
i9	17	0	10^7	10^7	0	10^7	10^7
i10	11	0	0	10^7	0	10^7	10^7
i11	91	0	0	10^7	659	10^7	10^7

the parameter spaces developed for the single objective problem and the solution of each single objective problem. The region below the curve is the feasible space.

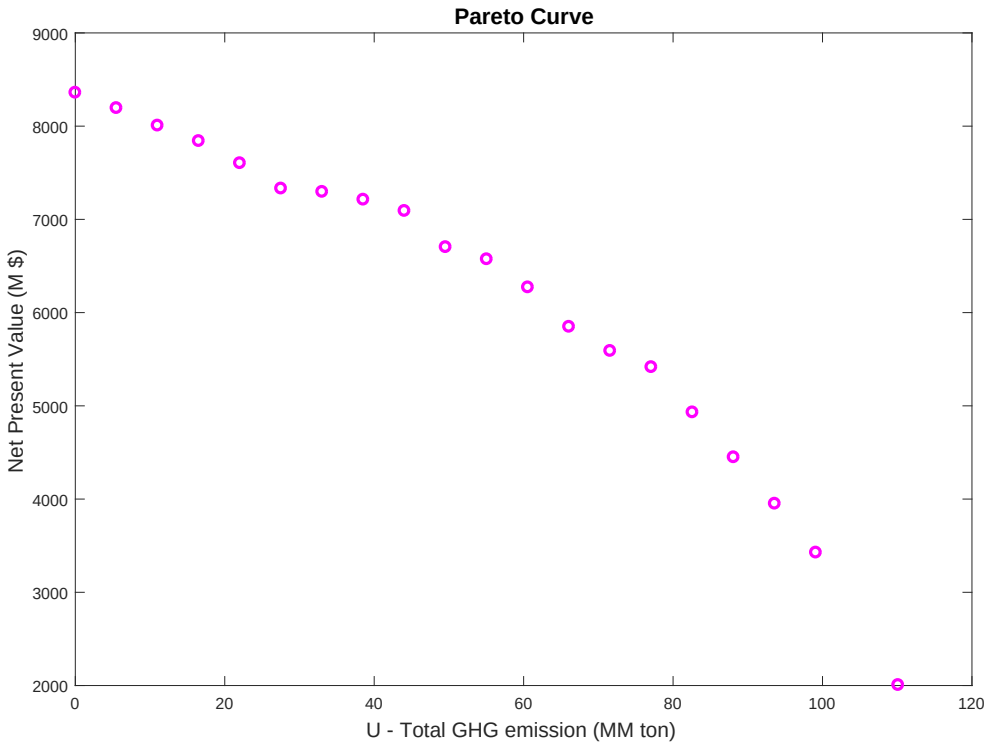

Figure 3.7: Pareto curve for hydrogen production network trading of the maximization of the net present value and the minimization of the greenhouse gas emission.

Further analysis and scenario checks are evaluated at the extreme points of the curve. A chart is used to show plant location, total hydrogen production capacity, hydrogen production technology mix at each region for any time period and the capacity change within the time horizon. Empty intersections of regions and time period indicate no hydrogen production plant is installed. Thus, the hydrogen demand in such region at the specific time period is met by importing hydrogen from other regions in an optimal transportation configuration. For brevity, not all transportation network are shown in this write up.

3.6.1 Case 1: Oxygen As a Discarded By-product

Here we consider a scenario where only hydrogen and GHG effluents are accounted for. This is the case in most hydrogen network studies. The optimal configuration of hydrogen supply chain network for the whole time horizon is shown in Figure 3.8. As expected SMR is the major

technology option at maximum net present value. The vertical axis represents the regions and the horizontal axis represents the time periods (5 years each). Regions 1,10 and 11 make use of electrolysis. Regions 3,6 and 7 started with electrolysis in the first period but SMR became more economical as hydrogen demand increased. This is because at large scale SMR the cost per hydrogen ratio is significantly lower. Region 8 which sits on a lignite deposit makes use of coal through out the period. SMR is obviously a more economic option when only hydrogen production (oxygen is vented) is considered. This result buttresses most studies done by researchers in this area.

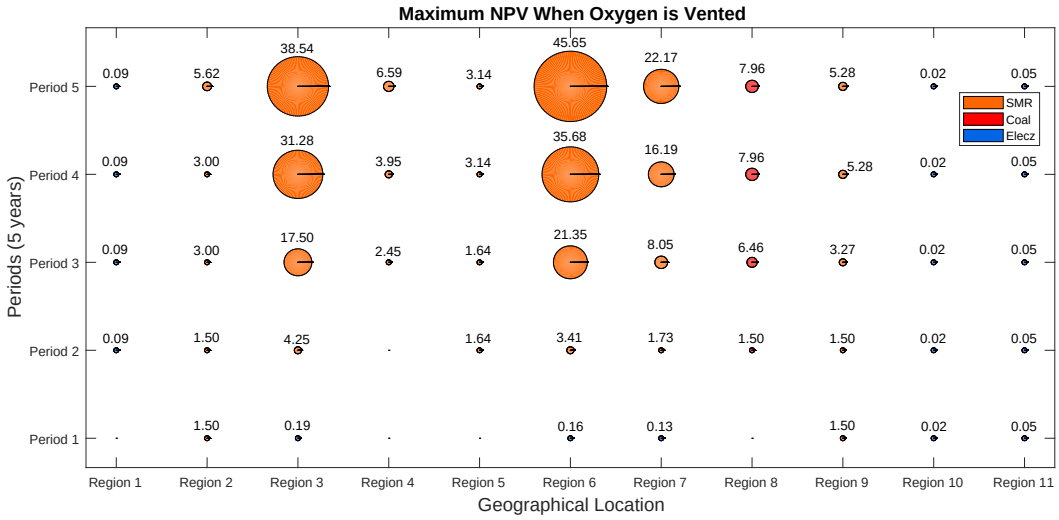

Figure 3.8: A chart showing the hydrogen producing plant location, total hydrogen production capacity per region (in metric tons) at any time period that maximizes the net present value within the planning horizon. The pie chart represents the technology share.

On the other extreme where GHG is minimized, more environmental friendly option dominate the chart as shown in Figure 3.9. Region 1 and 5 have a hydrogen production from biomass through the time horizon and the rest of the regions have a technology mix of biomass and electrolysis. It is important to note that biomass sequestrates CO_2 such that for every metric ton of biomass used, about 22 metric tons of CO_2 have been sequestrated. This result illustrates the impact of CO_2

sequestration on the technology choice.

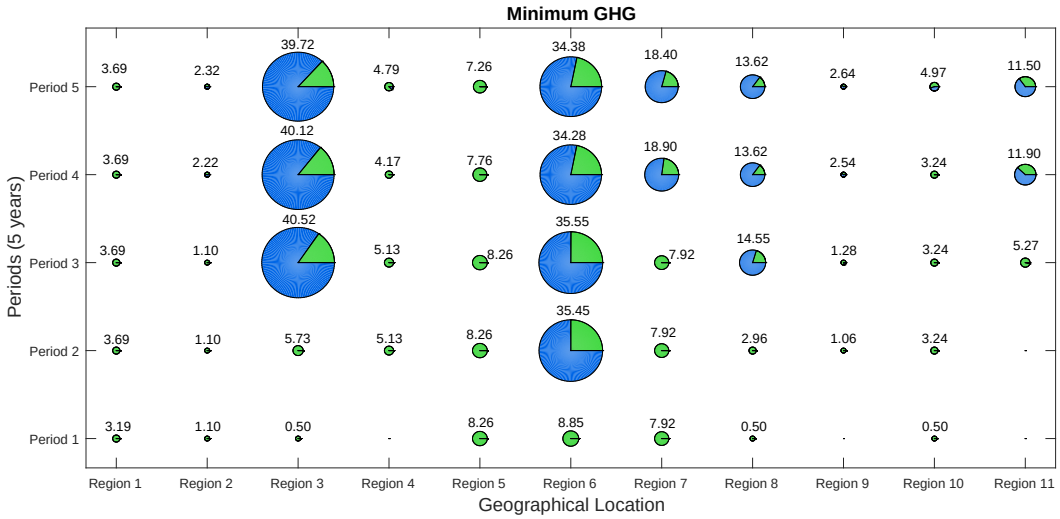

Figure 3.9: A chart showing the hydrogen producing plant location, total hydrogen production capacity per region (in metric tons) at any time period that minimizes the greenhouse gas emission within the planning horizon. The pie chart represents the technology share.

3.6.2 Case 2: Oxygen As a Revenue Generating By-product

When oxygen is collected and sold, hydrogen production from electrolysis becomes more economical as shown in Figure 3.10. Only the electrolysis option was selected in all the regions where hydrogen is produced. Hydrogen demand in other regions are met by transporting hydrogen for producing regions to none producing regions and the distribution network configuration changes with the time period. This is because more revenue is generated by the sell of oxygen. It can be seen that the use of electrolysis for producing hydrogen is an economically viable and environmental friendly option in this case. This result further emphasizes the need to consider oxygen as a valuable by-product in the production of hydrogen from electrolysis. One of the assumption here is that there was a steady demand for all the oxygen produced. This assumption can be supported by the assessment by Kato et al [79]. Figure 3.11 show the distribution network for the last period when only NPV is maximized.

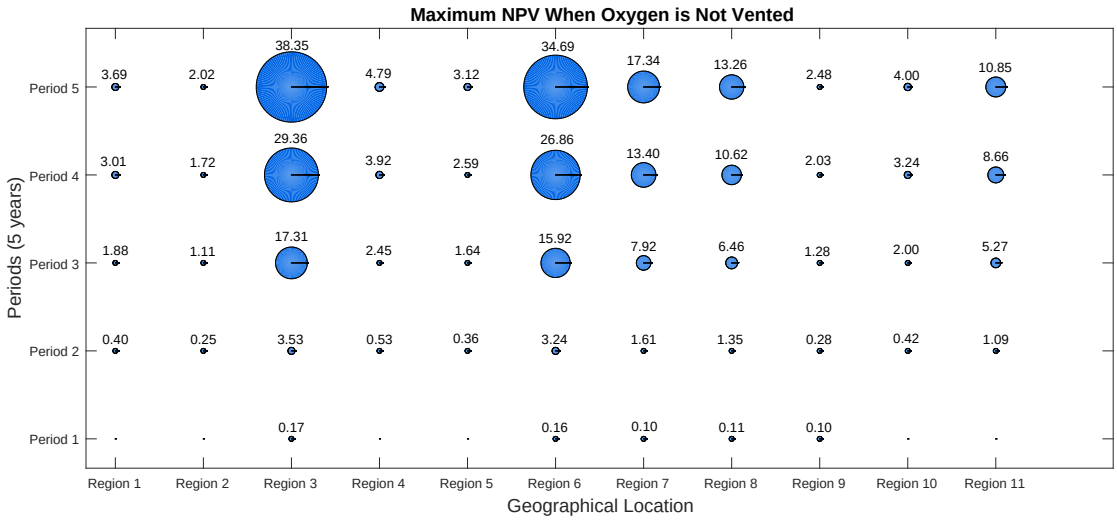

Figure 3.10: A chart showing the hydrogen producing plant location, total hydrogen production capacity per region (in metric tons) at any time period that maximizes the net present value within the planning horizon. The pie chart represents the technology share.

When GHG is minimized and revenue is generated from oxygen, as expected, the results are the same as shown in Figure 3.9. The consideration of oxygen as a revenue generating option only has economic implications.

3.6.3 Transport and Regional Connections

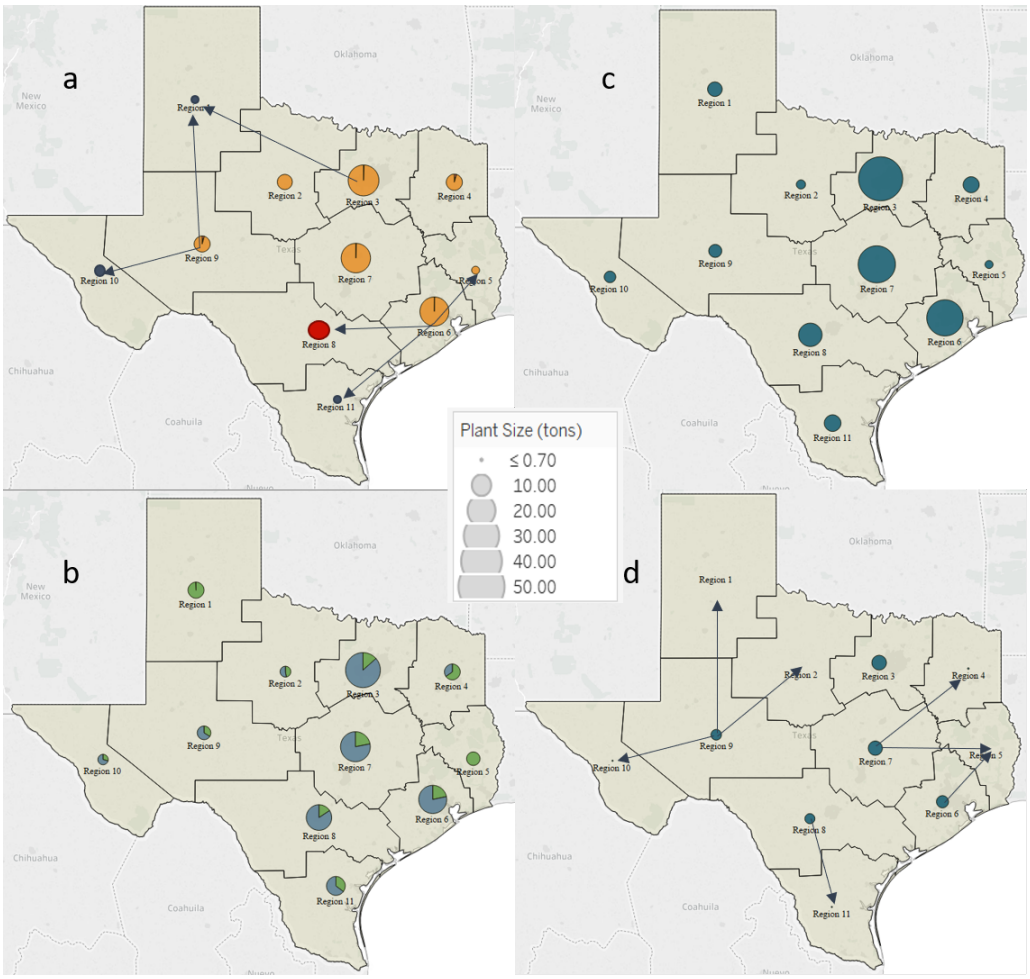

Figure 3.11: a, b, c shows optimal configuration for that plant location and distribution of hydrogen in the last time period for a maximum NPV (no oxygen),minimum GHG and maximum NPV (with oxygen) respectively. d shows the maximum NPV (with oxygen) in the first period

In the regional level, hydrogen is transported from the plants or storage facilities to the gas station. The supply chain within the regions would require a more detailed survey of the market which is beyond the scope of this work. Figure 3.11a,b and c shows the plant locations in the last period for the extreme points on the Pareto curve. The transportation mode for hydrogen (compressed gas) is the tube trailer. In figure 3.11a the hydrogen produced in region 1 is complimented

by the excesses in regions 3 and 9. Region 10 also gets hydrogen from region 9. Region 6 supplies hydrogen to regions 5, 8, and 11. In figures 3.11a and b the hydrogen produced in each region meets the demand. Figure 3.11d show the optimal portfolio for the first period when revenue generated from oxygen is considered. Only regions 3, 6, 7, 8, and 9 produce hydrogen and the other region depend on the excesses from the producing region.

A significant observation in the results shown is the time evolution of the hydrogen network. As expected, hydrogen plants are expanded as the demand of hydrogen increases and new plants of different technologies can be added to a region. This is attributed to the changes in hydrogen demand within the planning horizon and the corresponding cost effective technology option that satisfies the objective function.

3.7 California Case Study

3.7.1 California

California is chosen for this case study because it is more likely to quickly adopt a clean energy initiative. Data updated on 03/26/2019 shows that there are about 39 hydrogen gas stations in service and about 25 hydrogen gas stations either in the commissioning or planning phase [95]. While California is by far the state with the highest number of hydrogen gas stations in the US, the decision of where to build a hydrogen gas station might be based on limited data. Figure 3.12 shows that the population might be playing a major role in situating the hydrogen gas station where they currently are. The hydrogen supply chain provides a more systematic approach and will be demonstrated here.

3.7.2 Geographical Mapping

California is the most populous US state and the third largest by area. It has 58 counties and in order to reduce the size of the model the counties have been merged according to the California County Superintendents Educational Services Association service map [96] to 11 regions as shown in figure 3.13.

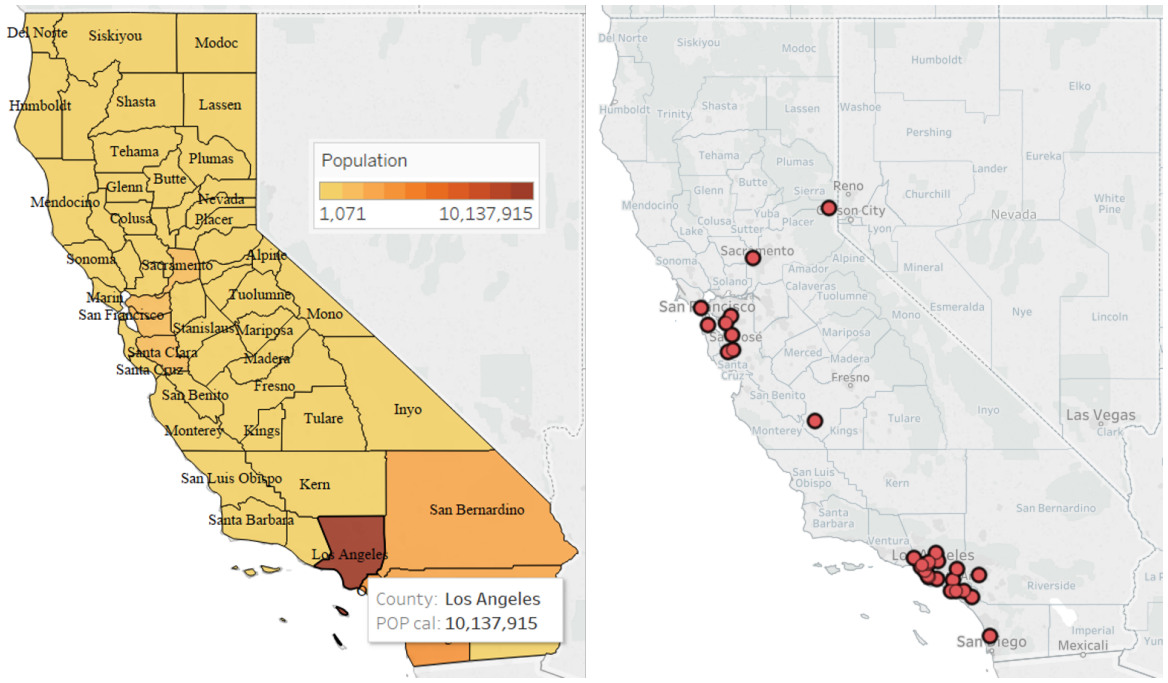

Figure 3.12: California maps showing (left) population distribution and (right) the operating hydrogen gas stations.

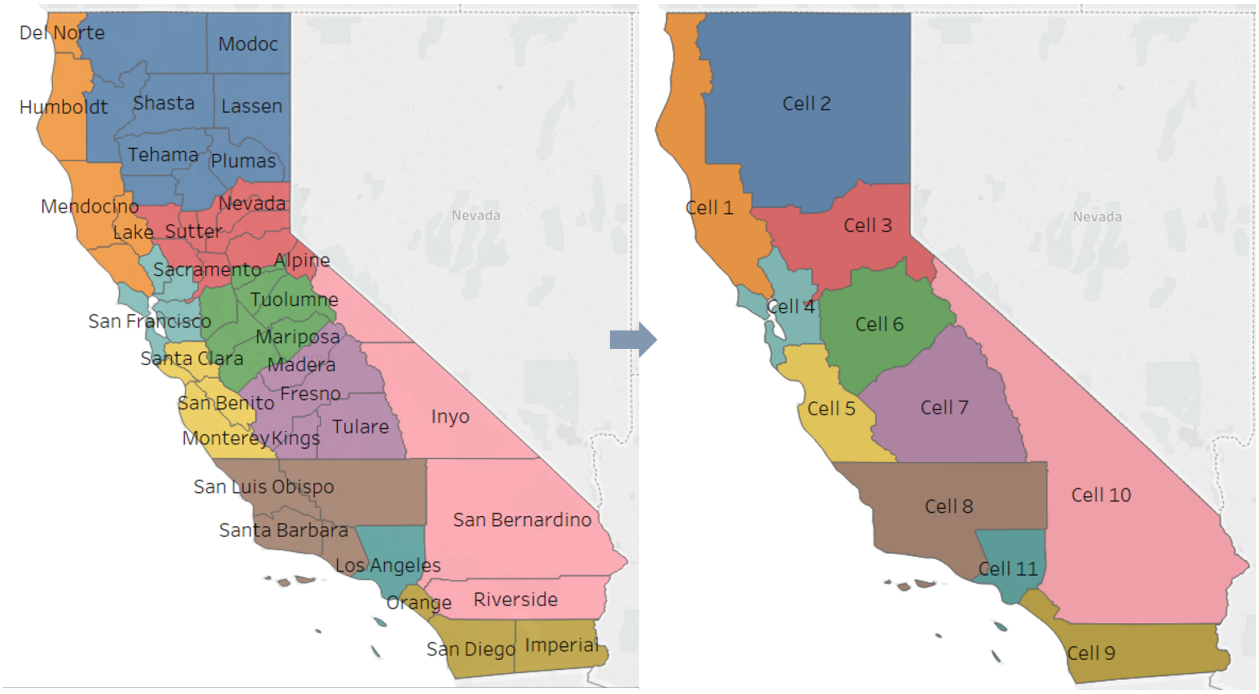

Figure 3.13: California maps showing (left) the counties and (right) the grouping of the counties into 11 regions.

3.7.2.1 Hydrogen Demand

The vehicle transport energy demand is estimated from the total number of registered vehicles in the state. The vehicles are said to be traveling an average of 12,000 miles per year, and the average miles per gallon (MPG) is dependent on vehicle type. It is assumed that 80% of the people above 18 years of age, leaving in California drives or owns a car. The results are validated by the population using a 45% commuter ratio. The hydrogen demand is derived from the gasoline demand for each commuter driving an average of 12,000 mile a year by using the equivalent hydrogen demand and a technology penetration factor during the time horizon considered (assuming that there is a full penetration of the technology by 2040). Table 3.4 shows the projected hydrogen demand for California. More information on considerations can be found in the work by Ogumerem et al. [20]. The data in Table 3.4 might be an over estimation but for the purpose of demonstration, the estimations were left as is.

Table 3.4: Projected hydrogen demand in each region in California (in ton)

regions	Period 1	Period 2	Period 3	Period 4	Period 5
i1	7.153	43.463	102.710	312.010	669.087
i2	8.522	51.652	121.829	369.503	791.511
i3	16.654	101.715	241.677	738.325	1592.633
i4	16.689	102.603	245.108	751.780	1626.476
i5	9.621	59.092	141.101	432.884	937.569
i6	10.595	64.666	153.488	468.296	1008.581
i7	12.473	76.057	180.474	550.689	1186.737
i8	14.130	86.072	204.182	622.860	1341.357
i9	23.880	146.034	346.941	1058.520	2278.407
i10	21.603	132.360	315.603	966.828	2090.332
i11	26.337	160.795	381.269	1160.405	2490.700

3.7.2.2 Hydrogen Production Technology

Three hydrogen production technologies are considered in this case study: Steam Methane Reforming (SMR), Biomass Gasification (BG) and water electrolysis (WE). Each technology pro-

duces hydrogen at 30 bar and is compressed for transportation. They require different raw material types and a certain amount of electricity to produce 1 kg of hydrogen. The operating conditions and other inputs for the hydrogen production technologies considered are taken from the work of [97].

3.7.2.3 Transportation

There are two transportation systems; tube trailer for compressed hydrogen and truck trailer for biomass. The natural gas is assumed to be supplied through the existing natural gas pipeline network. The parameters for the transportation modes used for this case study are similar to those in [17]. Google Maps was used to estimate distance (miles) based on the zip code.

3.7.3 Resource Availability

Renewable energy sources have temporal and geographical variabilities. Biomass, sunlight, and wind speed are unevenly distributed relative to the population throughout California, and their availability vary by season.The population is mostly concentrated in a few areas. Table 3.5 shows the available raw material in the regions adopted from [93]. It is assumed that there is abundance of fresh water in all the regions. Figures 3.13 and 3.14 highlights the geographical mismatch between the state's renewable energy sources and where most of the population lives.

Table 3.5: Daily extractable resource

Region	Natural gas (ton)	Biomass (ton)	Water (ton)
i1	34.854	6438.356	1000000
i2	674.903	10821.918	1000000
i3	1747.475	4383.562	1000000
i4	436.321	3424.658	1000000
i5	75.393	2054.795	1000000
i6	208.630	3835.616	1000000
i7	170.926	3561.644	1000000
i8	8882.076	1506.849	1000000
i9	106.747	3013.699	1000000
i10	0.004	3013.699	1000000
i11	834.704	2739.726	1000000

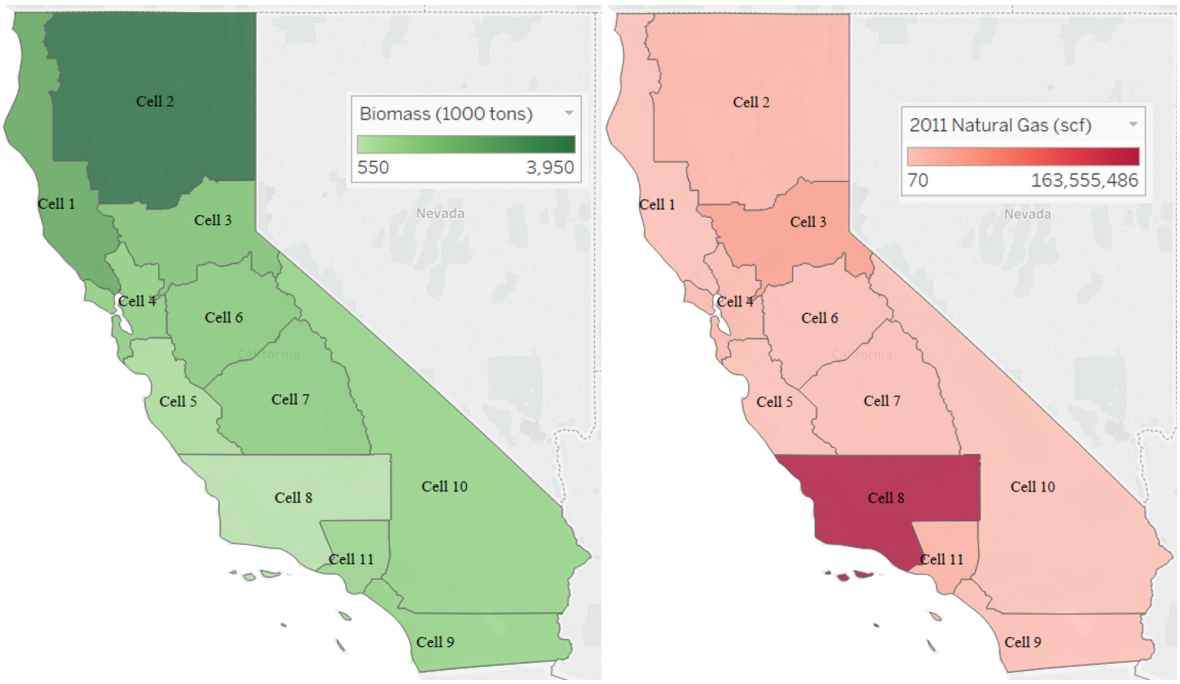

Figure 3.14: California maps showing the (left) distribution of biomass resource and (right) natural gas source

3.7.4 Results and Discussion

Like in the Texas case study, two scenarios are considered for the use of electrolysis. They are (1) when oxygen, which is a by-product in the electrolysis process, is not considered a revenue generating product and (2) when oxygen is considered a revenue generating product. Figure 3.15 t0 3.17 is used to show plant location, total hydrogen production capacity, hydrogen production technology mix at each region for any time period. The vertical axis represents the time periods (5 years each) and the horizontal axis represents the cells. Empty intersections of cells and time periods indicate that no hydrogen production plant is installed. Thus, the hydrogen demand in such region at the specific time period is met by importing hydrogen from other regions in an optimal transportation configuration.

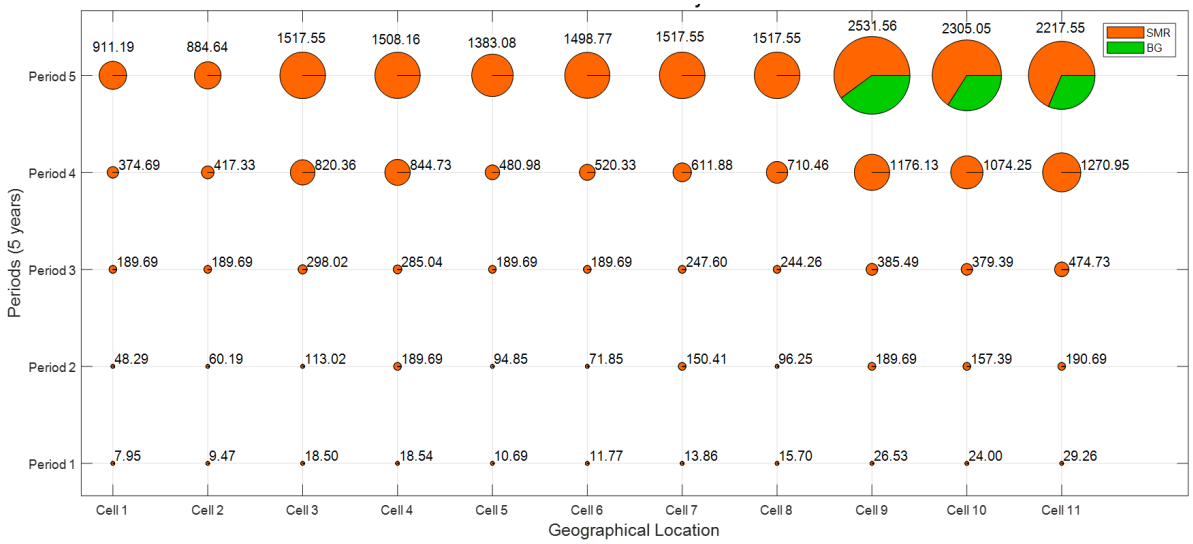

Figure 3.15: A chart showing the hydrogen producing plant location, total hydrogen production capacity per region (in metric tons) at any time period that maximizes the net present value within the planning horizon. The pie chart represents the technology share

3.7.5 Case 1: Oxygen As a Discarded By-product

The optimal configuration of hydrogen supply chain network for the whole time horizon is shown in Figure 3.15. As expected SMR is the major technology option at maximum net present value. At regions 9, 10 and 11 Biomass becomes a cost effective option as the hydrogen demand or the scale of the plant increases. This is attributed to fact that at large scale the biomass becomes cost effective. When compared to the Texas case study, it is obvious that the scale of the plant is pivotal to the choice of technology. As electrolysis does not appear in any of the regions when NPV is maximized.

On the other extreme where GHG is minimized, more environmental friendly option dominate the chart as shown in Figure 3.16. The regions have a technology mix of biomass and electrolysis. It is important to note that biomass sequestrates CO_2 such that for every metric ton of biomass used, about 22 metric tons of CO_2 have been sequestrated. This result illustrates the impact of CO_2 sequestration on the technology choice.

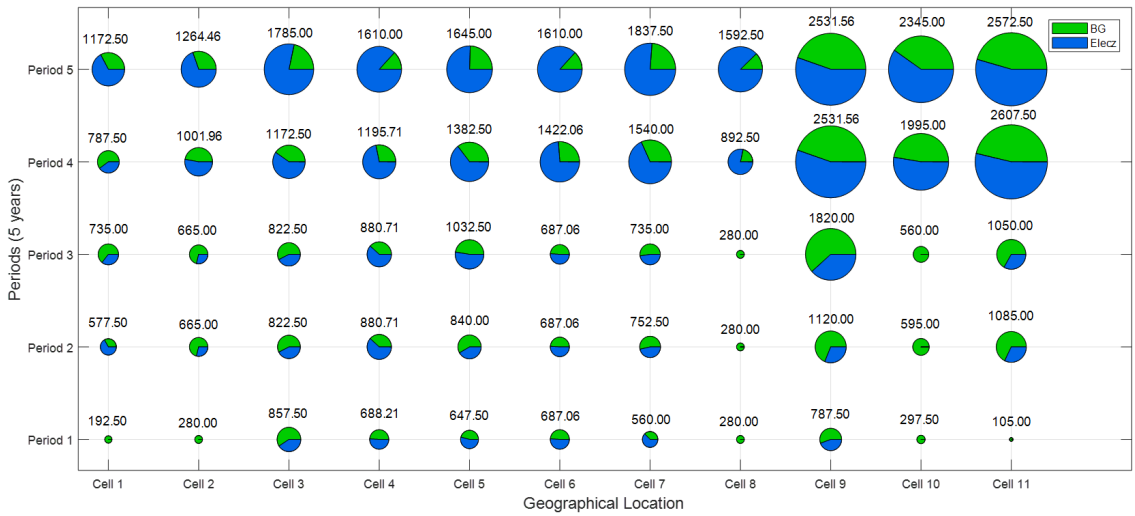

Figure 3.16: A chart showing the hydrogen producing plant location, total hydrogen production capacity per region (in metric tons) at any time period that minimizes the net present value and the GHG within the planning horizon. The pie chart represents the technology share

3.7.6 Case 2: Oxygen As a Revenue Generating By-product

When oxygen is collected and sold, hydrogen production from electrolysis becomes more economical as shown in Figure 3.17. This is because more revenue is generated by the sell of oxygen. However due to the scale of the hydrogen plants, SMR still dominates the mix. This result further emphasizes the need to consider oxygen as a valuable by-product in the production of hydrogen from electrolysis. One of the assumption here is that there was a steady demand for all the oxygen produced. This assumption can be supported by the assessment by Kato et al [79]. Figure 3.18 show the distribution network for the last period when only NPV is maximized and oxygen is considered a revenue generating by product.

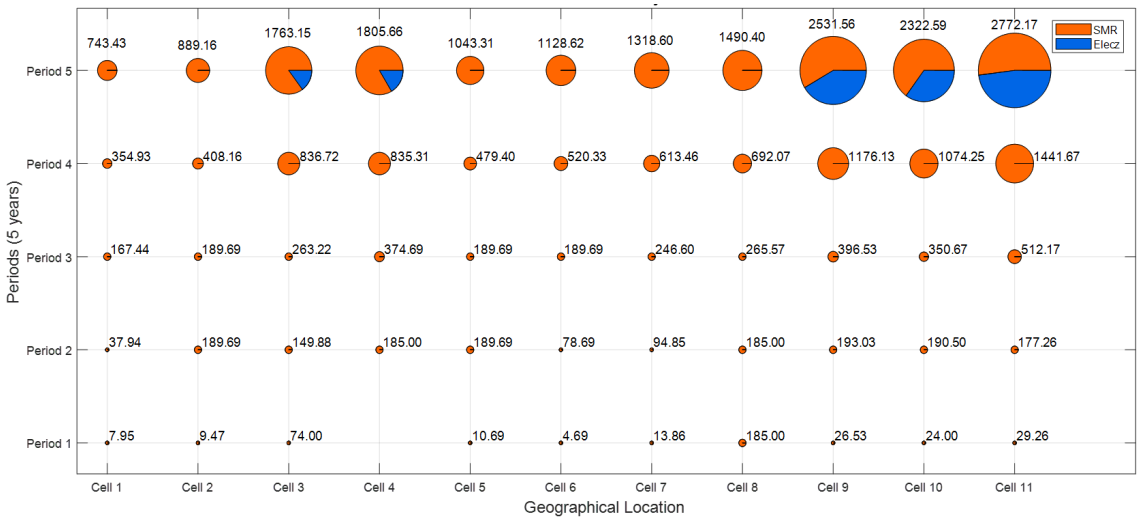

Figure 3.17: A chart showing the hydrogen producing plant location, total hydrogen production capacity per region (in metric tons) at any time period that maximizes the net present value when oxygen sale generates revenue. The pie chart represents the technology share

In the regional level, hydrogen is transported from the plants or storage facilities to the gas station. The supply chain within the regions would require a more detailed survey of the market which is beyond the scope of this work. Figure 3.18a,b and c shows the plant locations in the last period for the extreme points on the Pareto curve. The transportation mode for hydrogen (compressed gas) is the tube trailer. In figure 3.18a the hydrogen produced in region 1 is complimented by the excesses in regions 3 and 9. Region 10 also gets hydrogen from region 9. Region 6 supplies hydrogen to regions 5, 8, and 11.

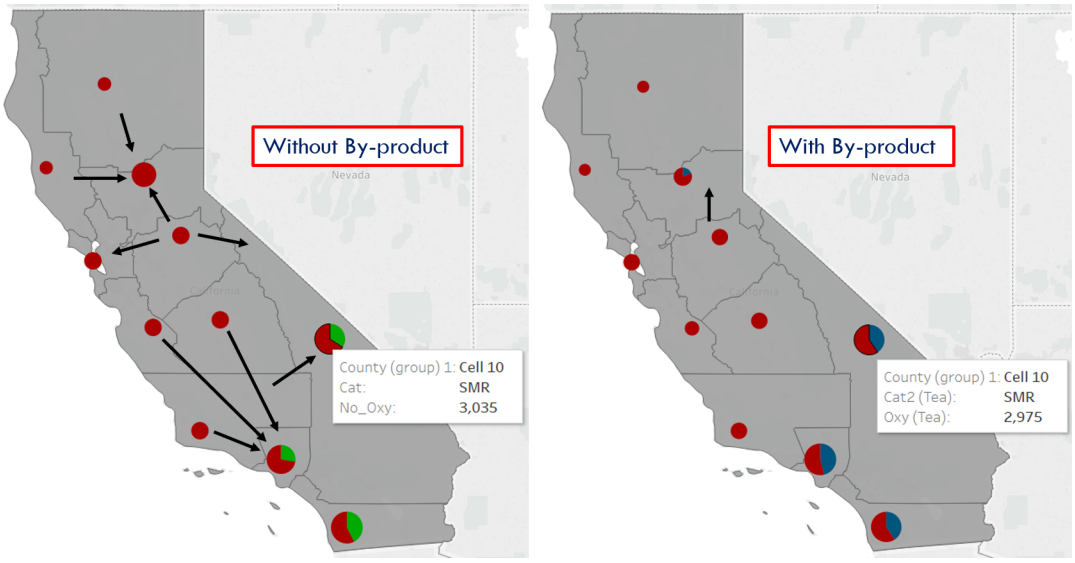

Figure 3.18: California maps showing the distribution route for hydrogen in the last period for when (left) oxygen is vented and (right) when oxygen is sold of revenue.

3.8 Concluding Remarks

In this study we developed a superstructure based mathematical programming model. Using this model we designed a multi-objective hydrogen supply chain network formulated as an MINLP model to simultaneously (i) maximize the NPV and (ii) minimize the GHG emission. The MINLP model was linearized to an MILP for simplification. We applied the model using Texas as a case study and evaluated two scenarios: (i) when oxygen (by-product of hydrogen production from the electrolysis technologies) is vented into the atmosphere and (ii) when oxygen is collected, compressed and sold for revenue. We deployed the ϵ-constraint algorithm in solving the formulated model and produced a Pareto curve with twenty data points. The scenarios were investigated and we found that hydrogen production from electrolysis is not only environmentally friendly but can also be an economically viable option especially when its valuable by-product (oxygen) is considered a revenue generating option.

4. PAROC DEVELOPMENT AND IN SILICO VALIDATION FOR HYDROGEN ENERGY SYSTEMS[1]

4.1 Synopsis

PAROC framework is an integrated framework and software platform that enables the use of model-based tools in the design, operational optimization and advanced control studies of process systems. In this chapter we will explain in details, the various aspects of the PAROC framework and adapt to the design of an explicit model predictive control for three hydrogen energy systems; (1) Proton Exchange Membrane Water Electrolysis(zer) (PEMWE), The Metal Hydride Refueling System (MHRS) and a Direct Internal Reformed Solid Oxide Fuel Cell (DIR SOFC).

[1]Reprinted with the permission from (i) “ASTM International" from - G. S. Ogumerem and E. N. Pistikopoulos, “Dynamic modeling and explicit control of a PEM water electrolysis process," Smart and Sustainable Manufacturing Systems, vol. 2, no. 2, pp. 25-43, 2018. (ii) “John Wiley and Sons" from - G. S. Ogumerem, N. A. Diangelakis, and E. N. Pistikopoulos, “Natural-gas-based sofc in distributed electricity generation: Modeling and control," Natural Gas Processing from Midstream to Downstream, pp. 509-525, 2018. (iii) “John Wiley and Sons" from - G. S. Ogumerem and E. N. Pistikopoulos, âĂIJParametric optimization and control towards the design of a smart metal hydride refueling system,âĂİ AIChE Journal, 2019.

4.2 Introduction

The process systems engineering community have been challenged with integrating detailed modeling, design and operational optimization, controller design and scheduling/planning policies in other to design economically profitable plants and improve their operational performance [33, 98]. In an attempt to address this challenge Pistikopoulos et al. [33] proposed the PARametric Optimization and Control (PAROC) framework which enables the representation and solution of demanding model-based operational optimization and control problems following an integrated procedure featuring high-fidelity modeling, approximation techniques and optimization-based strategies, including multi-parametric programming . A key advantage in the use of multi-parametric programming in the PAROC framework is that, the computational burden of the optimization is transferred offline, enabling its adaptability to more complex systems. Explicit/multi-parametric model predictive control (eMPC) is the most studied and well-known application of multi-parametric programming following the work of Bemporad et al. [71]. In this chapter we will explain in details, the various aspects of the PAROC framework and adapt to the design of an explicit model predictive control for three hydrogen energy systems; (1) Proton Exchange Membrane Water Electrolysis(zer) (PEMWE), The Metal Hydride Refueling System (MHRS) and a Direct Internal Reformed Solid Oxide Fuel Cell (DIR SOFC).

4.3 PAROC Framework

The PAROC framework is an integrated framework and software platform that enables the use of model-based tools in the design, operational optimization and advanced control studies of process systems. A key advantage of the PAROC framework is its ability to adapt to different classes of problems in an effortless manner. The main idea is to close the loop through a real-time implementation of the optimal feedback law generated using the PAROC framework. As shown in Figure 4.1 the PAROC framework involves (i) high fidelity modeling, (ii) model reduction, (iii) deploying multi-parametric programming (mpP) techniques to obtain mpP solutions and (iv) the validation of the mpP solutions.

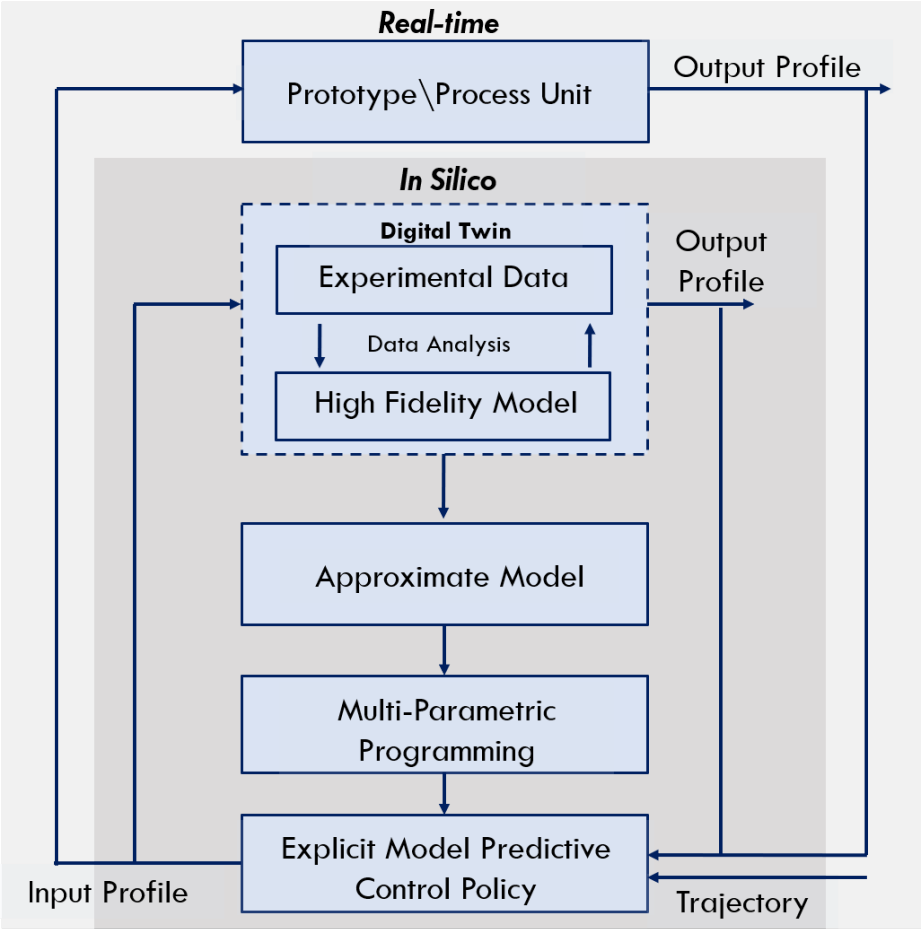

Figure 4.1: Schematic diagram of the PAROC framework.

4.3.1 High Fidelity Modeling

The first step in the PAROC framework is the development of a high-fidelity dynamic model and analysis of the system. The advancement and diversification of real-time and life-cycle modeling is indispensable to smart manufacturing. it is a common component in process system engineering techniques and it is at the core of existing ASCPM technology gaps [46]. The aim of this step is to develop a digital replica of the process system. It involves:

- developing a physics based or first principle model - the models are a combination of differential and algebraic equations that describe essential interactions in the process system.

- global sensitivity analysis - this technique is employed to capture the magnitude of the interactions between the variables, and
- parameter estimation - process data is an essential ingredient in the model development process and its particularly used in the validation of the model.

The system being modeled is fitted with sensors to enable system monitoring and data acquisition. The data acquired is used to validate the model using a parameter estimation technique. A validated high fidelity model of a system is also referred to as a digital twin of the system.

4.3.2 Model Approximation

The next step in the PAROC framework is model approximation. Though it is possible to use the high fidelity model in the design and operation decisions, it might be complex and computationally expensive. Thus, a model reduction step is required to reduce the complexity of the high-fidelity model while maintaining its accuracy. The model reduction is done using system identification techniques or other model reduction methods [99, 100]. The accuracy of the reduced model relative to the original model is an important determinant in the choice of model reduction technique employed. The reduced model is linear discrete time state space models.

4.3.3 Multi-parametric Programming

For operational optimization or control design, Model Predictive Control (MPC) algorithm are used to formulate an implicit receding horizon optimal policies with the reduced model. However, the application of this implicit policies requires solving the MPC optimization problem at every time step which can be avoided by employing Multi-parametric Programming (mpP) techniques. In the application of mpP, an exact reformulation of the MPC problem is obtained using procedures described in the work by Bemporad et al. [71]. The reformulated problem is solved using multi-parametric programming techniques which enables the optimization problem to be solved ones and offline as a function of a set of parameters. The mpP solution obtained is a set of piece-wise affine (PWA) functions of the parameters (measured at every sampling time), defining respective polyhedral critical region [71]. Several research have contributed to the development mpP and the work

done by Pistikopoulos et al. [33] reviewed key contributions in multi-parametric programming solution algorithms for solving various classes of problems. The PAROC framework employs a number of efficient mpP algorithms embedded in the POP toolbox [101, 33].

4.3.4 *In silico* Closed Loop Validation

The next step in the PAROC framwork is the *in silico* closed loop validation of the explicit control policies. The control policies are tested in a closed loop fashion with the original high-fidelity model for properties such as stability at a range of setpoints, effect of the initial conditions etc. This establishes the consistency of the approximate model and the accuracy of the controller. Given the outcome of the validation step the explicit controller can be redesigned and re-evaluated. The PAROC is process agnostic and have been used for system such as the combined heat and power (CHP) co-generation system for residential use, distillation column, a periodic chromatographic separation system of monoclonal antibodies[33].

4.3.5 Real-time Closed Loop Implementation

While there have been substantial progress in the development and *in silico* application of explicit MPC [102, 33], the same is not true for real-time application of explicit MPC on a physical system. This can be attributed to the cost of overhauling an existing control system and in some cases, the size of the mpP solution obtained. The size of the critical regions of the mpP solution easily increases exponentially with the number of active constraint in the MPC formulation. However a few researchers have proposed methods to address the issue [103] some of which compromise the optimality of the mpP solution. with the recent technological advances in embedded systems and micro-controllers, the cost of implementing the explicit control is reducing drastically. klauvco et al. [104] implemented an explicit MPC (embedded in an Arduino) on a magnetic levitation system.

4.4 High Fidelity Modeling of PEMWE System

A suitable model for prediction should capture the dynamics of the PEMWE in response to various inputs or disturbance. The HF model used in this thesis is adopted from by Ogumerem

et al. [105] and is presented below. It includes (i) a mass balance that captures the dynamic of various electrochemical phenomena such as; the electrochemical reaction to produce oxygen and hydrogen ions, the electro-drag of the hydrogen ion from the anode to the cathode where the hydrogen molecules are formed. It also includes equations describing (ii) the electro chemistry to determine actual voltage required for the reaction and (iii) an energy balance describing the heat generation and removal in the process. Also included in the HF model is an empirical relation of the voltage applied to the pump and the flow rate downstream of the filter. The HF model is developed and analyzed in gPROMS®. The model made up differential algebraic equations that have variable and parameters.

4.4.1 Mass Balance

4.4.1.1 Anode

During the operation of the PEMWE, deionized water is pumped into the anode. The deionized water flows across and percolates through the pores of the diffusion layer. When the water molecules reaches the catalyst layer, an electrochemical reaction (shown in equation 4.1) takes place producing protons (H^+) and oxygen ions.

$$\begin{aligned} &1 \quad \mathrm{H_2O(l)} \longrightarrow \tfrac{1}{2}\mathrm{O_2(g)} + 2\,\mathrm{H^+} + 2\,\mathrm{e^-} \\ &2 \quad 2\,\mathrm{H^+(aq)} + 2\,\mathrm{e^-} \longleftrightarrow \mathrm{H_2(g)} \end{aligned} \tag{4.1}$$

The Oxygen produced from the reaction leaves the catalyst layer through the diffusion layer. The reactions described in Equation 4.1 above is propelled by the flow of electrons - current. Increasing the current increases the flow of electron and thus the rate of rate of reaction. The gas phase in the anode is made of oxygen and water vapor. The pressure in the anode is 1 atm and the temperature is maintained well below the boiling point of water. The activities in the anode can be the described by the Equations 4.2 to 4.5.

$$\dot{N}_{\mathrm{H_2O}}^{out,an} = \dot{N}_{\mathrm{H_2O}}^{in,an} - \dot{N}_{\mathrm{H_2O}}^{drag} - \dot{N}_{\mathrm{H_2O}}^{diff} - \dot{N}_{\mathrm{H_2O}}^{rxn,an} \tag{4.2}$$

$$\dot{N}_{\mathrm{H_2O}}^{rxn,an} = \frac{n_{cell} I}{zF} \tag{4.3}$$

$$\dot{N}_{\mathrm{H_2}} = \frac{n_{cell} I}{zF} \tag{4.4}$$

$$\dot{N}_{\mathrm{O_2}} = \frac{n_{cell} I}{2zF} \tag{4.5}$$

Where $\dot{N}_i^{j,k}$ is the molar flow rate of substance i in j activity at location k. I is the current supplied per cell in the electrolyzer stack. F is the Faraday's constant and z is the charge per molecule formed and n_{cell} is the number of cells in the stack.

4.4.1.2 Membrane

The hydrogen ion passing through the membrane drags along some water molecule with it to the cathode. The flux of water through the membrane due to the flow of hydrogen ion is described by an electro-osmotic drag coefficient e_d which is a property of the membrane. The anode side of the membrane is in contact with liquid water and is considered saturated [106, 107] while the cathode side of the membrane accumulate water over time partly due to the electro-osmotic drag. Also given the difference between the chemical potential across the membrane, water diffuses through the membrane according to Fick's law. The activities in the membrane can be described by Equations 4.6 to 4.11

$$N_{\mathrm{H_2O}}^{drag} = \frac{n_{cell} e_d I}{F} \tag{4.6}$$

$$e_d = 0.029\lambda_m^2 + 0.05\lambda_m - 3.4 \times 10^{-17} \tag{4.7}$$

$$N_{\mathrm{H_2O}}^{diff} = \frac{n_{cell} D_m A \rho_m}{m_m} \left(\lambda_{an} - \lambda_{ca}\right) \tag{4.8}$$

$$D_m = 0.0021\lambda_{an} \exp\left(\frac{-2436}{T}\right) \tag{4.9}$$

$$\lambda_{ca} = 0.043 + 17.81a_m - 39.85a_m^2 + 36a_m^3 \tag{4.10}$$

$$\lambda_m = 0.5\left(\lambda_{an} + \lambda_{ca}\right) \tag{4.11}$$

where D_m is the diffusion coefficient water in the membrane, ρ_{mem} and m_{mem} is the membrane dry density and the mass respectively, A is the active area of the electrolyzer cell. λ_{an}, λ_{ca} and λ_m are the water content of the anode side, cathode side and middle of the membrane respectively. a_w is the water activity in the cathode.

4.4.1.3 Cathode

Hydrogen and water molecule flow in the cathode through the membrane electrode assembly. The outlet of the cathode can be controlled by a back-pressure regulator or a valve to maintain a certain outlet pressure and flow of hydrogen water mix. Water molecules flowing into the cathode accumulates to form a pool. Equations 4.12 - 4.16 represents the mass balance process in the cathode.

$$\frac{dN_{H_2}^{ca}}{dt} = \dot{N}_{\mathrm{H_2}} - y_{H_2}\dot{N}_{gas}^{out,ca} \tag{4.12}$$

$$\frac{dN_{\mathrm{H_2O}}^{ca}}{dt} = \dot{N}_{\mathrm{H_2O}}^{drag} + \dot{N}_{\mathrm{H_2O}}^{diff} - \left(1 - y_{\mathrm{H_2}}\right) N_{gas}^{out,ca} \tag{4.13}$$

$$p_{\mathrm{H_2}} = \frac{N_{\mathrm{H_2}}^{ca} RT}{V_{ca}} \tag{4.14}$$

$$y_{\mathrm{H_2}} = \frac{p_{\mathrm{H_2}}}{P_{ca}} \tag{4.15}$$

$$N_{gas}^{out,ca} = K_{ca}\left(P_{ca} - P_{amb}\right) \tag{4.16}$$

Where y_{H_2} is the mole fraction of hydrogen in the cathode. R and V_{ca} is the gas constant and volume of the cathode respectively, K_{ca} represents the valve constant of back pressure regulator constant. P_{ca}, P_{amb} and p_{H_2} are the total cathode pressure, the ambient pressure and the partial pressure of hydrogen respectively.

4.4.2 Electrochemistry

The actual voltage consumption in the PEMWE process is usually about 35% more than the reversible voltage. It is a sum of the open circuit voltage and the overpotentials as shown in the Equations below. The open circuit voltage is the reversible voltage with pressure correction. The reversible potential is independent of current density, It increases with increasing pressure and decreases with increasing operating temperature. The activation overpotential V_{act} stems from the energy barrier that the reactants must overcome before they can be converted to product. The activation overpotential expression is derived from ButlerâĂŞVolmer equation and given as equation [108]. The ohmic overpotential V_{ohm} stems from the resistant or inhibition to the flow of electron and flow of ions from the anode to the cathode. The electrochemical activities are described by the Equations 4.17 to 4.19

$$V = E_{oc} + V_{act} + V_{ohm} \tag{4.17}$$

$$E_{oc} = E^o + \frac{RT}{zF} \ln \frac{p_{\mathrm{H_2}} p_{\mathrm{O_2}}^{0.5}}{p_{\mathrm{H_2O}}} \tag{4.18}$$

$$E_o = 1.229 - 9.0 \times 10^{-4}(T - 298) \tag{4.19}$$

$$V_{act} = \frac{RT}{\alpha_{an} F} \sinh \frac{i}{2 i_{o,an}} + \frac{RT}{\alpha_{ca} F} \sinh \frac{i}{2 i_{o,ca}} \tag{4.20}$$

$$V_{ohm} = \delta_m \frac{i_c}{\sigma_m} \tag{4.21}$$

$$\sigma_m = (0.005139 \lambda_m - 0.00326) \exp\left[1268 \left(\frac{1}{303} - \frac{1}{T}\right)\right] \tag{4.22}$$

Where V is the actual voltage of the stack, V_{oc} is the open circuit voltage, V_{act} is the activation overpotential, V_{ohm} is the ohmic overpotential, E^o is a temperature dependent theoretical/reversible voltage derived from Gibb's free energy, $i_{o,an}$ and $i_{o,ca}$ are the exchange current density for the anode and cathode respectively and σ_m is the membrane conductivity.

4.4.3 Energy Balance

The electrochemical reaction in the PEMWE is theoretically endothermic however, heat is generated in the PEMWE process. The heat generated stems the joule heat effect and it is captured by the energy in excess of the enthalpy of reaction (which is expressed as the thermo-neutral voltage) or the overpotentials. Increase the current supply results in a increase in the heat generation rate and a rapid increase in the generated can is detrimental to the membrane of the Membrane Electrode Assembly (MEA) which is made of polymers. Therefore, maintaining the PEMWE at an efficient temperature is of immense value to it operation. In the PEMWE operation, water is not only a reactant but also a coolant. Consequently, the inlet temperature of water and the flow rate are important parameter to considered in maintaining the temperature of the stack. The temperature gradient across the stack is an important indicator of the rate of heat generation in the PEMWE. To retain the integrity of the PEMWE, the temperature gradient across the stack should be maintained below a certain threshold. The energy balance of the PEMWE is described by the Equations 4.23 to 4.26 [109, 110].

$$m_{stack}C_p\frac{dT}{dt} = n_{cell}I\left(E_{oc} - V_o\right) + \dot{m}_{\mathrm{H_2O}}^{in,an}C_{p,\mathrm{H_2O}}\left(T - T^{in,an}\right) - H_{rad} \tag{4.23}$$

$$V_o = 1.4756 + 2.252(10)^{-4}(T - 273) + 1.521(10)^{-8}(T - 273)^2 \tag{4.24}$$

$$Power = n_{cell}IV \tag{4.25}$$

$$H_{rad} = A_s\delta\sigma\left(T^4 - T_{amb}^4\right) \tag{4.26}$$

Where $\dot{m}_{\mathrm{H_2O}}^{in,an}$ is the mass flowrate of water in the anode, V_{th} is the therm-neutral voltage expressed as a function of temperature, $Power$ and H_{rad} are the power supplied to the stack and the heat loss from radiation respectively. A_s is the surface area of the stack, δ and σ are constants and T_{amb} is the temperature of the surrounding.

4.4.4 Simulation

The model is developed and analyzed in gPROMS® modelbuilder and the simulation results are presented below. One important aspect of the PEMWE is the polarization curve. It is a characteristic curve that conveys the performance or efficiency of the PEMWE. Figure 4.2a show the polarization curve of the PEMWE modeled above. Its shows how the cell voltage changes with the current density. High cell voltage change per current density (or steeper polarization curve) indicates a high power consumption per kilogram of hydrogen produced. The current density is the ratio of the current and the area which is a design parameter. Figure 4.2b shows how the power changes with the current density and 4.2c shows how temperature changes with current density. Increasing the current density increases also increases the joule heating effect which raises the temperature.

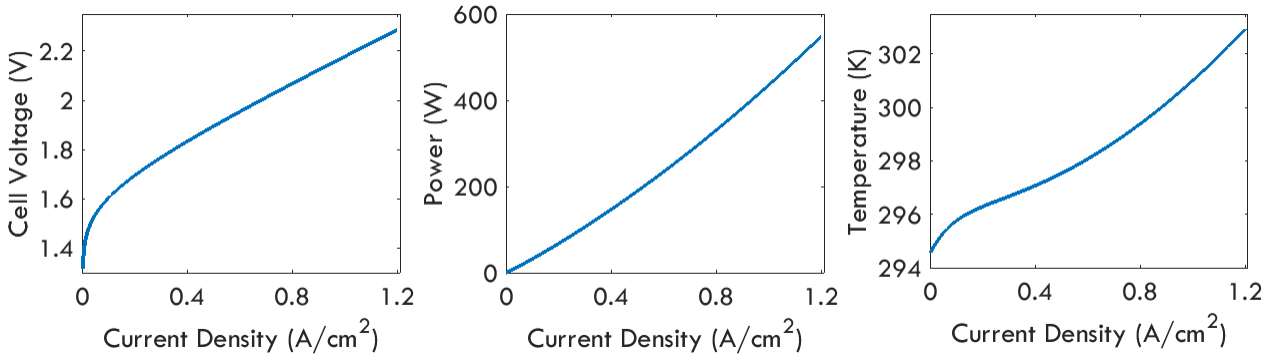

Figure 4.2: Simulation results showing the how current density affects (left) cell voltage (middle) power and (right) temperature

Figure 4.3 demonstrates the impact of varying the control parameters on some keys variables during the operation. The PEMWE is simulated to operate at an inlet water temperature of 297 K and varying flowrate as shown in Figure 4.3f. The current is also varied as shown in 4.3e. From Figure 4.3a, the cell voltage has slight sensitivity to the water flowrate while in 4.3b, the hydrogen and oxygen production has a high sensitivity to current and none to water flowrate. As expected,

the PEMWE operating temperature is sensitive to changes in the current and water flowrate as shown in Figure 4.3c and 4.3d.

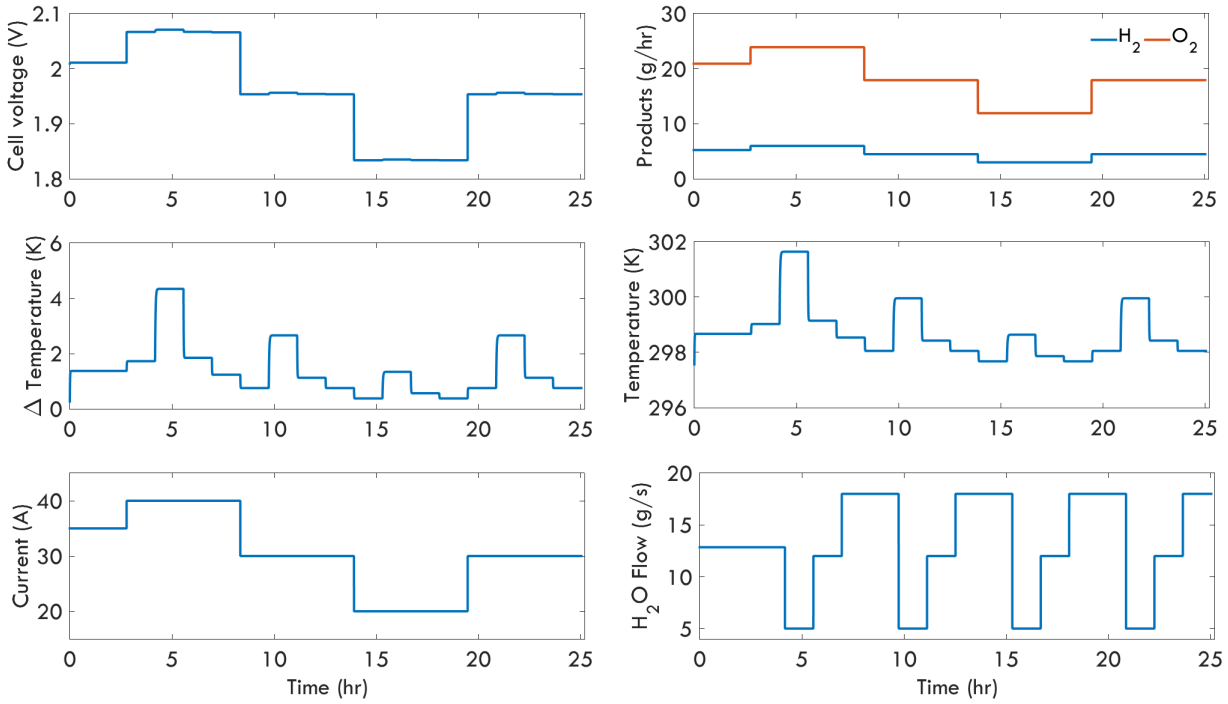

Figure 4.3: Simulation results showing dynamic response of various process variable in the PEMWE

4.4.5 Model Reduction

The digital twin is highly nonlinear thus, for a linear MPC, the model is reduced to a linear discrete time state space model. For the temperature change across the electrolyzer (ΔT), the water flow rate is perturbed at a specific hydrogen production and the corresponding temperature change dynamic is obtained. Using the data and the system identification toolbox in MATLAB®, a linear discrete time state space model is developed such that the accuracy of the original model is not compromised. The linear state space model generated is given in equation A.7 below with a sampling time of 1s. The accuracy of the reduced model is determined by a fitting parameter value which is 97.04 % and 99.97 % for the ΔT and the total voltage curve respectively. Figure

4.4 shows a chart juxtaposing the total voltage and the ΔT profiles for the high fidelity model and the reduced model. Figure 4.4 also shows the water flowrate and current inputs profile used.

$$
\begin{aligned}
x_{k+1} &= \begin{bmatrix} 1 & 2.785e^{-5} \\ 3.959e^{-3} & 0.9959 \end{bmatrix} x_k + \begin{bmatrix} -7.346e^{-7} & 7.761e^{-7} \\ 1.066e^{-4} & -1.062e^{-4} \end{bmatrix} u_k \\
y_k &= \begin{bmatrix} 53.47 & 0.2515 \\ -22.64 & 13.71 \end{bmatrix} x_k
\end{aligned} \tag{4.27}
$$

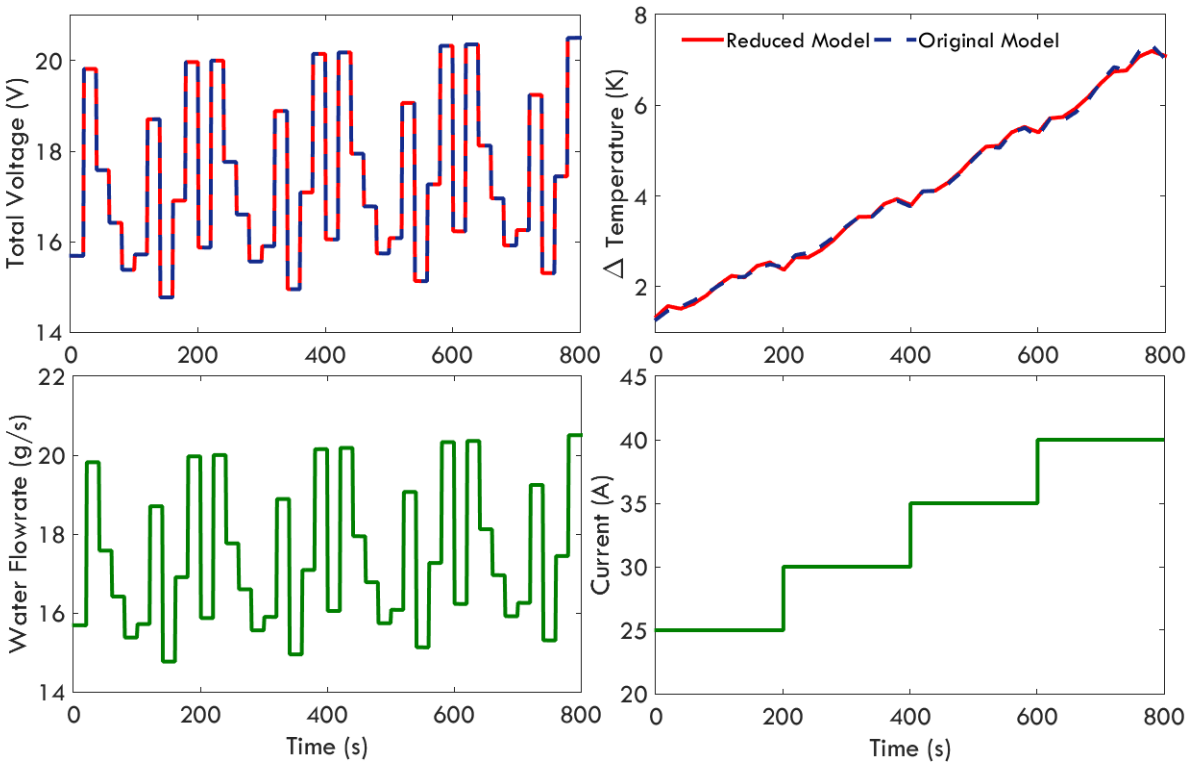

Figure 4.4: Diagram comparing the original model and the reduced model prediction of the total (top left) and the ΔT (top right) while randomly perturbing the the water flowrate (bottom left) and the current (bottom right).

When using the system identification model reduction method, the states of the linear state

space model do not translate to the states of the original model. Therefore an observer is used to make this translation. The Kalman filter is used for as an observer in this study [111].

4.4.5.1 Control Problem

The PEMWE system produces hydrogen and oxygen and the amount of produced gases is determined by the current supplied to the system. The power utilized by the PEMWE is a product of the current supplied to the system and the resultant voltage. The resultant voltage is used to determine the efficiency of the PEMWE and it depends on the temperature of the system. The present study focuses on the thermal management of the PEMWE operation to mitigate the long-term effect of exposing the membrane to high temperature. As discussed earlier, such exposure to higher temperature increases the susceptibility of the membrane to degradation. The flowrate and temperature of the water entering the PEMWE stack has a significant impact on the temperature of the stack as shown in Figure 4.2. Though the inlet temperature has a significant impact on the stack temperature, it is considered a measured disturbance in the present study because the water is recycled. The current is also considered a disturbance in the study since change in current significantly affects the heat generation in the stack. The goal is to maintain the temperature difference across the PEMWE stack at a specified setpoint amid change current (or hydrogen production rate) and inlet water temperature by controlling the water flowrate.

4.4.6 Formulation of the Multi-parametric Model Predictive Controller

The objectives of the receding horizon optimal policy is to reject measured and unmeasured disturbances while maintaining certain operating set-points. The current supply (hydrogen production rate) and the water flowrate are two variables with the most impact on the ΔT or the output temperature. The hydrogen production is not included in the control design because it has a direct translation to the current supplied (Equation 4.4), thus its already controlled. For the MPC formulation, the manipulated variable is the water flowrate and the ΔT is the measured output or the control variable. The linear model developed in section 4.4.5 is used to formulate an MPC optimization problem.

The MPC is exactly reformulated into a multiparametric quadratic programming problem (mpQP) as shown in equation A.9 [71, 59]. The parameters realized at every sampling are denoted as θ and are bounded. The parameters include the initial states x_0, the output y_k the set points y_k^R, and previous control actions u_{-1} for evaluating Δu_k. The multi-parametric model predictive controller problem (equation A.9) is solved using POP toolbox in MATLAB® [101]. The solution obtained is of the form $\mathbf{u} = f(\theta)$ mapping the parameters θ to a sequence of control actions $\mathbf{u}$. Figure 4.5 shows the map of solution when all but the water flowrate and the ΔT are assigned a feasible value.

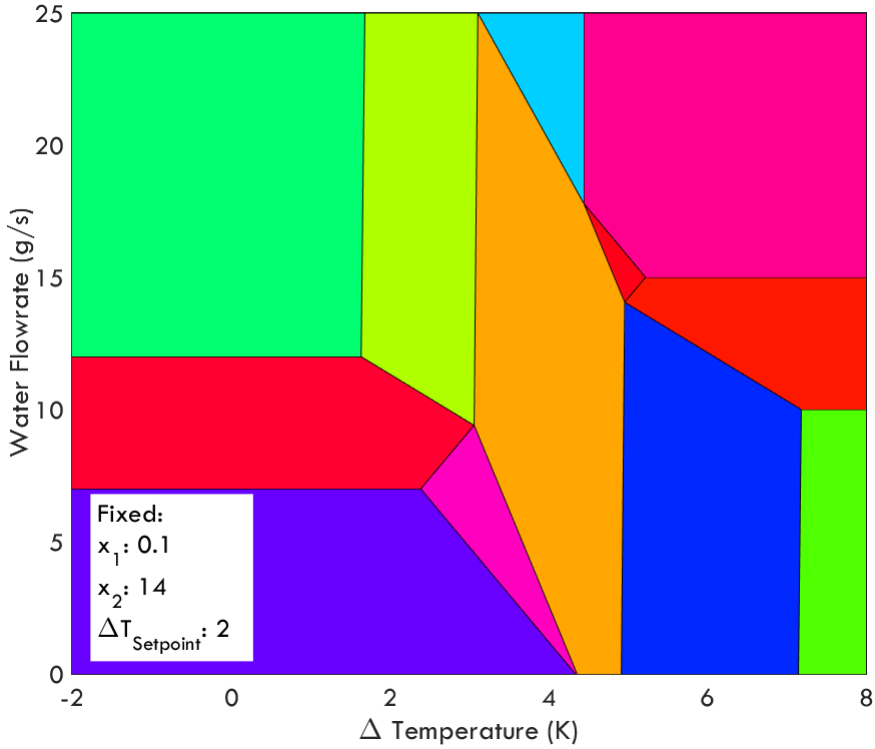

Figure 4.5: Critical regions for the explicit MPC solution - where all the parameters are fixed except the water flowrate and ΔT .

With the explicit MPC feedback law constructed (equation B.4), the next step from the PAROC framework is a closed loop validation of the feedback law with the high fidelity model. Hosting the high fidelity model in gPROMS® and the feedback control policy in MATLAB®, and through

a data exchange protocol provided by gOMATLAB®, the controller is tested in a closed loop fashion. The result of the closed-loop validation is shown in Figure 4.6. It shows the process variable and set-points for ΔT, the water flowrate and the current changes during the *in silico* validation. The ΔT tracks the setpoint well even with changes in current which corresponds to changes in the rate of heat generation.

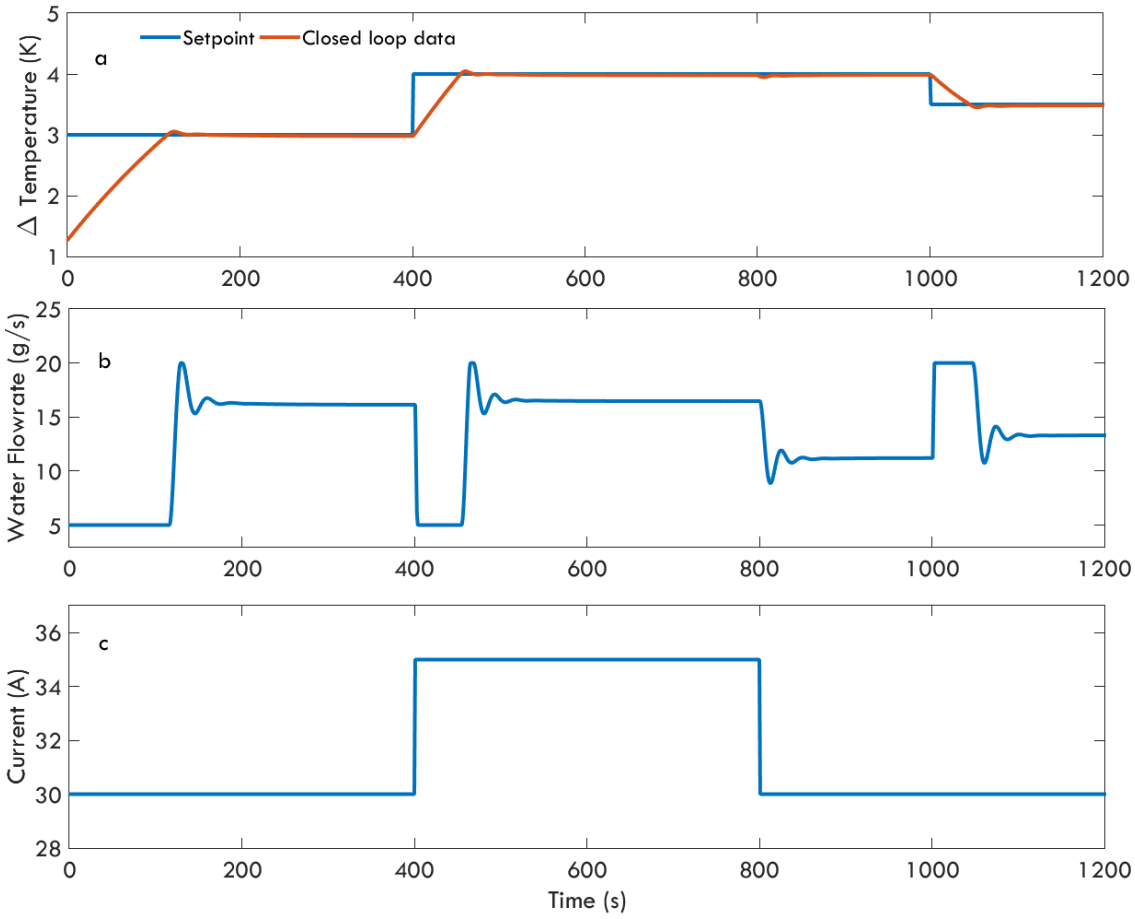

Figure 4.6: *In silico* closed loop validation of the control policy on the PEMWE prototype: (a) ΔT, (b) water flowrate (c) current

4.5 High Fidelity Dynamic Model of Metal Hydride Hydrogen Storage System

There are several mathematical models with various level of complexities that have been used to describe the processes in the metal hydride [112, 113, 31, 114]. The model used in this studied is a physics based lumped dynamic model with parameters that describe the $LaNi_5$ metal hydride. It includes the mass and energy balance equation, the rate equation and a variant of the Van't Hoff equation for the PCT isotherm relation. The mathematical equations are presented below.

4.5.1 Mass Balance

During the refueling process, the hydrogen gas enters the metal hydride canister and adsorbs on the surface of the metal hydride granules. depending on the operating pressure and the concentration of the adsorbed hydrogen, the hydrogen fused into the lattice (absorption) of the metal hydride. The mass balance in the metal hydride is described by equation 4.28. Gas phase hydrogen accumulation in the free volume of the MH pod is assumed to be negligible.

$$\frac{dm_{mh}}{dt} = rm_{sm} \tag{4.28}$$

where m_{mh} is metal hydride mass, r is the reaction rate and m_{sm} is the mass of a hydrogen saturated metal hydride.

4.5.2 Reaction Kinetics

The adsorption and subsequent absorption is described by an pressure-concentration-temperature isotherm. Equations 4.29 describes the hydriding reaction as a function of the reaction temperature, the equilibrium pressure, the hydrogen supply pressure, and hydrogen content [31, 115, 114]. The equilibrium pressure is related to the changes in enthalpy (ΔH) and entropy (ΔS), according to the Van't Hoff's equation and its expressed by Equation 4.29.

$$r = C_a \exp\left(\frac{E_a}{RT}\right) \ln\left(\frac{P_g}{P_{eq}}\right)\left(1 - \frac{m_{mh}}{m_{sm}}\right) \tag{4.29}$$

$$P_{eq} = P_0 \exp\left(\frac{\Delta H_{rxn}}{RT_{mh}} - \frac{\Delta S}{R} + a\tan\left[x\left(\frac{m_{mh}}{m_{sm}} - b\right) + c\right]\right) \tag{4.30}$$

where C_a is material depended constant, m_{sm} and m_{mh} are the mass of the solid phase at hydrogen capacity and actual content respectively. P_{eq} and P_g is the equilibrium pressure and the hydrogen inlet pressure respectively. R and T are the gas constant and the MH pod core temperature respectively. ΔS and R are entropy change and gas constant respectively

4.5.3 Energy Balance

The metal hydride reactor is enclosed with a water jacket with flowing coolant (water), thus the energy balance accounts for the heat generated during the reaction and the heat loss to the water jacket. The energy balance is described by Equations 4.31 to 4.33.

$$m_s C_{mh}\frac{dT_{mh}}{dt} = \dot{Q}_w - \Delta H_{rxn} r \frac{m_{sm}}{M_{H_2}} \tag{4.31}$$

$$V\rho_w C_w \frac{dT_w}{dt} = \dot{m}_w C_w (T_w^{in} - T_w) - \dot{Q}_w \tag{4.32}$$

$$\dot{Q}_w = \epsilon A_s h_w (1-\phi)(T_w - T_{mh}) \tag{4.33}$$

where C_{mh} is the effective heat capacity of the metal hydride, T_{mh} is the temperature of the metal hydride core, ΔH_{rxn} is the heat of reaction, $\dot{Q}_w$ is the heat flow through the surface of the MH pod M_{H_2} is the molecular weight of hydrogen. C_w is the heat capacity of the water, T_w and T_w^{in} are the temperature of jacket water or water leaving the jacket and the inlet water temperature respectively, V and ρ are the volume of the reactor jacket and the density of water respectively, $\dot{m}_w$ is the mass flowrate of water. A_s and h_w are the reactor surface area and the heat transfer coefficient respectively.

4.5.4 Simulation

The model is developed in gPROMS® modelbuilder and the simulation results are presented in Figure 4.7. Figure 4.7a shows te evolution of the state of charge (SoC). SOC is the ratio of the actual hydrogen content to the capacity of the Metal hydride canister. Figure 4.7b shows

the temperature inside the metal hydride canister and the temperature of the water in the jacket. The temperature difference is about 40 K which is high and this is this attributed to the thermal conductivity of the metal hydride and the flowrate of the water in the jacket.

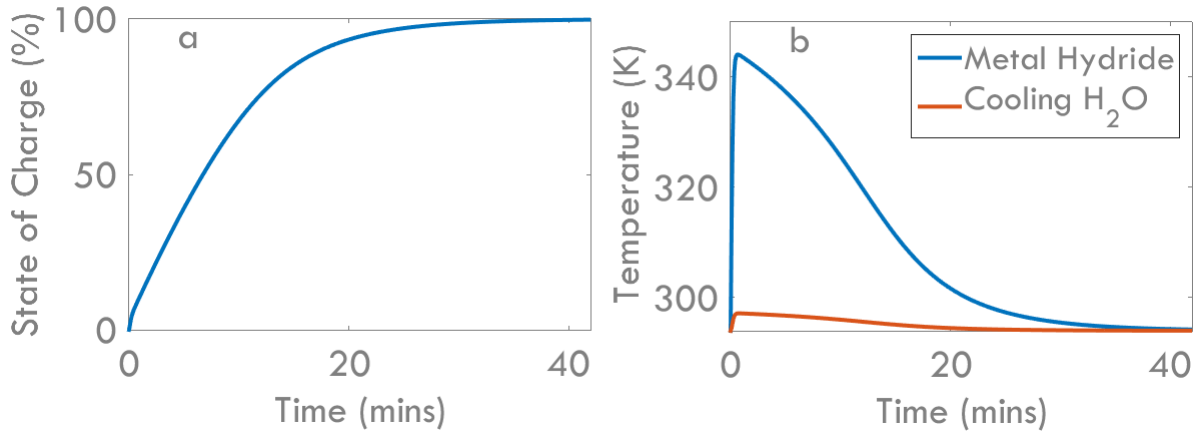

Figure 4.7: Simulation results showing dynamic response of the (a) state of charge of the metal hyride and (b) temperatures of the metal hyride core and outlet coolant water

With the high fidelity model developed, the next step in the PAROC framework is the control design. This includes reducing the complexity of the model to make it tractable for control design, formulating the MPC and reformulating the MPC into an mpMPC.

4.5.5 Model Reduction

The digital twin is highly nonlinear thus, for a linear MPC, the model is reduced to a linear discrete time state space model. Data is generated from the high fidelity model by randomly perturbing the filling pressure to generate the corresponding the temperature and hydrogen charge data. Using the data and the system identification toolbox in MATLAB®, a linear discrete time state space model is developed such that the accuracy of the original model is not compromised. The linear state space model generated is given in equation 4.34 below with a sampling time of 1s. The accuracy of the reduced model is determined by a fitting parameter value which is 86.53 % and 98.11 % for the temperature and the filling profile curve respectively. Figure 4.8 shows

the profiles for the high fidelity model and the reduced model for the temperature and the state of charge of the MH pod respectively.

$$x_{k+1} = \begin{bmatrix} 0.9999 & -1.295e^{4} & 4.287e^{-4} & -1.273e^{-5} \\ -2.895e^{-5} & 1 & -8.987e^{-6} & 1.176e^{4} \\ -6.672e^{-3} & -8.829e^{-3} & 0.9687 & -1.569e^{-2} \\ -3.38^{-3} & -1.491e^{-2} & -3.048e^{-2} & 0.9741 \end{bmatrix} x_k + \begin{bmatrix} 1.28e^{-8} \\ -1.008e^{-7} \\ 3.877e^{-5} \\ 4.632e^{-5} \end{bmatrix} u_k \tag{4.34}$$

$$y_k = \begin{bmatrix} 950.6 & 564.6 & 25.79 & -0.9191 \\ 199.2 & 6675 & 303.2 & -10.81 \end{bmatrix} x_k$$

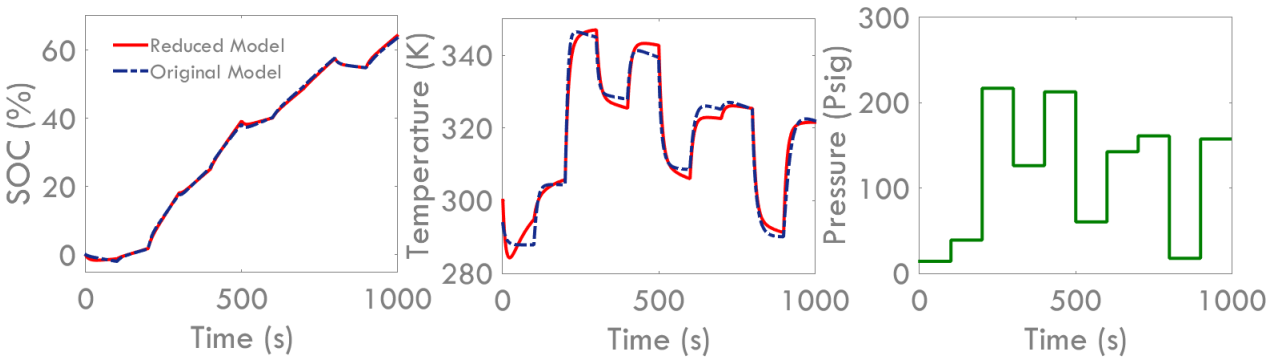

Figure 4.8: Diagram comparing the original model and the reduced model prediction of the the state of charge of the MH pod (right) and the MH core temperature (middle) while randomly perturbing the refill pressure (left).

It is important to note that when using the system identification model reduction method, the states of the linear state space model do not translate to the states of the original model. Therefore an observer is used to make this translation. The Kalman filter is used for as an observer in this study.

4.5.6 Formulation of the Multi-parametric Model Predictive Controller

The primary objective is to develop control policies that will maintain the temperature of the hyriding operation below a certain threshold while maximizing the State of Charge (SOC). The manipulated variables for the hydriding operation are the filling pressure and the water flow rate. During the hydriding process, an important objective is to remove as much heat as possible because, the higher the rate of heat removal the faster the filling. In the hydriding operation, there exist a trade-off between the temperature, the pressure and the filling rate. The higher the filling pressure, the faster the reaction rate (high filling rate) and the higher the maximum operating temperature. The MPC is formulated to optimize the filling pressure profile within the control horizon such that the temperature and other constraint are not violated and also that the output trajectory reaches or maintains the set-points as much as possible. The MPC optimization for the hydriding operation is formulated according to Equation A.8 and the setpoints are based on a time invariant optimal trajectory obtained from a dynamic optimization of the original model. Using the linear discrete model developed in 4.5.5 an we formulate an MPC optimization problem as shown in Equation A.8.

The quadratic problem formulated using equation A.8 can be reformulated into a multi-parametric quadratic programming problem (mpQP) as shown in equation A.9 [71, 59]. The uncertain parameters are denoted by θ and they include the initial states x_0, the output y_k the set points y_k^R, and previous control actions u_{-1} for evaluating Δu_k. The multi-parametric model predictive controller problem (equation A.9) is solved using POP toolbox in MATLAB® [101]. The solution obtained is of the form $\mathbf{u} = f(\theta)$ mapping the parameters θ to a sequence of control actions $\mathbf{u}$. $f(\theta)$ is a piece-wise affine function of the uncertain parameters as shown below . For the MH system, there are ten uncertain parameters measured at every sampling time. Figure 4.9 shows the map of solution when all but the previous input (filling pressure) and the SoC are assigned a feasible value.

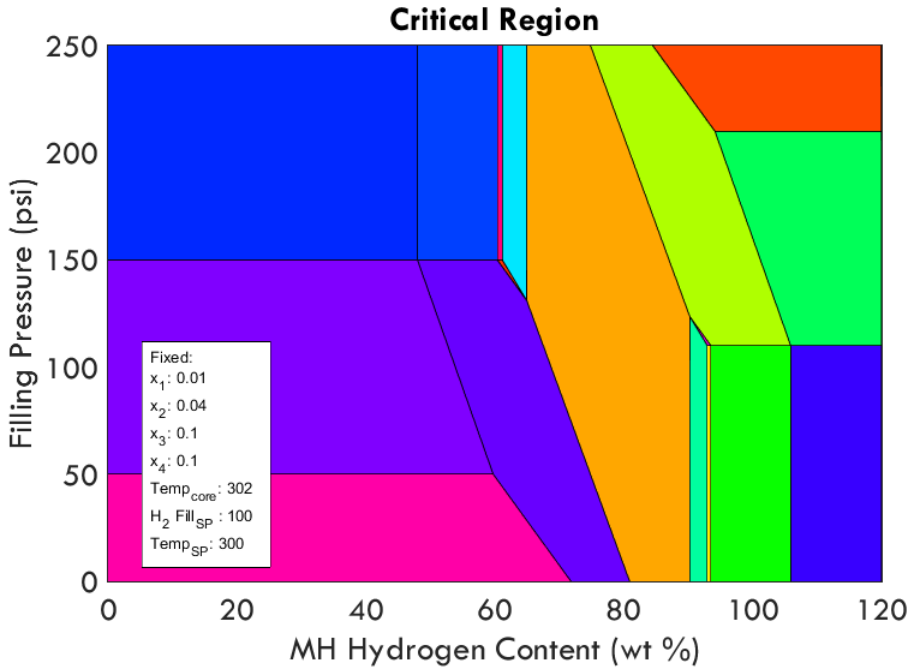

Figure 4.9: Critical regions for the explicit MPC solution - where all the parameters (states x, setpoints and output are fixed except the filling pressure and the SoC of the MH pod.

With the explicit MPC feedback law constructed (equation B.4), the next step from the PAROC framework is a closed loop validation of the feedback law with the high fidelity model. Hosting the high fidelity model in gPROMS® and the feedback control policy in MATLAB®, and through a data exchange protocol provided by gOMATLAB®, the controller is tested in a closed loop fashion. The result of the closed-loop validation is shown in Figure 4.10. It shows the process variable and set-points for the temperature and MH pod SoC and the manipulated variable - the filling pressure and water flowrate. The filling pressure and the water flowrate profiles shows the sequence of optimal control action required to keep the MH core temperature on the setpoint for most of the alpha-beta reaction phase while filling up the metal hydride to 100% full.

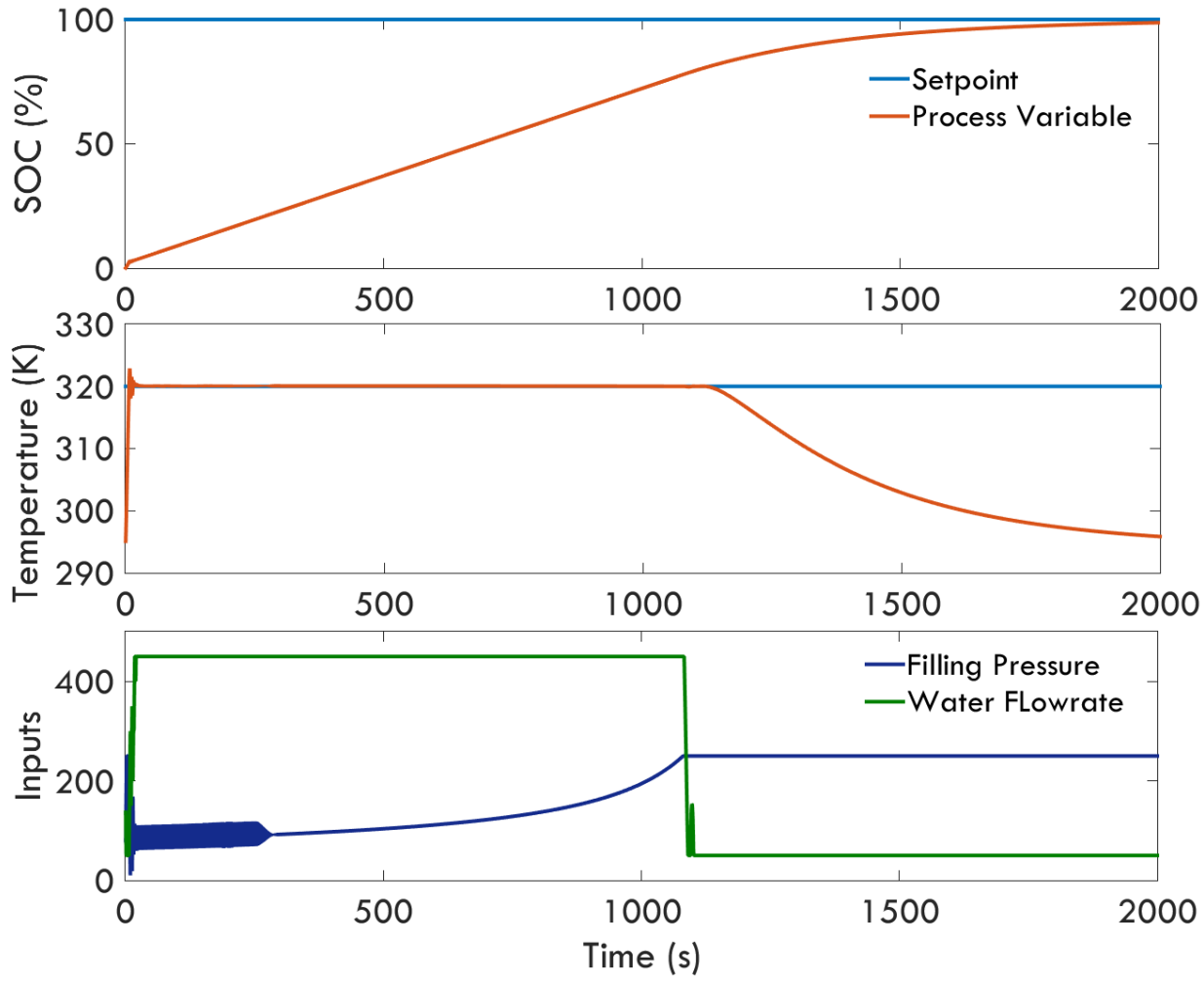

Figure 4.10: Insilico closed loop validation results of the control policy for the SoC of the MH pod (top), the MH core temperature (middle) and the filling pressure (bottom)

4.6 Direct Internal Reforming (DIR) SOFC

Several integration strategies for SOFC have been reviewed [116]. One of the design approaches considered is the external reforming SOFC. Here, the reformer is spatially close to the SOFC and the heat generated for the SOFC is transferred to the reformer through heat integration [117]. Contrariwise, in the internal reforming approach the reforming process is within the SOFC. Generally, two design techniques exist for the internal reform of natural gas in SOFC and they are the Direct Internal Reforming DIR and Indirect Internal Reforming IIR. In the latter, the stack and

the reformer are in thermal contact and the reformate is fed to the to the adjacent anode. Also, the electrochemical reaction and the reforming reaction are separated. While in the DIR the NG reform take place in the anode. The heat generated by the exothermic electrochemical and shift reaction is utilized by the endothermic reforming reactions. Tubular, planar and monolithic are the predominant geometric configurations of a SOFC[118, 119]. Westinghouse, now Siemens-Westinghouse developed the tubular SOFC [120]. Planar designs are popular for their compact nature and higher power density. A schemcatic diagram of a DIR SOFC Cell is shown in figure 4.11. Due to its high operating temperature, the electrolyte is a nonporous ceramic; Y_2O_3 stabilized ZrO_2 (YSZ). The anode face is made of a porous Nickel/Yttria-stabilized zirconia (Ni/YSZ) cement and the nickel serves as a catalyst for the reform reaction. The cathode face is porous Sr-doped $LaMnO_3$.

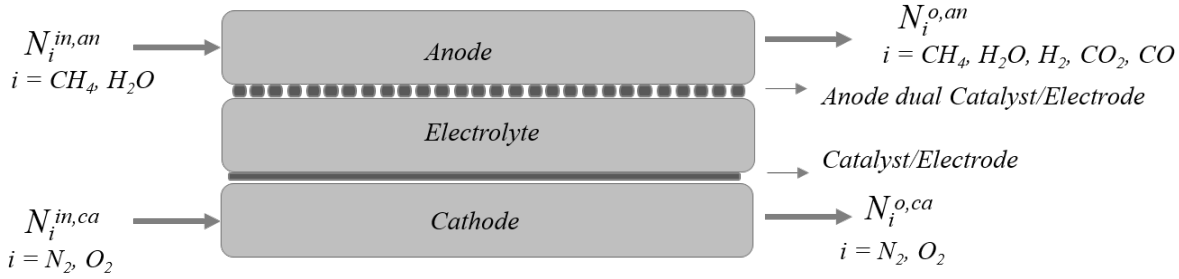

Figure 4.11: Schematic diagram of a DIR SOFC cell

During the startup operation of the direct internal reforming, natural gas and steam is fed to the anode. Air is fed to the cathode and oxygen ion percolates through the electrolyte to the anode where it reacts with the hydrogen ion to form steam. At continuous operation, the steam from the electrochemical, heat and the nickel catalyst sustains the reforming reaction producing hydrogen H_2 and carbon monoxide CO and carbon dioxide CO_2. The shift reaction also utilizes the CO and

steam to produce more CO_2 and H_2.

$$\begin{array}{lll} 4 & H_2 + O_2{}^- \longleftrightarrow H_2O + 2\,e^- & -285\ kJ/mol \\ 5 & CO + O_2{}^- \longleftrightarrow CO_2 + 2\,e^- & -283\ kJ/mol \\ 6 & O_2 + 4\,e^- \longleftrightarrow 2\,O_2{}^- & 0\ kJ/mol \end{array} \tag{4.35}$$

4.6.1 Mathematical Model

Mathematical models can be used to estimate the required amount of input steam by analyzing the interactions between various components of the system. A few researchers have developed models for internal reforming SOFC [118]. Here we develop a dynamic model describing various fundamental principles of a DIR SOFC similar to the model developed by Ogumerem and Pistikopoulos [121]. The system adopted is a 12 kW SOFC and the following assumption were made in developing the hypothetical model used here;

- The gases behave like ideal gas
- The pressure correction on the voltage i dependent of hydrogen oxygen and steam.
- The kinetics developed through the experiments conducted by Jianguo Xu and Gilbert Froment [122] is the same for a direct internal reforming SOFC since nickel base catalyst is used in both cases.
- The anodic and cathodic chambers are well mixed and the oxidation of hydrogen happens in the anode

4.6.2 Mass Balance

4.6.2.1 Anode

The anode takes in NG and steam at a molar ratio of 3:1 in a reforming reaction to produce a CO and H_2. The CO produced is shifted with steam to produce more H2. The H_2 produced undergoes an electrochemical reaction with oxygen to produce steam and electricity. The steam

produced in the electrochemical reaction augments the steam in the inlet stream. At the cathode, Air flows in and the oxygen from air sips through the electrolyte and into the anode as oxygen ion where it reacts with hydrogen ions to form water. The composition of the air is assumed to be 21% oxygen and 79% nitrogen. The material balance is as follows

$$\frac{V_{an}}{RT}\frac{dp_i}{dt} = N_i^{i,an} - N_i^{o,an} - r_i^{an} \tag{4.36}$$

$$\frac{V_{ca}}{RT}\frac{dp_i}{dt} = N_i^{i,ca} - N_i^{o,ca} - r_i^{ca} \tag{4.37}$$

Where V_{an} is the volume of the anode, p is the partial pressure of specie i, R and T are gas constant and temperature respectively, N_i is the molar flowrate of specie i, r_i is the sum of reactions involving specie i and i represents all the species in the anode $(\mathrm{CO}, \mathrm{CO_2}, \mathrm{H_2O}, \mathrm{CH_4}, \mathrm{H_2})$. Where V_{ca} is the volume of the anode, i represents all the species in the cathode $(\mathrm{O_2}, \mathrm{N_2})$

4.6.3 Energy Balance

The thermal integration that takes place in the DIR SOFC creates a state where endothermic reaction is complimented by the exothermic reactions. Here the streams are preheated to 950^0C before they are fed into the anode. The partial enthalpies of the inlet and outlet streams of the anode and the cathode make up the first two terms in equation A.6. The combination of the reaction enthalpies and reacted quantities produces a net heat generation which depends on the kinetic of the reaction with respect to the equilibrium. About 235 kJ of energy generated for every mole of water produced contributes to power and some of the heat generated are lost due to radiation.

$$\frac{dT}{dt} = \sum_{i=1}^{n_a} N_i^{an}\left(h_i^{in} - h_i^{st}\right) + \sum_{i=1}^{n_c} N_i^{ca}\left(h_i^{in} - h_i^{st}\right) + \sum_{j=1}^{m} \Delta H_j r_j - P_{st} - H_{rad} \tag{4.38}$$

$$H_{rad} = A\delta\sigma\left(T^4 - T_{surr}^4\right) \tag{4.39}$$

Where ΔH_j is the enthalpy of reaction j, h_i^{in} and h_i^{in} are the enthalpy of the fluid entering and leaving the stack, na nc are the number of species in the anode and the cathode respectively. P_{st}

and H_{rad} are the power of the stack and the heat loss from radiation respectively. A is the surface are of the stack, δ and σ are constants and T_{surr} is the temperature of the surrounding.

4.6.4 Kinetics

The Langmuir Hinshelwood kinetics is used to describe the reforming reaction according to [122]. The rate expressions for the reaction given by equations 4.40 to 4.48.The kinetic model for the electrochemical reaction is based on a Butler Volmer reaction mechanism where the rate expressions for reactions is given by 4.47 and 4.49.

$$r_1^{an} = \frac{\frac{k_1}{p_{\mathrm{H_2}}^{2.5}}\left[p_{\mathrm{CH_4}}p_{\mathrm{H_2O}} - \frac{p_{\mathrm{H_2}}^3 p_{\mathrm{CO}}}{K_1}\right]}{DEN^2} \tag{4.40}$$

$$r_2^{an} = \frac{\frac{k_2}{p_{\mathrm{H_2}}}\left[p_{\mathrm{CO}}p_{\mathrm{H_2O}} - \frac{p_{\mathrm{H_2}}p_{\mathrm{CO_2}}}{K_2}\right]}{DEN^2} \tag{4.41}$$

$$r_3^{an} = \frac{\frac{k_3}{C^{3.5}}\left[p_{\mathrm{CH_4}}p_{\mathrm{H_2O}}^2 - \frac{p_{\mathrm{H_2}}^4 p_{\mathrm{CO}}}{K_3}\right]}{DEN^2} \tag{4.42}$$

$$DEN = 1 + K_{\mathrm{CO}}^{ads}p_{\mathrm{CO}} + K_{\mathrm{H_2}}^{ads}p_{\mathrm{H_2}} + K_{\mathrm{CH_4}}^{ads}p_{\mathrm{CH_4}} + K_{\mathrm{H_2O}}^{ads}\frac{p_{\mathrm{H_2O}}}{p_{\mathrm{H_2}}} \tag{4.43}$$

$$k_j = A_j \exp\left[\frac{E_j}{R}\left(\frac{1}{T} - \frac{1}{T_{ref}}\right)\right] \tag{4.44}$$

$$K_i^{ads} = A_i \exp\left[\frac{\Delta H_i^{ads}}{R}\left(\frac{1}{T} - \frac{1}{T_{ref}}\right)\right] \tag{4.45}$$

$$K_j^{equ} = A_j \exp\left[\frac{\Delta H_j^{rxn}}{R}\left(\frac{1}{T} - \frac{1}{T_{ref}}\right)\right] \tag{4.46}$$

$$r_4 = \frac{I}{zF} \tag{4.47}$$

$$r_i = \sum_{j=1}^{4} v_{ij} r_j \tag{4.48}$$

$$I = I_o\left[\exp\left(\frac{\alpha_a z F \eta}{RT}\right) - \exp\left(\frac{\alpha_c z F \eta}{RT}\right)\right] \tag{4.49}$$

where k_j is the rate constant of reaction j; K_j is the equilibrium constant of reaction j and K_i is the adsorption coefficient of component i. I is electrode current density, I_o exchange current density, z number of electrons involved in the electrode reaction, F Faraday constant, α_c cathodic charge transfer coefficient, α_a anodic charge transfer coefficient, η activation overpotential.

4.6.5 Electrochemistry

The theoretical or reversible voltage can be derived from the standard Gibbs free energy at any defined temperature. However, the actual cell voltage is less then the theoretical voltage due to overpotentials. The overpotentials are caused by the activation barriers, V_{act} and resistances to electron, ion and bulk mass transport through and to the electrolyte, charge leaks. Io is the exchange current, and it varies with temperature as shown in equation 4.53 [123]. The limiting current density I_L is the current density at which the flow to the triple phase boundary is not sufficient to meet the power demand. V_{conc} related to the current as follows according to 4.55.

$$V = n\left(E_{oc} - V_{act} - V_{ohm} - V_{conc}\right) \tag{4.50}$$

$$E_{oc} = E^o + \frac{RT}{zF}\ln\frac{p_{\mathrm{H_2}}p_{\mathrm{O_2}}^{0.5}}{p_{\mathrm{H_2O}}} \tag{4.51}$$

$$V_{act} = \frac{RT}{F}sinh^{-1}\frac{I}{2I_o} \tag{4.52}$$

$$I_o = A\exp(-E/RT) \tag{4.53}$$

$$V_{ohm} = \gamma\exp\left[\beta\left(\frac{1}{T_o} - \frac{1}{T}\right)\right]I \tag{4.54}$$

$$V_{conc} = \frac{RT}{zF}\ln\left(1 - \frac{I}{I_L}\right) \tag{4.55}$$

Where V is the actual voltage of the stack, V_{oc} is the open circuit voltage, V_{act} is the activation overpotential, V_{ohm} is the ohmic overpotential, V_{conc} is the concentration overpotential. Where E^o is a temperature dependent theoretical/reversible voltage derived from Gibb's free energy. T_0 is the fuel cell reference temperature; T_0 = 973 K, γ = 0.2Îl', and β = âĹŠ2870 K are the constant coefficients of the fuel cell.

4.6.6 Simulation

The Model was developed and simulated in gPROMS. The dynamic model is simulated to investigate the interactions between the manipulated and controlled variables, and for the characterization of the effect of disturbances. The results from the simulations shows the transient behavior of the materials and how the temperature changes. The inlet stream is a mixture of methane and steam at 950 K and a composition ratio of 3:2. The reforming reactions, shift reaction and the electrochemical reactions occur simultaneously. The model is initialized with some hydrogen in the anode. A polarization curve was derived from the model at constant temperature (950 K) (figure). Figure 4.12 shows the cells polarization curve. It also shows how the power changes with current density. The limit current density used for the hypothetical model is 2 A/cm2.

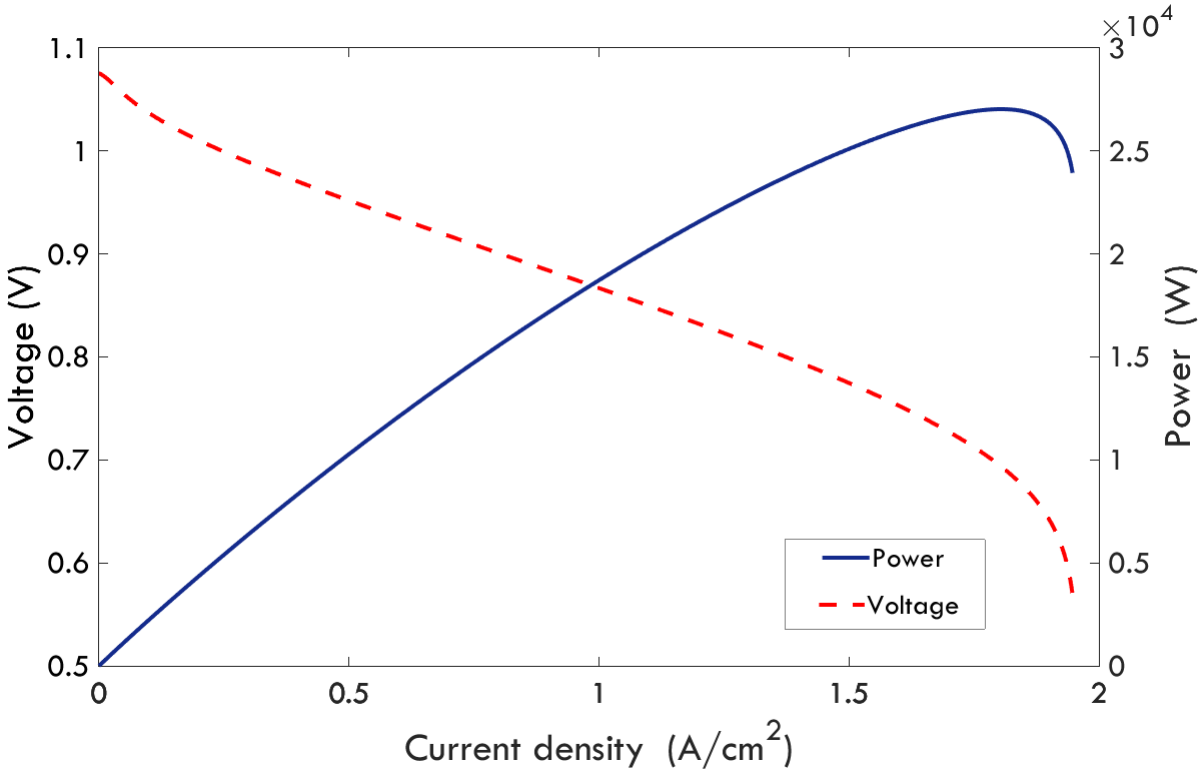

Figure 4.12: Polarization curve.

Fuel cells in general are subjected to varying power demand. The DIR SOFC should be robust

to enough meet varying power demand. All the components in the anode and the cathode respond to change in current demand. Consequently, an increase in the power demand results in a depletion of the hydrogen and an accumulation of steam which in turn favors the reforming reaction. Moreover, if the reforming reaction is more favorable than the electrochemical reaction (probably due the current demand), the temperature of the system might start decreasing and will tend to slow down the reforming reaction.

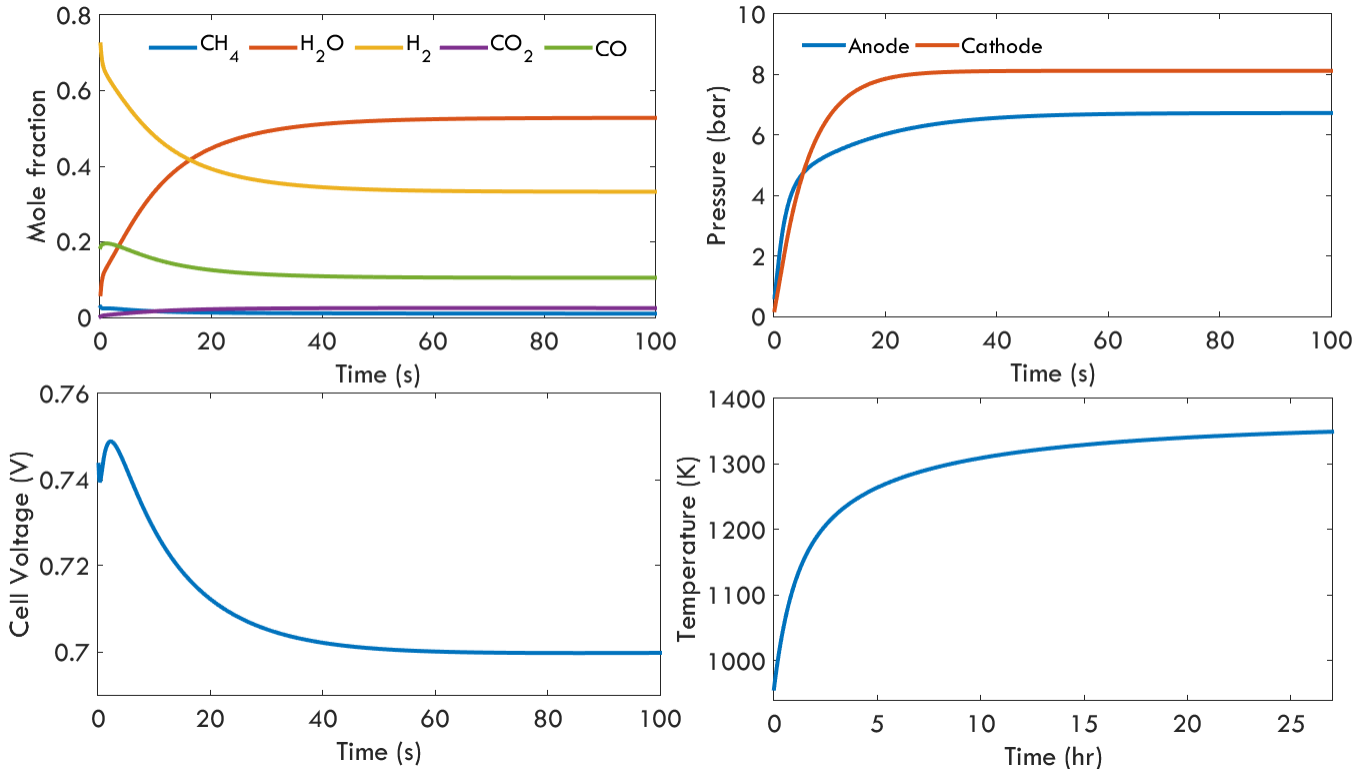

Figure 4.13: Transient change in mole fraction with change in power demand.

One of the major challenges of Fuel cells is the voltage fluctuation that accompany a change in current or power demand. This phenomenon is associated with the (multiple) time constants of the various interactions in the operation of the system. A controller can be used to regulate voltage to a set point, for slight change in the power demand. This combination of exothermic and endothermic reactions at varying reaction rate (or time constant) has a significant impact on the

thermal management of the system. The control developed here will attempt to maintain a voltage set point while constraining the temperature of the system within a bound.

4.6.7 Linear Model Approximation

A series of simulations of the dynamic model for different input is used to construct a meaningful linear state-space model of the process using statistical methods. The inputs are the inlet flowrate for the anode and the cathode while we measure voltage current and temperature. The current is a disturbance One of the most widely applied tools within this area is the System Identification Toolbox from MATLAB®. The sampling time for the input-output data is 200ms. A discrete linear state space model is obtained from the input-output data using the System identification toolbox. The mathematical expression of the SS model is of the form The SS model generated have 4 states, 2 outputs, 2 inputs and 1 disturbance. The state space model is given in equation 4.56

$$
\begin{aligned}
x_{k+1} &= \begin{bmatrix} 1 & 2.75e-5 & 2.9e-5 & 2.14e-6 \\ -0.064 & 0.922 & 0.065 & -0.0233 \\ 0.0696 & 0.0526 & 0.887 & -0.223 \\ 9.23e-3 & -0.239 & -0.0397 & -0.0472 \end{bmatrix} x_k + \begin{bmatrix} -5e-6 & 1.05e-4 \\ -1.532 & 0.85 \\ -1.523 & -5.093 \\ -12.12 & -18.07 \end{bmatrix} u_k \\
y_k &= \begin{bmatrix} -1875 & -0.01 & -0.0336 & 5.97e-4 \\ -1.756 & 0.049 & -0.0022 & 1.41e-4 \end{bmatrix} x_k + \begin{bmatrix} 0.2357 & 0.1143 \\ 0.0628 & 0.00248 \end{bmatrix} u_k \\
T_s &= 0.2s
\end{aligned}
\tag{4.56}
$$

The approximate model was compared to the original nonlinear model in figure 4.14. Only one input (anode inlet flowrate) and output is shown here, however the inlet flow of the cathode was varied too and temperature fitting curve was obtained. The temperature has an R^2 value of 99% while that of the voltage (figure 4.14) is 79%.

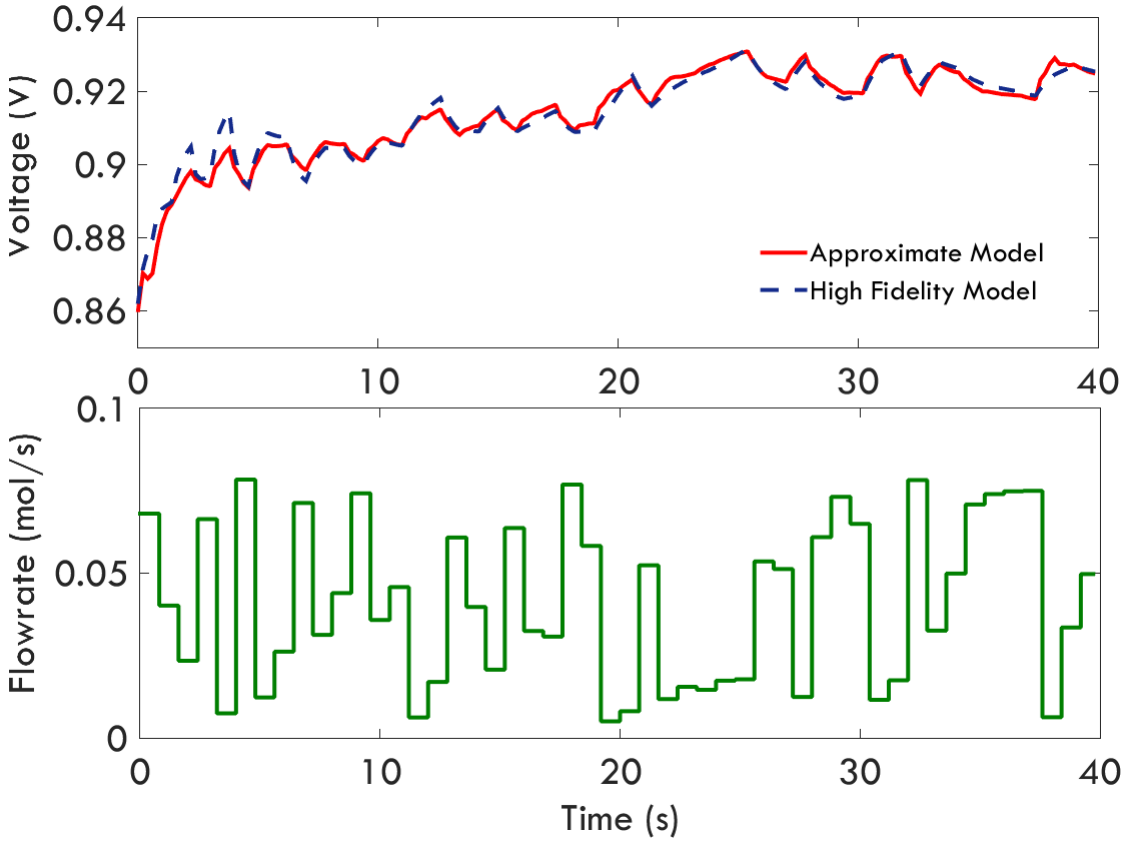

Figure 4.14: Comparison of linear SS model and the original model.

There are eight states in the original dynamic model however, for simplifications, the linear discrete state-space model has only four states. Not only are the states unequal but the state of the linear state space model looses it physical meaning during the system identification process. To maintain an even better representation of the original complex dynamic model a state observer is employed to estimate the state of the system using the linear model. The Kalman filter is a type of observer that uses a least square estimation approach to characterize the current state of a dynamic system based on the influence of past measurement. Its prime feature is the iterative propagation of the noise measurement risk. For further reading on the Kalman Filter used in this work see reference article [124].

Table 4.1: Weight Tuning for the mpMPC of the DIR SOFC Unit

mpMPC design parameters	Value
N	5
M	2
$QR_k, \forall k \in \{1, \ldots, N\}$	100
$R1_k, \forall k \in \{1, \ldots, M\}$	$\begin{bmatrix} 10^{-4} & 0 \\ 0 & 10^{-4} \end{bmatrix}$
x_{min}	$-500[1 \quad 1 \quad 1 \quad 1]$
x_{max}	$500[1 \quad 1 \quad 1 \quad 1]$
u_{min}	$[0.002 \quad 0.004]$
u_{max}	$[0.1 \quad 0.1]$
y_{min}	$[900 \quad 0.1]$
y_{max}	$[2000 \quad 1.2]$
Δu_{min}	$-[0.05 \quad 0.05]$
Δu_{max}	$[0.05 \quad 0.05]$

4.6.8 Formulation of Multiparametric Model Predictive Control (mpMPC)

4.6.8.1 mpMPC Controller Design

This quadratic problem in equation B.2 can be reformulated into a multiparametric quadratic programming problem (mpQP) B.3 The uncertain parameters are denoted by θ and they include are the initial states x_0, the set points y_k^R, previous control actions u_{-1} for evaluating Δu_k, and the disturbances (dk). The mpQP is given as follows:

The multi-parametric model predictive controller problem is formulated and solved using POP toolbox in MATLAB®.The objective of the mpMPC is to meet the electrical power demand at a constant voltage amid the current change and to maintain the temperature within 1500 K. The optimal control action is generated as a map of solutions and as an affine function of the aforementioned parameters. Thus, at every time step a set of parameters, realized from measurements and estimations is used as inputs to evaluate the affine function generated from solving the mpQP. The solution of the affine function evaluated is the MPC solution at the that time step. The bounds on the output variable u and y have been set according to the complex dynamic model simulation results. However the bounds on x are exaggerated since the states of the linear state space model do

not necessarily represent the state of the original system. They bounds on x are also not too large to avoid the explosion of the critical regions. The tuning parameters of the controller is presented in Table 4.1

4.6.9 Closed-Loop Validation and Results

The controller is validated by closing the loop on the controller design. The controller is used on the original complex dynamic model to check if the controller can actually control the system from which it was designed. The validation process involves, calculating the control action from the realized parameters and the mpQP generated affine function. The control action calculated is used as input to the original dynamic model. The output Voltage is measured to and compared with the set-point value as shown in figure 4.15 . This is enabled through gO:MATLAB®, an application that links the gPROMS® with MATLAB®. Figure 4.15 also shows how the flow of NG in the anode and flow of air in the anode changes with changes in current. The power demand is varied by changing the current.

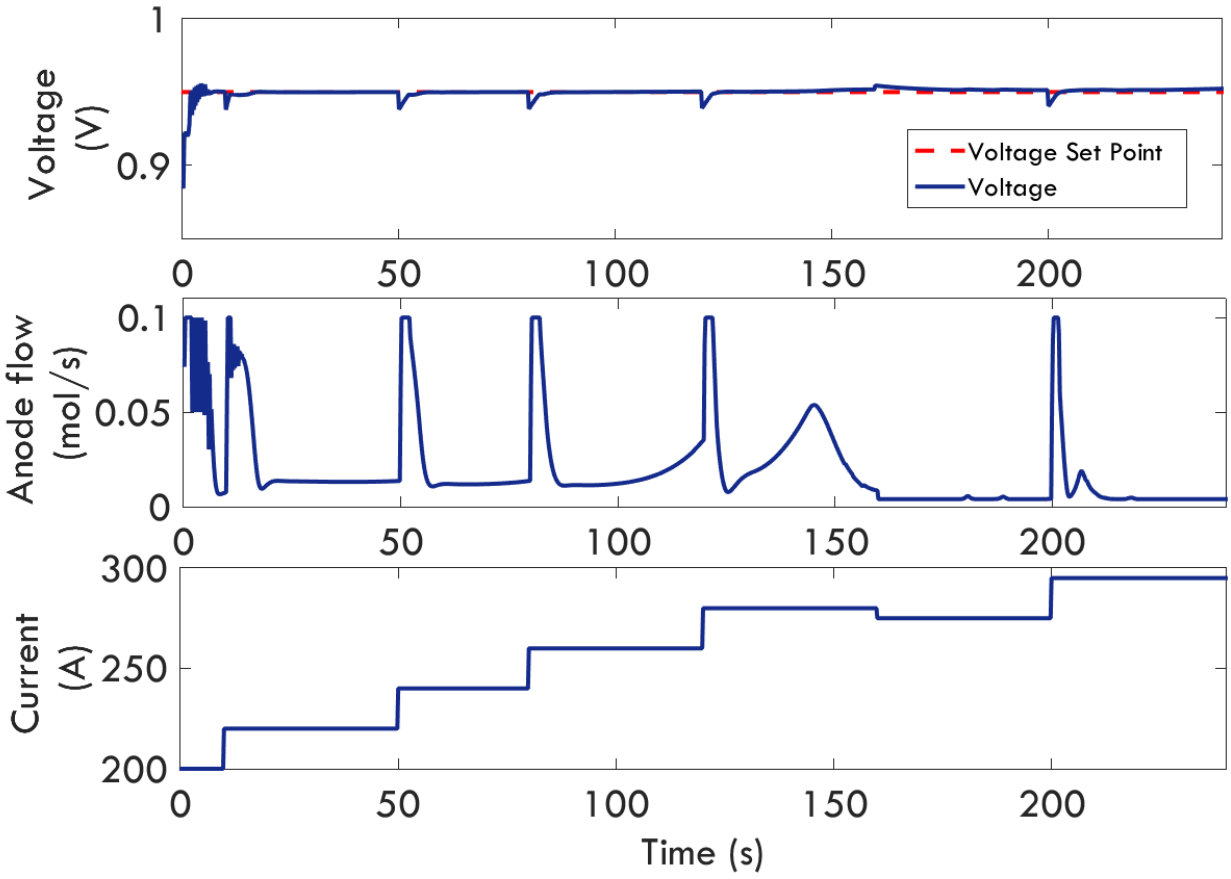

Figure 4.15: Closed-loop validation results of the mpMPC controller showing the voltage set point tracking (top) the anode and cathode flowrate (mid) and the current profile (bottom)

4.7 Conclusion

This work demonstrates the PAROC framework as a smart manufacturing tool that uses high fidelity models to develop optimal control strategy for chemical processes. We developed a complex dynamic model of a hypothetical DIR SOFC to describe the various interactions between the reforming reaction, transport phenomenon and the electrochemical reaction. Using the PAROC framework we designed an multi-parametric model Predictive controller for regulating the voltage of the power generated by the DIR SOFC. The controller was validated with the complex dynamic model. In future work, we intend to explore the how the DIR SOFC compares with other intensified distributed electricity generation unit. An economic analysis of the DIR SOFC and other

auxiliary unit that make up the balance of plant will be essential for benchmarking it with other technologies. Wes also demonstrated the PAROC framework as a smart manufacturing tool for developing optimal control strategy for a novel integrated metal hydride system. For the hydrogen production, we presented a dynamic process model of a PEMWE that describes complex interactions like transport phenomenon, electrochemical reaction, thermodynamics. Using the PAROC framework we designed an multiparametric model Predictive controller for regulating the cell voltage and temperature of the PEMWE system. The controller was tested on the complex dynamic model in a closed loop validation scheme. In future work, we intend to perform experiments on the electrolyzer purchased from Giner Inc. to validate the process model presented in this work. In addition, we will also deploy the control design developed in the this work to the operation of the electrolyzer.

5. PEMWE AND SMHRS LABORATORY SCALE PROTOTYPE DEVELOPMENT AND EXPERIMENTAL VALIDATION[1]

5.1 Synopsis

This Chapter describes the development and operation of two laboratory scale prototypes: smart Proton Exchange Membrane Water Electrolysis (PEMWE) system amd Smart Metal Hydride Refueling System (SMHRS). The high fidelity mathematical models of both systems developed in Chapter 3 is also validated based on which the application of the PARameteric Optimization and Control (PAROC) framework results in the design of an explicit model predictive controller for its efficient operation in in the next Chapter.

[1]Reprinted with the permission from "John Wiley and Sons" from G. S. Ogumerem and E. N. Pistikopoulos, âĂIJParametric optimization and control towards the design of a smart metal hydride refueling system,âĂİ AIChE Journal, 2019.

5.2 Introduction

In the previous chapter we presented the development high fidelity model for a Direct Internal Reforming Solid Oxide Fuel Cell (DIR SOFC), Metal Hydride Hydrogen Storage (MHSS) and Proton Exchange Membrane Water Electrolysis (PEMWE). In this chapter we will describe the experimental validation of some of the models developed in the previous chapter. The model validation step includes (i) the development of a lab-scale prototype (ii) running experiments and (iii) parameter estimation of the model using the data generated from the experiments. The model validation is performed for the PEMWE and the MHSS model only. The rest of the chapter is structured as follows: the next section describes the experimental validation of the MHSS model starting with an introduction into the state of art of hydrogen storage in the commercial landscape. section 5.5 describes the experimental validation of the PEMWE model starting with a brief history of electrolysis.

5.3 Onboard Hydrogen Storage in Fuel Cell Electric Vehicles

A Fuel Cell Electric Vehicle (FCEV) utilizes hydrogen stored onboard to generate electricity to power the electric motor that turns its wheels. Though FCEV does not produce greenhouse during its operation, its driving range is excepted to be up to par with the Internal Combustion Engine Vehicles (ICEVs) which has a median driving range of about 400 miles for light-duty vehicles [65]. while FCEV are known for high fuel economy (60 miles/gasoline gallon equivalent which is 1kg of H_2) they would require about 5 - 7 kgs of hydrogen to travel more than 300 miles without the need for refueling [125, 126]. Hydrogen has a low volumetric energy density and storing 5 - 7 kg of hydrogen onboard is saddled with challenges. There are three main onboard hydrogen storage options; the compressed hydrogen gas storage, the liquid hydrogen storage, and the solid hydrogen storage. The compressed hydrogen storage is considered a feasible option and is currently being used, given that there are already existing matured technologies for handling other gaseous fuels that can be adapted for hydrogen. However, to store 5 - 7 kg of hydrogen onboard, requires a hydrogen density of about 42 kg/m^3 which necessitate a operating pressure of about 10,000 psi at

$15°$C.

The Department of Energy (DOE) has set targets for onboard hydrogen storage , which includes limits on the operating temperature and pressure of the hydrogen storage system, refuel rate (of about 3 - 5 mins) to match the gasoline refueling rate etc[65]. Due to the thermodynamic properties of hydrogen under compression, fast refuel is accompanied with increased operating temperature which becomes an issues because of the materials used for the canisters. The materials used to build the compressed hydrogen canisters for FCEV are selected because of its high strength to weight ratio which enables it to withstand pressure as high as 10,000 psi. However these materials start to degrade when continuously exposed to temperatures above $85°$C or below $-40°$C [65]. To ameliorate this issues, the Society of Automotive Engineers (SAE) developed a fueling protocol J2601 for light-duty FCEVs to enable fast refueling time (3 - 5 mins) for different ranges of hydrogen amount with increasing the temperature of the storage canister above a given threshold [127]. The J2601 fueling protocol is based on a lookup table (LT) strategy that comprises 44 individual tables that specify pressure ramp rates for given combinations of FCEV onboard storage capacities (2 - 4 kg, 4 - 7 kg and 7 - 10 kg), station/hose delivery pressure (10,000 psi and 5,000 psi), station types/fuel delivery temperature ($-40°$C, $-30°$C and $-20°$C), type of vehicle dispenser interface (communication and non-communication) and temperature at the dispenser outlet [126]. The LT strategy is currently used in hydrogen fueling stations. Another refueling strategy that can meet the DOE target and out perform the LT strategy in some cases is the MC-Formula.

The MC-Formula proposed by Kiyoshi el al. [128] at Honda, is a refueling method that uses the same inputs as the LT but instead of the lookup table, uses continuous measurements and numerical equations to calculate the pressure ramp rate in an adaptive control fashion. The MC-Formula method has a substantial fueling time advantages in certain conditions when compared to the lookup table method [126]. Both methods were developed for compressed gas hydrogen storage system.

The solid hydrogen storage option is a plausible option for on-board hydrogen storage especially for more compact or sporty FCEV design. it comprises a canister filled with metal alloys

that reacts with hydrogen to form metal hydride. It has numerous advantages over the compressed hydrogen option but its has a low gravimetric which a material constrain [65, 127]. Research in this area is ongoing and a study done by Sakintuna el al. [64] reviewed the development of metal hydride material for hydrogen storage and a more recent work by Lai et al. [129] reviewed the progress of hydrogen storage material in general. This paper focuses on developing a control strategy similar to the MC-Formula but are optimal. It involves using the PAROC framework to develop an explicit MPC which are embedded into a micro-controller and deployed for the optimal operation of hydrogen storage in a metal hydride storage system (MHSS) to demonstrate its potential to effectively control the metal hydride operation.

5.4 Hydrogen Refueling Process

When activated, metal hydrides are powdery and form a packed bed in a canister. There are two main processes involved in the operation of onboard metal hydride storage system: (1) the filling or hydriding of the metal hydride with hydrogen which is an exothermic process and (2) the discharge or dehyriding of hydrogen from the metal hydride, which is an endothermic process. In both processes, the temperature, the pressure and the hydrogen content are the main variables that determine the state of the metal hydride. The interaction of these variables is characterized by a Pressure Composition Temperature (PCT) isotherm curve. The metal hydride used in this study is the $LaNi_5$. Figure 5.1 shows the isotherm curve for the hydriding and dehydriding process of the particular $LaNi_5$ used in the project. The isotherm curve was generated by the metal hydride supplier (Hydrogen Component Inc) at 25°C.

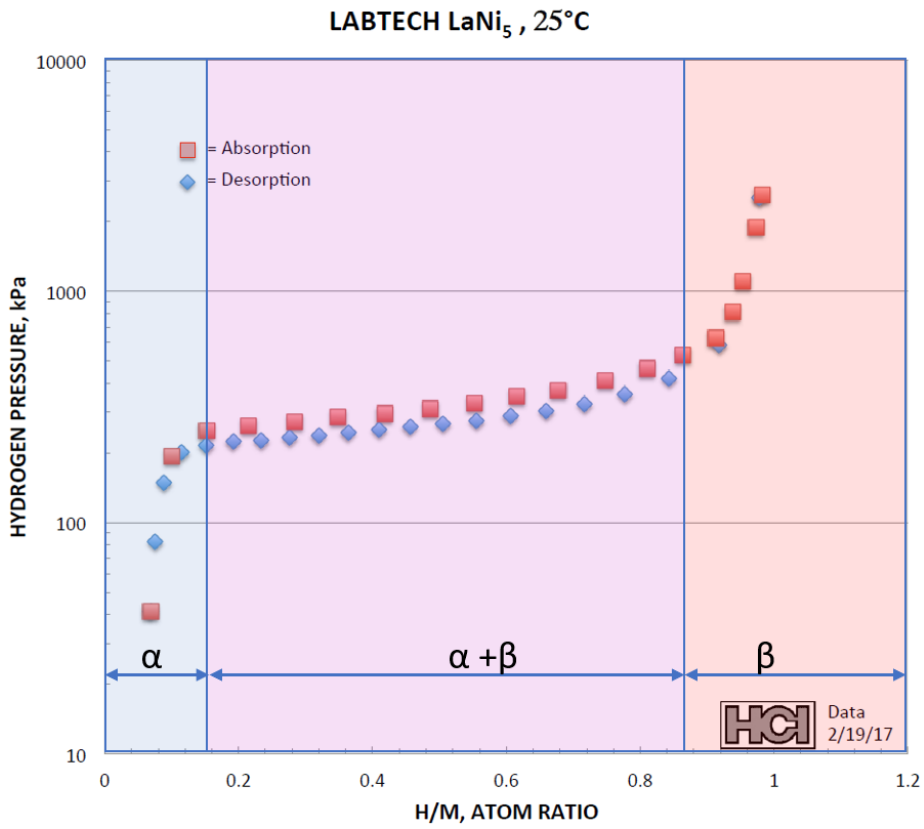

Figure 5.1: P-C-T isotherm for $LaNi_5$ provided by Hydrogen Component Inc.

On a continuum scale, the hydriding and dehydriding process occurs in three phases : the alpha phase, the alpha-beta phase and the beta phase as shown in Figure 5.1. In the alpha phase, the hydrogen adsorbed on the surface, diffuses in the lattice. The hydrogen content of the MH increases mildly with substantial increase in pressure till the plateau pressure region. The plateau is derived from the coexistence of the solid solution (alpha phase) and the hydride (beta phase) and the length of the plateau region determines the amount of hydrogen that can be stored. The beta phase is characterized by the covalent bond formation of the metal complex and hydrogen ion. The Isotherm curve in Figure 5.1 does not depict the pressure-temperature interaction of the $LaNi_5$ which the most important interaction needed in the development of the thermal management strategy. In the work done by Gkanas [130], Figure 5.2 shows the phase diagram of metal hydrides which portrays the thermodynamic interaction of the pressure and temperature. In general, in-

creasing the operating pressure results in an increase in temperature according to the Van't Hoff's equation thus, The hyriding process does not strictly follow the hydriding curve in figure 2.4. To illustrate the thermodynamic interaction, we conducted various experiments which are discussed in Section 5.4.1.1.

In an isothermal condition where the heat generated is efficiently removed, the rate of hydrogen uptake depends largely on the operating pressure. The heat transfer mechanism in a powdery substance is poor thus, creating isothermal condition for onboard MH storage system is infeasible. Moreover, the effective thermal conductivity, which is a combination of the conductivity across the regimes present in the MH bed, is relatively low. The thermal conductivity is a an inherent property of the MH system and a pivotal parameter in the development of a thermal management strategy. The effective heat conductivity of MHs is within 0.1 W/mK which is low compared to that of aluminum which is 204 W/mK. Since the effective conductivity of the MHs is low, the design of the MH Hydrogen storage system should be such that optimizes the heat removal. Effective heat removal in a MHSS is a design problem and a number of studies have suggested design strategies that address this issue [131, 132, 133]. A plausible design approach is an integrated active cooling and heating strategy to improve Hydrogen uptake and discharge. This involves having conducting plates between thin layers of MH bed and running coolant. The thinner the MH bed the better the heat removal but given the required amount of MH for about 5 kg of hydrogen, the size and weight of the MH storage system becomes a major consideration. To address this, a distributed model can be optimized for heat removal given the size and weight constraints [134, 112].

The control challenge in the refilling operation stems from poor thermal conductivity of the activated metal hydrides thus the temperature control add ons such as the cooling jacket are not sufficient to maintain operating temperature of the system within a threshold. Therefore the inlet pressure is also manipulated to control the temperature and they a direct proportional relation. However faster filling operation requires increased pressure which results in high temperature which can cause hot spots and temperature runaways.

5.4.1 Smart Hydrogen Refueling for MH storage in FCEV

The Smart MH Refueling System (SMHRS) is a setup that uses explicit MPC control policies to maintain optimal refueling process. It integrates an explicit MPC with a MH storage system. The smart MH refuel technology is similar to the MC-Formula described earlier in that the control algorithm recalculates the control actions (pressure ramp rat)e using continuous measurement of the filling parameters however, unlike the MC-Formula, SMHRS employs optimization techniques thus the control actions are optimal. Using strategically installed sensors, the SMHRS measures the parameters at every sampling time and calculates the control action from the explicit control policy. The control action will include the filling pressure and the coolant flow rate. In scenarios when hydrogen precooling is not available the SMHRS will also operate at the cost of a longer filling time. A key advantage of the SMHRS is that the control policies are embedded on a chip using the MPC-on-a-chip concept described in section 4.4.6 and can be built into the FCEV refuel system (Figure 5.2). Thus the FCEV will have a built-in control system derived from model based explicit MPC strategy that is unique to the MH material and storage unit design. The current hydrogen gas pumping device in the gas stations are heavily automated to meet the DOE requirements and requires frequent maintenance. With SMHRS a significant part of the automation burden is shifted away from hydrogen gas station pumping device (shown in Figure 5.1) to the FCEV and this enables more sophistication and specialization of the refueling strategy within various FCEV manufacturing companies. The MPC-on-a-chip can also be adopted for currently used compressed gas storage system for optimal solution.

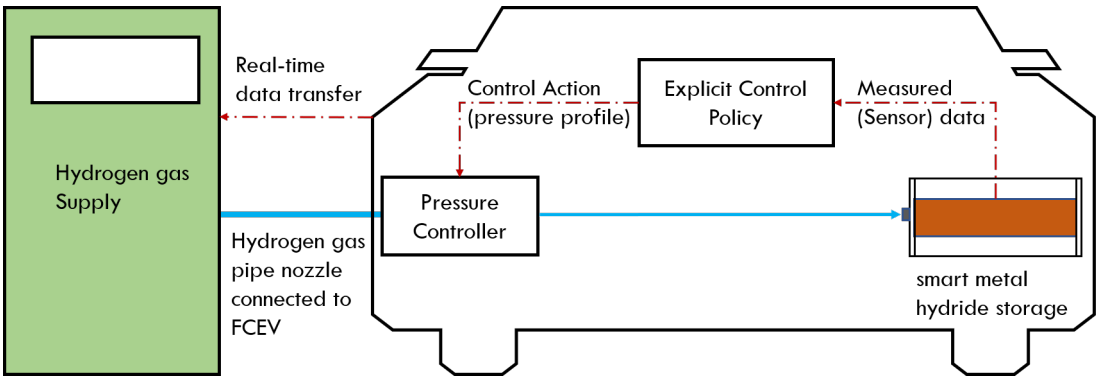

Figure 5.2: Schematic of a refueling operation in SMHRS

The SMHRS is demonstrated using a laboratory scale prototype setup described in the next section. The prototype is intended to replicate the hydrogen filling process in a gas station.

5.4.1.1 SMHRS Experimental Setup

The experimental setup for SMHRS comprises three main units. The primary unit is a jacketed MH reactor or canister referred to as MH pod which represents the FCEV fitted with a MHSS 5.3 . The MH pod is a sealed 563.74 cm^3 volume canister made of stainless steel that contains 488 g of $LaNi_5$ MH capable of storing about 6 grams of hydrogen (Figure 5.3). At the center of the MH pod is a stainless steel filter that prevents any particle from entering the MH bed. As shown in Figure 5.3 the MH pod has three thermocouple inside it; one half-way between the core and the wall and another at the wall on the opposite side. The MH canister is made of stainless steel and was built in collaboration with Hydrogen Component Inc. A water jacket made of acrylic is built around the MH canister (Figure 5.3)to enable temperature control of the MH pod operations. Two thermocouple are connected to the inlet and outlet of the temperature control jacket on the reactor. Water is used as the cooling and heating medium and it is supplied from a temperature controlled water reservoir.

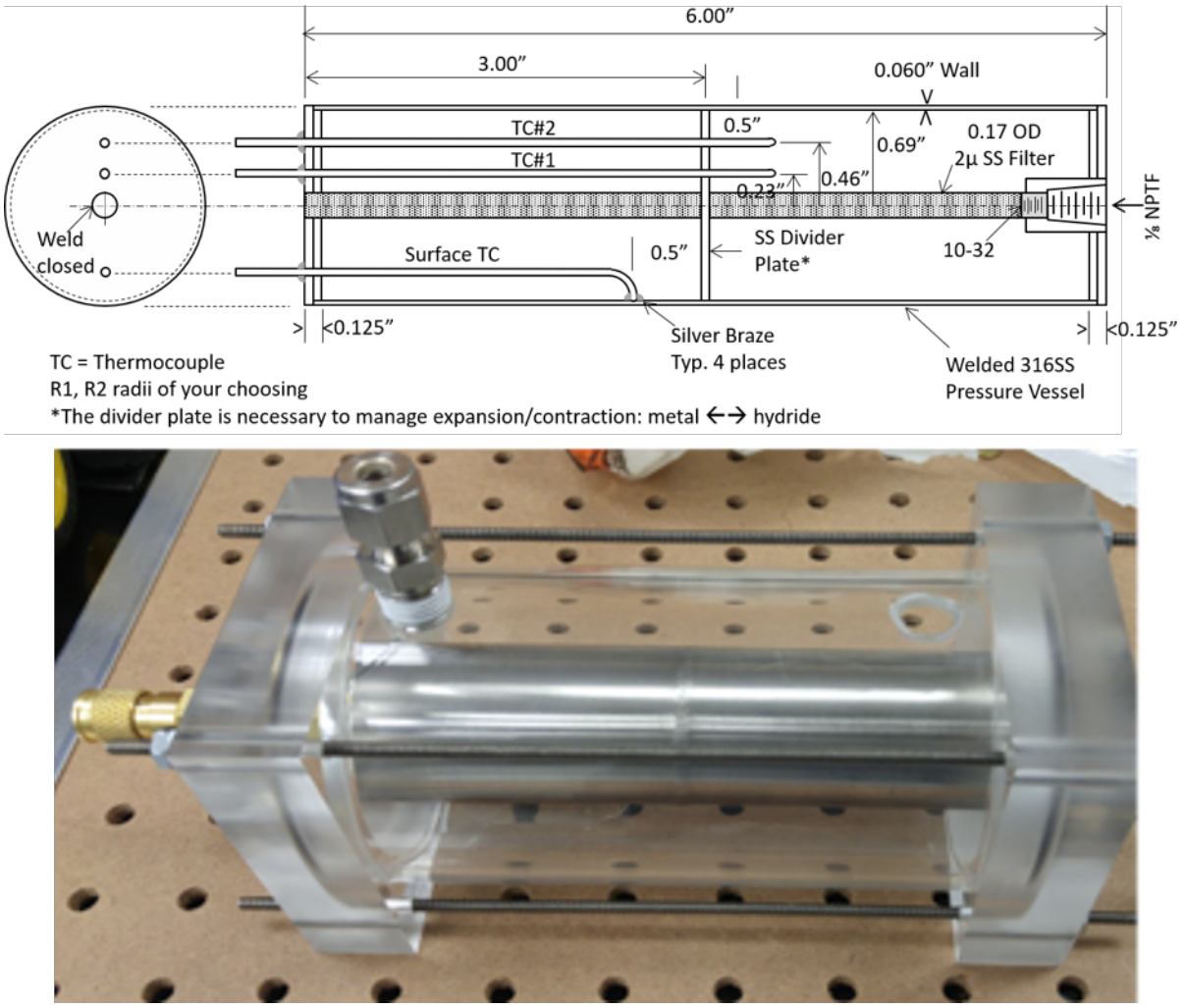

Figure 5.3: Metal hydride pod schematic diagram (top) and image (bottom).

The hydrogen supply unit is another main unit and it comprises a 1700 cm^3 canister (shown in Figure 5.5)fitted with a thermocouple, a pressure transducer and a two stage pressure regulator. The canister is capable of withstanding pressures as high as 2500 psi. It is filled with hydrogen up to 1000 psi from a compressed hydrogen gas cylinder. The pressure regulator is connected to an electronic pressure controller which is connected to a manifold then to the MH pod. The manifold is is fitted with a relief valve, a pressure transducer and a thermocouple.

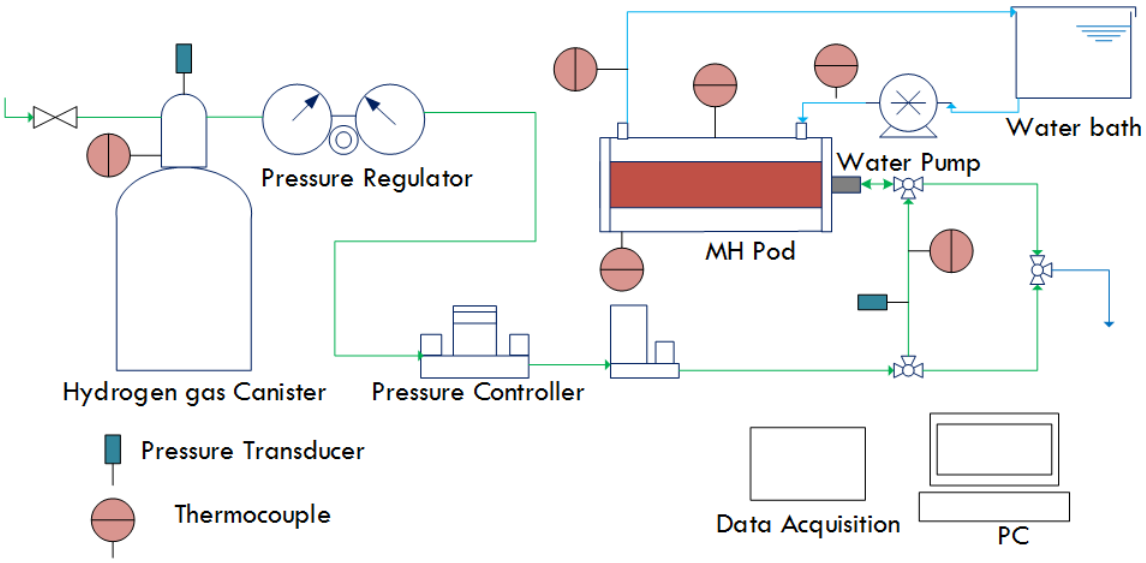

Figure 5.4: Schematic diagram of the experimental setup of SMHRS.

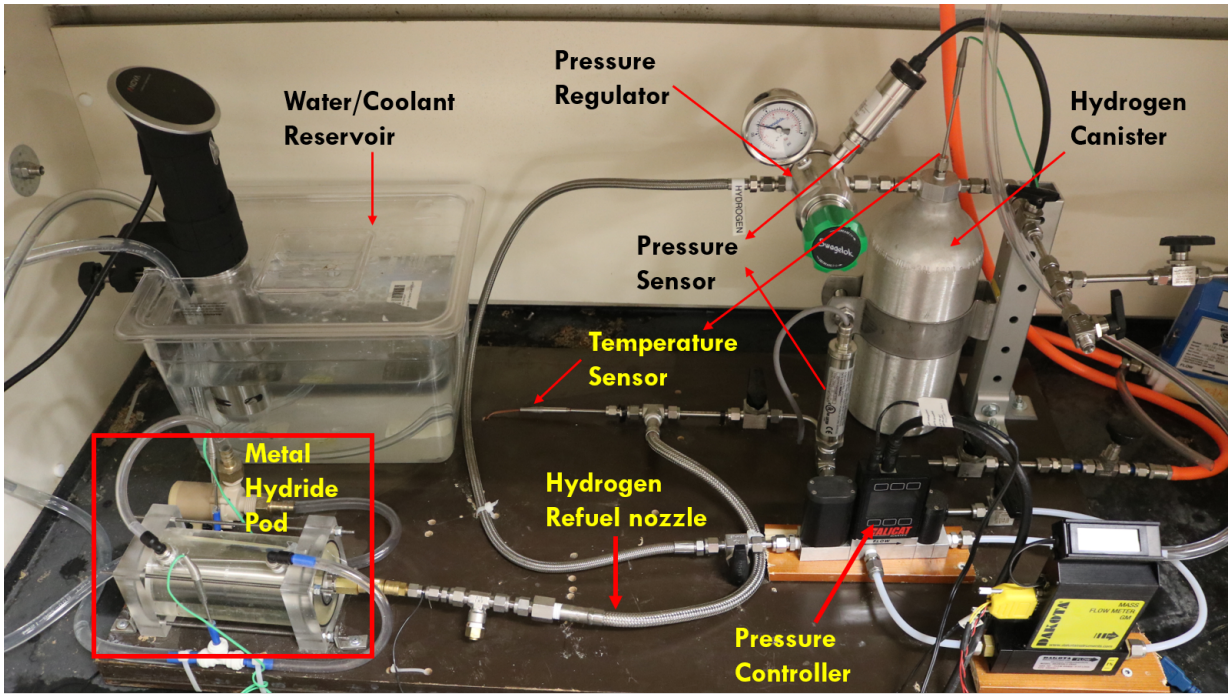

Figure 5.5: Image of the experimental setup of SMHRS.

Another main unit is the power electronics. This is primarily made up of the USB TC from Measurement and Computing (MC) for acquiring the thermocouple data and myRIO from National Instrument for acquiring pressure data and implementing the control policy on the system through the pressure controller and the water pump. The data acquisition (DAQ) systems are connected to a computer for data analysis and visualization.

5.4.1.2 SMHRS Prototype Operation

The experiments are cycles of filling and discharge operations of the MH pod with hydrogen however, the focus of this study is in the filling operation. During the discharge operation, water at 340 K is pumped through the jacket of the MH pod while the pod's outlet valve is open. The discharge operation runs for about 20 mins to ensure most of the hydrogen gas has been discharged. The filling operation is initialized by closing the outlet valve and pumping water at 273 K or 295 K through the jacket to bring the core temperature of the MH pod to the jacket temperature. The goal of the discharge and initialization operation is to bring the MH pod to an initial state where the core temperature is 273 K or 295 K and the MH pod pressure is 14.7 psi. In the initial state, the MH pod has some hydrogen gas in it. In the filling operation, the hydrogen reservoir canister is filled with hydrogen to 1000 psi at 295 K (ambient temperature) and water at a specific temperature is pumped through the jacket at a constant flow rate. The pressure of the inlet is set and the valve is opened. The temperature data are acquired using an MC DAQ system. The hydrogen content in the metal hydride is estimated from the hydrogen that leaves the reservoir which is calculated from the temperature and pressure profile using the gas law. Results of the experiments are presented in Figure 5.6

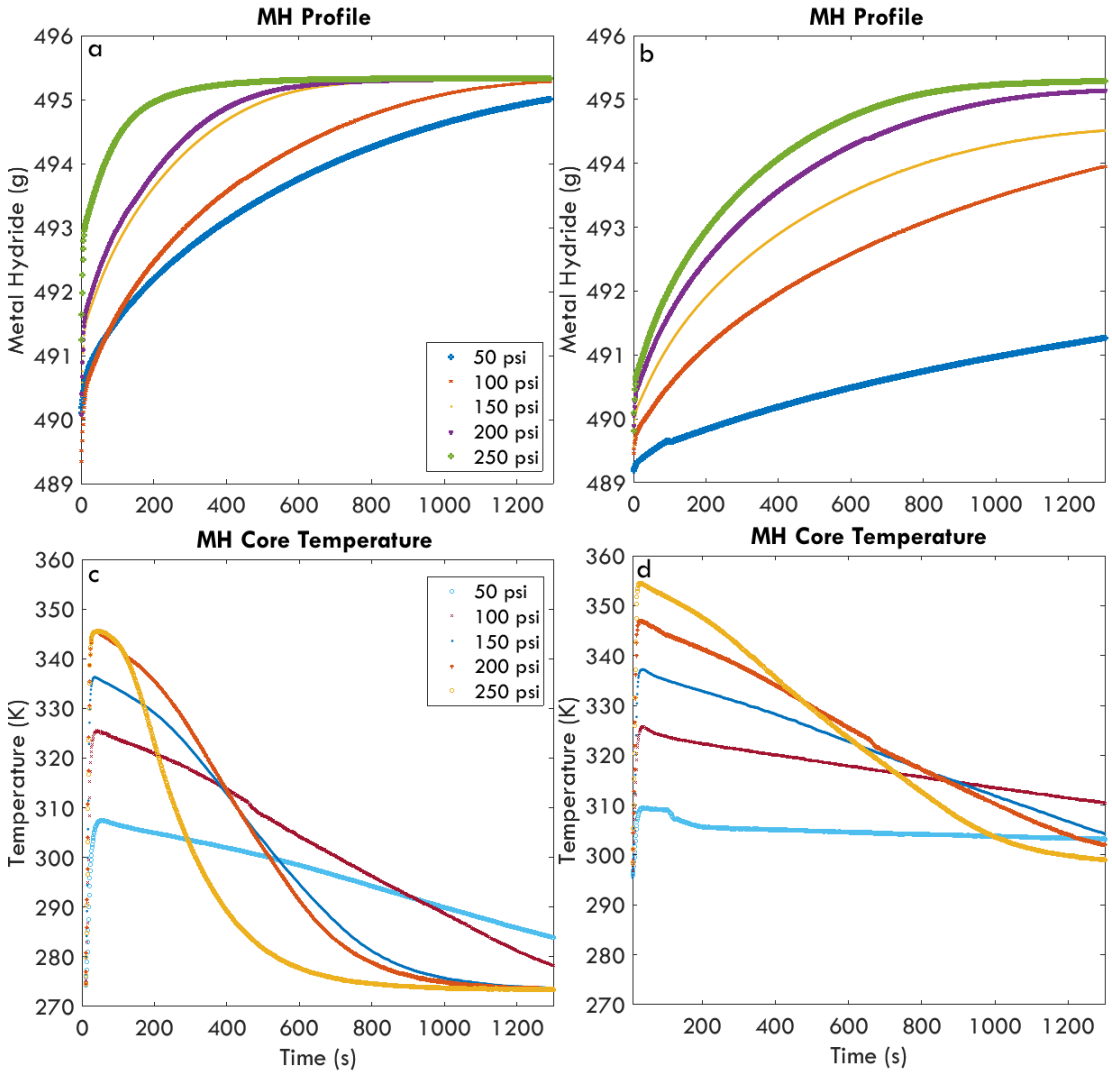

Figure 5.6: (a) MH profiles for five refueling pressure at coolant temperature of 273 K (b) MH profiles for five refueling pressure at coolant temperature of 295 K (c) MH core temperature profile for five refueling pressures at coolant temperature of 273 K and (d) MH core temperature profile for five refueling pressures at coolant temperature of 295 K

Figure 5.6a and 5.6b shows the MH formation profile for five different refill pressures (50 to 250 psi with 50 psi increments) at 273 K and 298 K coolant temperatures respectively. Figure 5.6c and 5.6d shows the corresponding temperature profile for 273 K and 298 K coolant temperatures respectively. In Figure 5.6a and 5.6b, the refueling rate reduces with increasing pressure and also refueling rate increases with decreasing coolant temperature. While in Figure 5.6c and 5.6d, the

temperature increases with increasing pressure and as expected, the heat removal is faster with lower coolant temperature. Thus, there is a faster hydrogen uptake at higher pressure and lower coolant temperature. Notice that at a coolant temperature of 273 K and hydrogen inlet pressure of 250 psi, the MH pod reaches 95% charge (5.7 g of hydrogen) in less than 4 mins and the operating temperature is less than the 85°C set by DOE. With the experiment results, the next step is to develop and validate the high fidelity model.

5.4.2 Parameter Estimation

The relevant measured variable are the operating temperatures of the core and the wall of the MH pod, the temperatures of water at inlet and outlet of the jacket, temperature and pressure of the hydrogen reservoir canister, pressure of the MH pod. A distributed model would have captured different temperature profile at different node but validating a distributed model will require as many thermocouple as the nodes considered which will be more challenging and might result in a marginal improvement in the predictability of the original model. A simplifying assumption is to assume a single temperature profile for the MH pod. The lumped model used in this work make considers the simplifying assumption. The data obtained from the experiment are processed using a filter to remove the noise and outliers. The processed data is then imported in the gPROMS® environment for the parameter estimation. The parameter estimation is done using gPROMS® modelbuilder and the criteria used is the maximum likelihood method [135]. Figure 5.7 shows the results of the parameter estimation.

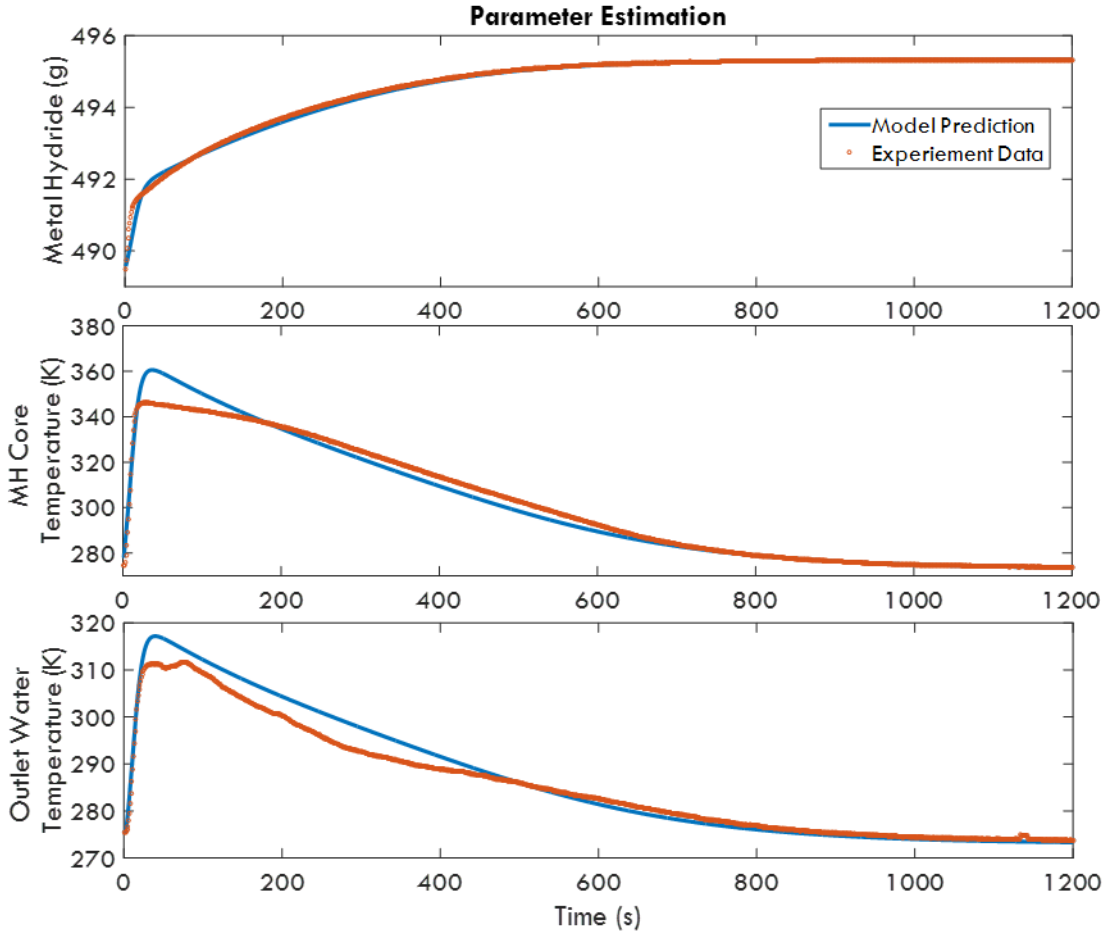

Figure 5.7: Parameter estimation result showing the experimental and predicted profile for the MH evolution (top), MH core temperature (middle), coolant outlet temperature (bottom)

5.5 Water Electrolysis

The electrolysis phenomenon was discovered in by Troostwijk and Diemann in 1789 and in 1800, William Nicholson and Anthony Carlisle applied the electrolysis phenomenon to water splitting. [136, 137] In water electrolysis, a direct electric current (DC) source is connected to two electrodes; a cathode and an anode (typically made from inert metals e.g. platinum, stainless steel or iridium) which are immersed or in contact with an electrolyte. As electrons flow, hydrogen gas is produced at the cathode where electrons enter the electrolyte and oxygen gas is produced at the anode where electrons leave the electrolyte to complete the circuit.

5.5.1 Alkaline Water Electrolysis

Since the electrolysis phenomenon was discovered, there have been tremendous improvements in the design and efficiency of the water electrolysis process. The alkaline water electrolysis (AWE) is the most developed and commercialized water electrolysis technology. The characteristic property of AWE is that it uses a liquid alkaline electrolyte made of a caustic potash solution at concentrations of 20 - 30% KOH. Also, a diaphragm permeable to the hydroxide ion and water molecule is used to keep the product gases separate for efficiency and safety. Though the AWE has been used extensively in the production of hydrogen, it has a low maximum current density which drastically affects the operational cost. Another type of water electrolysis technology is the solid oxide electrolysis.

5.5.2 Solid Oxide Water Electrolysis

The Solid Oxide Water Electrolysis (SOWE) is another type of water electrolysis technology that was first reported in 1985 by W. Donitz and E. Erdle as part of the HotElly project at Dornier System GmbH [138]. The SOWE is characterized by a ceramic electrolyte, high operating temperature and a low operating voltage. The SOWE technology is still under development but research has grown exponentially [136]. It has the potential to be used in large scale hydrogen production in the future if issues with its ceramic electrolyte durability under high operating temperatures are solved.

5.5.3 PEM Water Electrolysis

In the 1960s General Electric developed the first water electrolyzer based on solid polymer electrolyte following a concept idealized by Grubb [139, 140]. This technology became the Proton Exchange Membrane Water Electrolysis (PEMWE). The PEMWE has gained attention due to its advantages over other water electrolysis technologies [136]. It is characterized by a solid sulfonated polymer membrane (eg Nafion, fumapem) which has a high proton conductivity, low product gas crossover, compact system design and high-pressure operation. It can be operated at relatively high current density which reduces its operating cost. Also, unlike the AWE, the

PEMWE can operate below 30% of its nominal operating capacity.

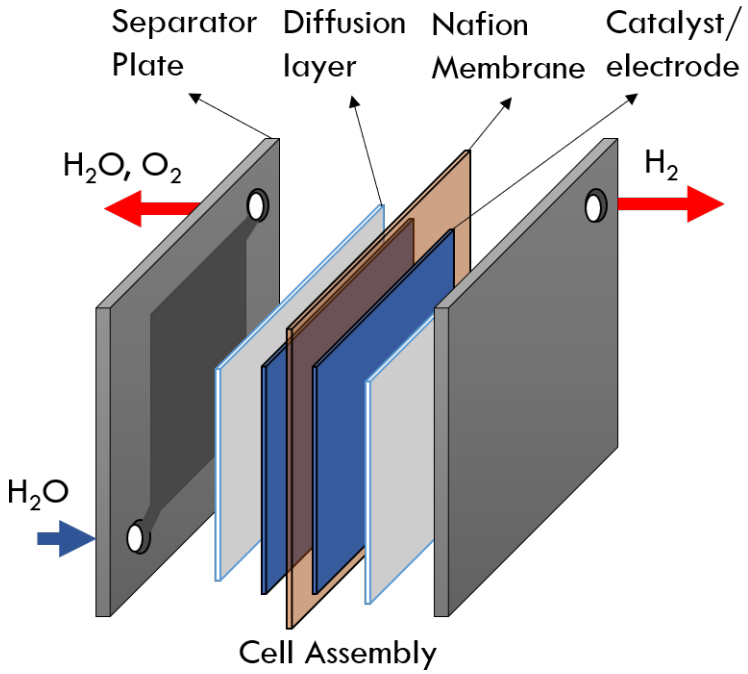

Figure 5.8: Exploded view of a PEMWE cell.

The solid sulfonated polymer membrane are thin and they make a compact system design with structural properties that can maintain high operational pressure. PEM Water Electrolyzers (PEMWE) are made up of electrolysis cell stacked together. Each cell is made up of separator plates with grooves or water channels, and a membrane electrode assembly (MEA) as shown in 5.8. The MEA is made up of a current collector, diffusion layers and a catalyst coated membrane.

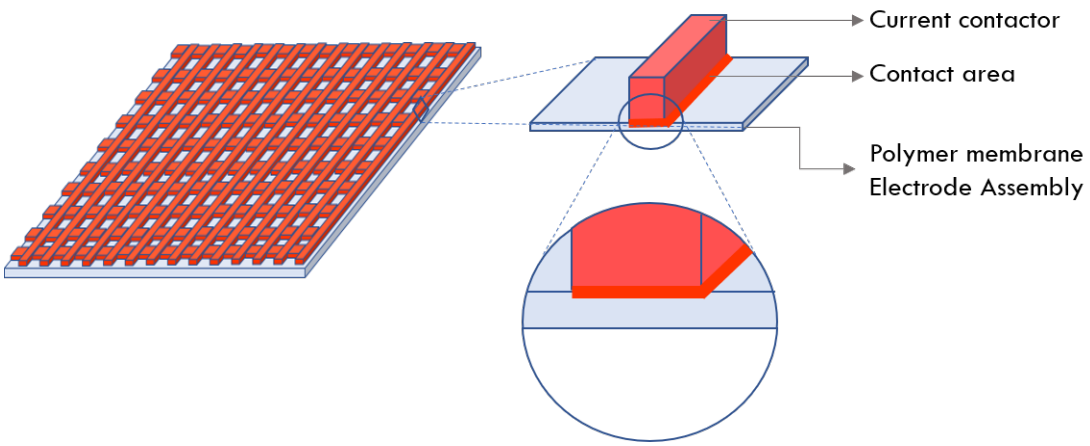

Figure 5.9: Schematic showing the placement of the current contactor and the membrane

Though the water electrolysis reaction is endothermic heat is generated in the process. The heat generated is attributed to the joule heating effect. Joule heating or Ohmic heating is the process where by the passage of electric current through a conductor produces heat. The heat generated is proportional to the current supplied and the resistance of the material. In the PEMWE, the current contactor is a conductor through which current is supplied to the membrane electrode assembly (MEA). Figure 5.9 shows the placement of the current contactor (usually made of Ti) with the polymer membrane. During the operation of the PEMWE, heat is generated in the current contactor due to joule heating and the area of the membrane in contact with the current contactor will be at the same temperature with the current contactor. Though cell interior of the PEMWE is flooded with water the area of the membrane pressed on the current contactor is still exposed to localized higher temperatures making it more susceptible to degradation. Thus, it is important to estimate the stack temperature and the heat generation rate. The temperature of the outlet water is used to estimate the temperature in the stack however the change in water temperature across the stack is a more appropriate parameter to estimate the heat generation in the PEMWE. As expected, increasing the current supplied will increase the heat generated in the PEMWE. Results from the experiment presented in Section 5.6 also demonstrates this phenomenon. Though the PEMWE is known for it dynamic nature, a steep increase in hydrogen production (or current supply) will rapidly increase

the heat generation and thus the operating temperature which will have a devastating effect of the stability and durability of the membrane. In an operating manual for the G5 PEMWE series, Giner Inc recommends that the differential water temperature across the stack be maintained below 5°C [141]. Controlling the differential water temperature across the electrolyzer will drastically reduce the devastating effect of prolonged exposure of the membrane to higher temperature. Thus, it is important to develop a thermal management strategy for the operation of the PENWE.

5.6 PEMWE Lab-scale Experimental Setup

The operation of an electrolyzer required other peripheral devices or units that make the balance of plant. These units are used to (i) purifies or deionizes the water used to prevent the deativation of active catalyst cites, (ii) pump the water through the system, (iii) acquires and analyzes data etc. Figure 5.10 shows the essential units that make up PEMWE plant or prototype. The lab-scale prototype used in the experiment was design and built from scratch.

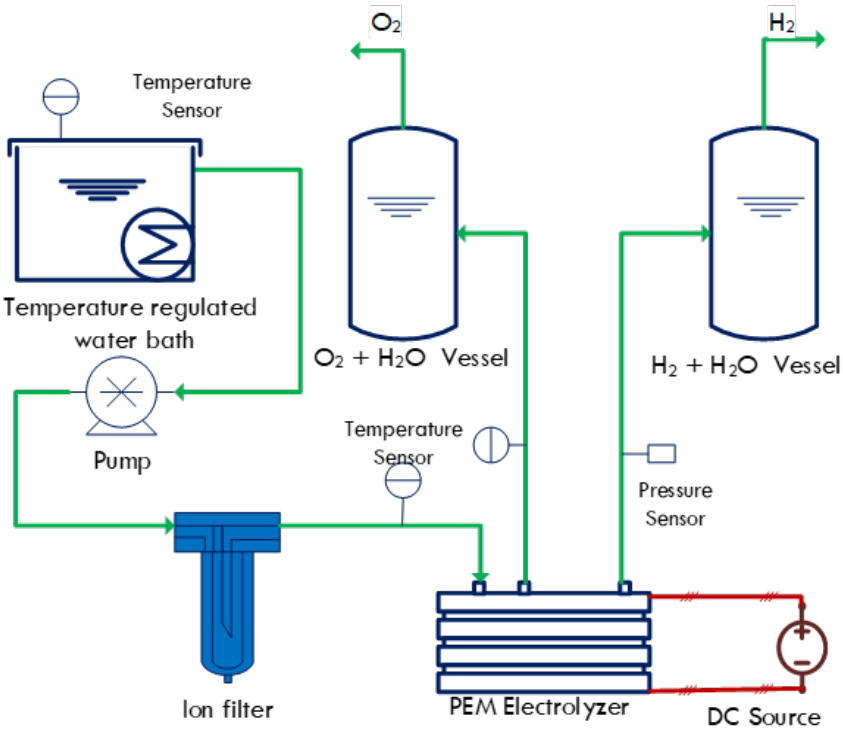

Figure 5.10: Schematic of PEMWE prototype.

5.6.1 Experimental Setup

The experimental setup consists of four main units: (1) the water supply, (2) the electrolyzer, (3) the power supply and (4) the data acquisition and control unit. The water supply unit includes a temperature regulated water bath. The temperature in the water bath is regulated by a device from Anova that has a heating coil, a stirrer and a temperature control system. The device is inserted into the water bath and used to increase the operating temperature of the water when needed. The heating coil heats up the water while the stirrer is used to distribute the water to maintain a uniform temperature in the bath. The temperature control system in the Anova device allows a temperature setpoint to be inputed by the user. An immersible pump is placed inside the water bath and used to channel the water to the filter. The filter is made up of a cartridge housing and a 20" cartridge deionizer able to maintain the filtrate at >14 million ohms. The conductivity of water filtrate is measured using a conductivity meter to maintain the integrity of the electrolyzer.

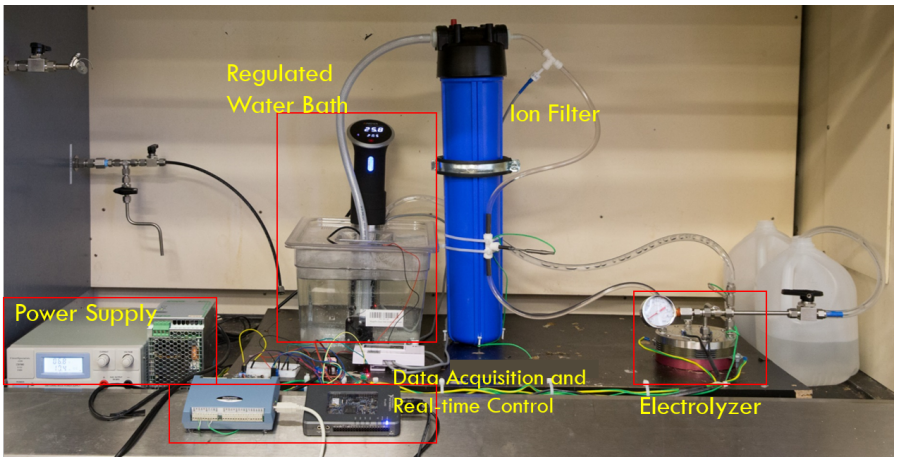

Figure 5.11: Image of the lab-scale PEMWE prototype.

The water filtrate is channeled to the electrolyzer where the reaction takes place to produce hydrogen and oxygen and unreacted water. Oxygen and the unreacted water is channeled back to the water reservoir where oxygen is vented and the water is recycled. Hydrogen leaves the cathode

Table 5.1: G5 PEM Electrolyzer Specifications

Characteristics	**Specification**
Number of cells	4 cells
Active area	50 cm^2
Operating pressure	0 - 20.7 bar(0 - 300 psig)
Operating temperature	278 - 313 K
Current (I)	15 - 60 Amp
Water quality	$>$ 10MΩ-cm, TOC $<$ 30 ppb
Water flowrate	100 - 500 mL/min/cell
Max O_2 & and H_2 Production (At max I)	1,192 mg/min & 149.2 mg/min

and is vented. During the operation of the PEMWE water accumulates in the cathode over time and flows out with the hydrogen. Temperature sensors are installed at the inlet and outlet of the electrolyzer. The electrolyzer used for the prototype in figure 5.11 is a G series Giner electrolyzer and its specifications are given in table 5.1.

Power is supplied to the electrolyzer using a current control device from CircuitSpecialists. The current is set on the power supply device which directly translates to the hydrogen production rate. As discussed in section 4.6.5 the actual voltage is made up of the reversible voltage, ohmic overpotential and the activation overpotential. The power supply device shows the voltage reading but to only one decimal place approximation, which is not suitable for the our for our application.

The current and voltage supplied are measure using sensors. The current is measured using a ACS712 current sensor with a total output error of 1.5% at 25^0C while the voltage is measured using an arduino voltage sensor with an accuracy of + 40mV. The data from the thermocouples are retrieved using a data acquisition device (USB TC) from Measurement and Computing (MC) while the voltage and current sensors are acquired using the myRIO-1900 from National Instrument (NI). The NI myRIO-1900 is a portable reconfigurable input/output device used to acquire sensor data and also used to implement the real-time control actions.

The various sub unit described above are connected to form a the PEMWE prototype. The prototype is operated within the safe bounds of the G5 electrolyzer according to the operating manual [141] and the ion filter unit. A key operating requirement for the electrolyzer is to maintain the

temperature difference (ΔT) across the electrolyzer below a certain threshold. The ΔT across the electrolyzer is an indication of the rate of heat generation within the electrolyzer. Since the heat is generated as a result of current flow through the metal plates in the electrolyzer unit (joule heating), the part of the membrane in contact with the metal plate is exposed to scorching or deformation if the temperature is not controlled. The deformation may result in product gas crossover to form an explosive mix which jeopardizes safety and durability of the system. Also during the operation of the PEMWE prototype described, there is an expected increase in the operating temperature since the water used is recycled. Recycling the water is a more efficient way to manage the ion filtration process since the ion loading in the water per pass through the electrolyzer is negligible compared to those in the tap water. Most of the heat generated in the electrolyzer is lost to the water which recirculates through uninsulated channels. The heat in the water is lost to the environment through radiation and the rate of heat loss is determined by the temperature gradient (of the outlet water and the ambient temperature) and the magnitude is determined by the residence time (before it reenters the electrolyzer).

During the operation of the PEMWE, the current is set using the knob in the power supply unit. The current or electron flow translates to the hydrogen or oxygen production rate. However increasing the current increases the rate of heat generation from the unit. The generated from the unit is removed by the water flowing through the unit. Thus water is not just a reactant but also a temperature control agent. The flowrate of water is used to regulate the temperature of the unit. Figure 5.12 show the sensitivity of the temperature and cell voltage of the electrolyzer unit to changes in current and water flowrate. Also the effect of the temperature change to the cell voltage. The data from the experiments are used to validate the high fidelity model developed in section 4.6.1

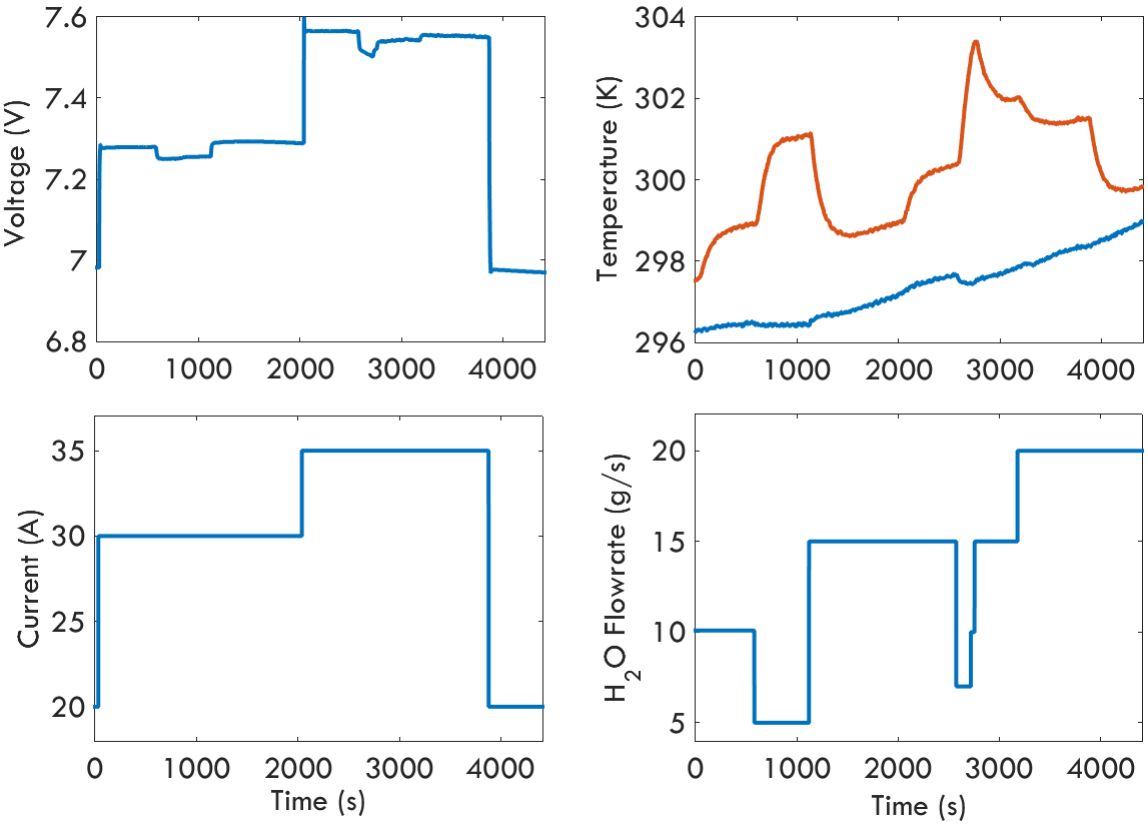

Figure 5.12: Experimental data showing the effect of current change (bottom left) and water flowrate changes (bottom right) on stack voltage (top left) and temperature (top right).

Equations 5.1 and 5.2 describe the empirical relation of the voltage applied to the pump and the water flow rate downstream of the filter. The control mechanism sends Pulse Width Modulation (PWM) signals to the pump driver and it is translated to the voltage.

$$V_{pump} = 8.8567 Z_{PWM} + 1.3829 \tag{5.1}$$

$$\dot{m}_{\mathrm{H_2O}}^{in,an} = 2.4882 V_{pump} - 6.2772 \tag{5.2}$$

Where V_{pump} and Z_{PWM} are the voltage and pulse width modulation values sent to the pump. $\dot{m}_{\mathrm{H_2O}}^{in,an}$ is the flowrate of water

5.6.1.1 Parameter Estimation

A parameter estimation step is needed to tailor the HF model to the lab scale PEMWE prototype. Data from the experiment is used to validate the model in gPROMS®. During the data generation, inputs such as flowrate and current are varied and the corresponding output dynamics are captured. The data generated is loaded into gPROMS® experiment module for the parameter estimation. gPROMS® uses the maximum likelihood estimation (MLE) technique, and its main objective is to find estimates of the model parameters such that the probability of the sample is as great as possible. Unlike the least square estimation (LSE) method an initial set of parameters must be chosen to begin the model fitting.

Two parameter estimation procedure were performed. The first one which is on the polarization curve (shown in figure 5.13) is aimed at capturing the electrochemical interactions involved in the splitting water in the Giner electrolyzer. The polarization curve parameter estimation is implemented in a steady state fashion. The optimal parameters generated from estimating the polarization curve is used in the original model. With the parameters for the electrochemistry part fixed, a second parameter estimation is performed to determine the optimal parameters for other parts of the model that describes various phenomena such the energy balance, the hydrogen ion transport through the membrane etc. The second parameter estimation is implemented in a dynamic fashion and figure 5.14 shows the result.

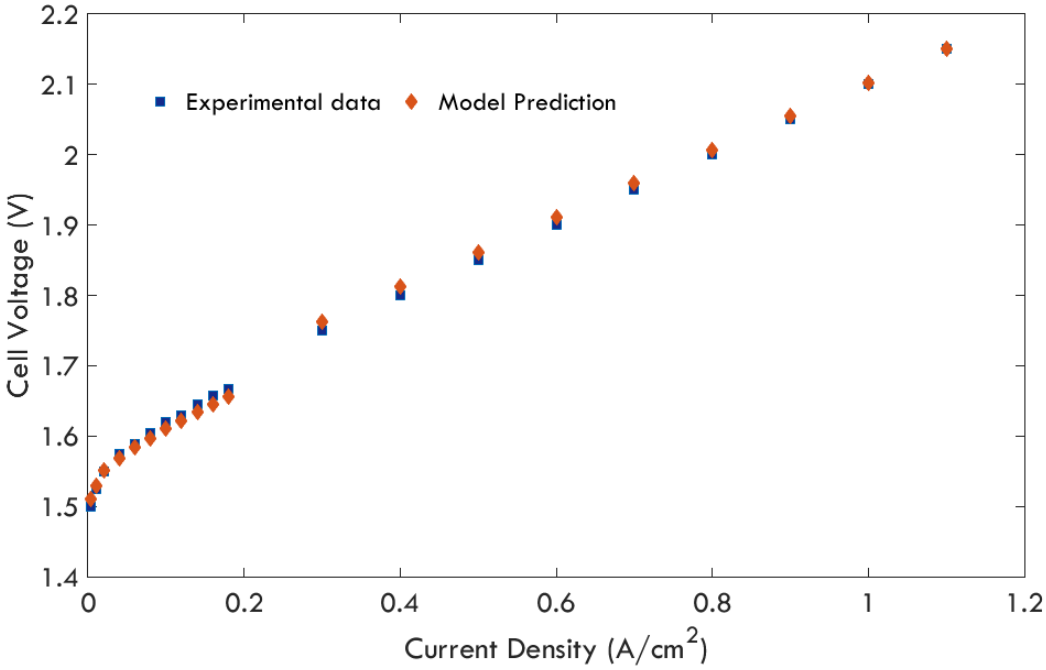

Figure 5.13: Parameter estimation results of the polarization curve.

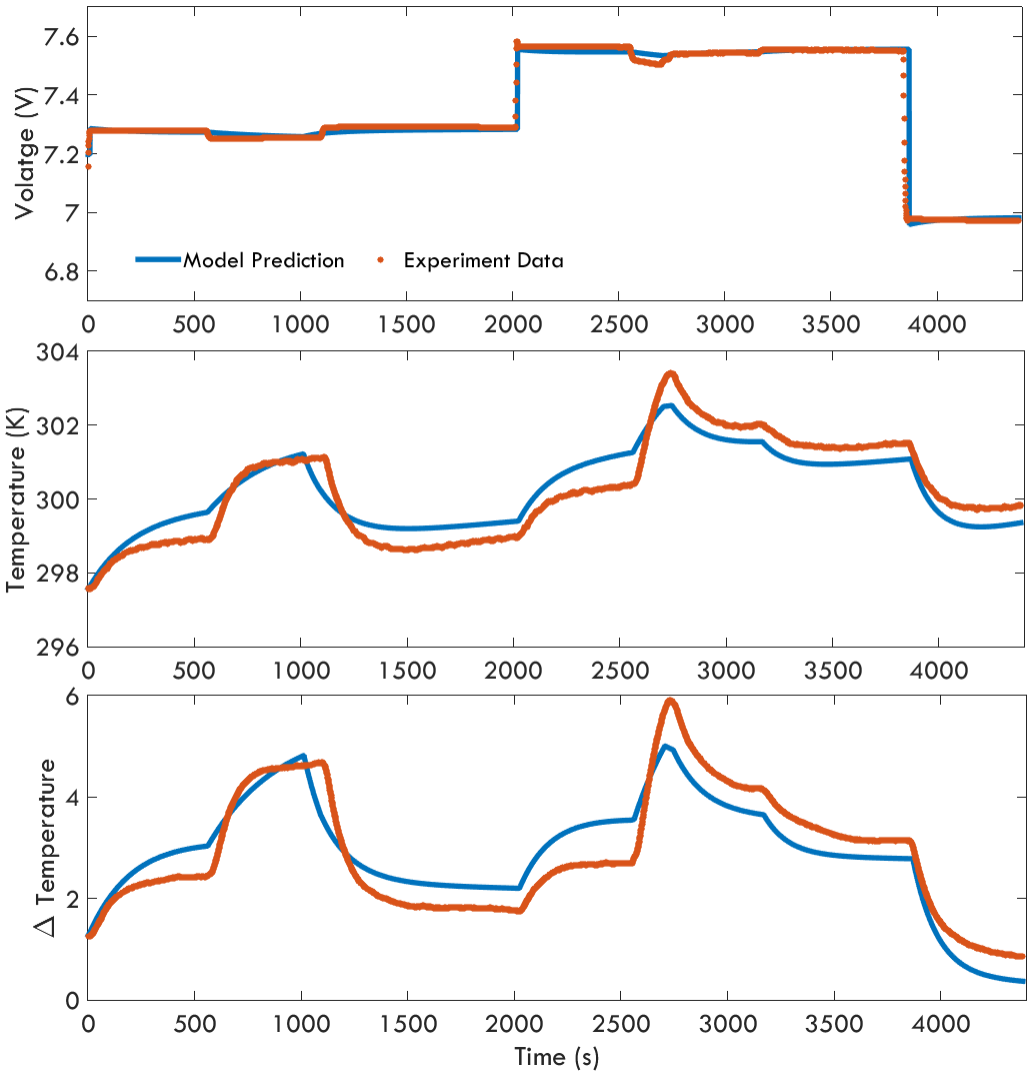

Figure 5.14: Parameter estimation results for the HF model (a) voltage (b) outlet temperature (c) ΔT.

With the digital twin developed, the next step in obtaining the receding horizon optimal polices for PEWME using the PAROC framework is the reduction of the HF model to an approximate model.

5.7 Conclusion

In this chapter we described the prototypes for the PEMWE system and the SMHR system. The PEMWE system consisted of a water ionization process (with a pump as the water mover), the

electrolyzer for splitting water into hydrogen and water with electrical energy from a power supply system and the data acquisition system/ control system. Temperature, voltage and current sensors are installed at strategic points to capture the data needed to validate model. The SMRH system is made up of two hydrogen storage units. One of the storage is a 1.7 liter volume canister that holds hydrogen at 1000 psi which represents the hydrogen gas dispenser at the gas station and the other hydrogen storage unit is a canister with metal hydride in it and represents the a storage unit in a fuel cell electric vehicle. The SMRH system also has a multiple senors strategically placed and a data acquisition/control system.

The parameter estimation results for both prototype system was performed in gPROMS and the resultant model (validated model) shows good agreement with the experimental data. The validated model are used to develop the controller that will be deployed to the prototype for the real-time demonstration of the application of eMPC to the prototypes.

6. SMART OPERATION OF THE PEMWE AND MHRS LABORATORY SCALE PROTOTYPES[1]

6.1 Synopsis

The last two Chapters discussed the development of explicit MPC feedback control design strategies and the design and fabrication of two laboratory scale prototypes. This Chapter looks at the integration of the explicit MPC feedback control strategy into the prototype systems to creates a smart metal hydride storage technology that can be deployed for on-board hydrogen storage in an FCEV and a smart PEM water electrolysis system. The results obtained from the real-time implementation of the explicit feedback law demonstrates an effective thermal management of both systems.

[1]Reprinted with the permission from “John Wiley and Sons" from - G. S. Ogumerem and E. N. Pistikopoulos, âĂIJParametric optimization and control towards the design of a smart metal hydride refueling system,âĂİ AIChE Journal, 2019.

6.2 Introduction

In the last three decades, Model Predictive Control (MPC) methods have become a popular and highly sought after control design method for the process industry [2]. Variants of the MPC methods has been built into several software packages (eg. Dynamics Matrix Control) that enables its deployment to process manufacturing systems [142, 32]. An online application of MPC involves solving a finite horizon, discrete-time, constrained, optimization problem on-line, recursively when the state of the system becomes available at every sampling time. The solution obtained is a sequence of optimal control actions. The duration of the time step used in the MPC design takes into consideration; the time constant of the system, the sampling rate and the time it takes to solve the optimization problem. MPC gained its popularity mainly due the simplicity of its concept and its ability to effectively handle complex problems with hard constraints and multiple variables that interact. Also, logical conditions for the process operation can be incorporated into the open-loop optimization and phenomena such as time delays and inverse responses can be effectively captured by the scheme.

Although the use of MPC within the process industries has been extensive, existing MPC strategies have limitations in its application. They require solving an optimization problem at every sampling time, which largely confines its application to systems with relatively slower dynamics. Secondly, the control policy is implicit since it must be obtained by solving the optimization problem. Thus, there are no close loop analysis of the control policy which is needed to gain insight on features such as stability and good initial conditions. Thirdly, due to their computational complexity, MPC control application requires control hardware and software that have the ability to not only set up the optimal control problem but also embed the optimization solvers. Devices with such computational ability are not cheap.

The aforementioned limitation of the MPC can be addressed by explicit MPC also referred to as multi-parametric Model Predictive Control (mpMPC) [71]. In explicit MPC, the original MPC formulation is reformulated into a multi-parametric programming problem which enables the optimization problem to be solved once and off-line. The solution obtained from solving the

parametric programming problem off-line is a set of piece-wise affine (PWA) functions of the parameters (states measured at the sampling time), defining respective polyhedral critical region. Thus, instead of solving an optimization problem at every sampling time to obtain the control policies, in an explicit MPC, the control policies are obtained from function evaluation of the PWA functions. With the PWA there is an explicit relation between the control actions and the parameters or states of the system, which enables a closed-loop analysis of the control design. Also, it is relatively easier and less expensive to embed and implement the explicit MPC strategies on a control hardware than it is embedding the MPC strategies which necessitates a solver.

Though the implementation of explicit MPC generally has a lower computational expense when compared to the original MPC formulation, there could be an explosion of critical regions that will potentially increase the computational expense of implementing the explicit MPC. The computational burden in implementing the explicit MPC feedback law is mainly in identifying the critical region for the parameter vector realized at every sampling time. While it is possible to exhaustively enumerate all the polytopes to find the region with the parameter vector, it maybe computationally expensive for systems with larger number of critical regions. Larger number of critical regions also creates the issue of storage space. The benefits of implementing the explicit MPC instead of the original MPC will in most cases outweighs the implementation expense. [103] reviewed some of the techniques proposed by various researchers in the field to address issues with the explicit MPC implementation. The computational burden in implementing the explicit MPC feedback law is mainly in identifying the critical region for the parameter vector realized at every sampling time. While it is possible to exhaustively enumerate all the polytopes to find the region with the parameter vector, it maybe computationally expensive for systems with larger number of critical regions. The goal is to use an efficient amount of computational expense and storage space. There are various options available and they defer in search structure [143, 144] or control action evaluation or in the ability to compromise optimality for a simpler implementation [103]. A simple and common approach is the sequential search. The sequential search procedure also requires looping through the critical regions to identify the polytope where the parameter vector lies at every sampling time

as described by the point location algorithm 6.2 below (defined in POP [101]).

There has been substantial progress in the development and *in silico* application of explicit MPC [105, 33, 102], but very few researcher have implemented a real-time explicit MPC [103, 104, 145]. The work of [104] actually embedded the explicit MPC feedback law into an Arduino and used it in a reference-governor set-up to control a magnetic levitation system. This Chapter describes the real-time implementation of the explicit MPC on two chemical prototypes described in chapter 4.

6.3 Embedding the Multi-parametric Programming Solution

The real-time application setup of the controller is done in LabVIEW®. The device used to implement the on-line evaluation is the National Instrument portable reconfigurable I/O (RIO) device myRIO-1900. It uses a Xilinx Z-7010 dual core Processor, (FPGA type) with speeds of 667 MHz and RAM of 256 MB.

The POP toolbox in MATLAB is used to solve the multi-parametric programming problem and the solutions are given in a structured form in MATLAB. The process of embedding the solution into the myRIO device in shown in figure 6.1. The mpP solution obtained is of the form $\mathbf{u} = f(\theta)$ mapping the parameters θ to a sequence of control actions $\mathbf{u}$. $f(\theta)$ is a piece-wise affine function of the uncertain parameters as shown below .

$$f(\theta) = \begin{cases} a_1\theta + b_1 & \text{if } \theta \in \mathbf{CR}_1; \\ \vdots & \vdots \\ a_m\theta + b_m & \text{if } \theta \in \mathbf{CR}_m. \end{cases} \tag{6.1}$$

where $\mathbf{CR}_i = \{\theta \in \mathbb{R}^q | \mathbf{Z}_i\theta \leq \mathbf{z}_i\}, \quad i = 1, ..., N_m$ are polyhedral critical regions which are half-spaces defined with $\mathbf{Z}_i \in \mathbb{R}^{c \times d}$ and $\mathbf{z}_i \in \mathbb{R}^c$. $\mathbf{a}_i \in \mathbb{R}^{Nx \times d}$ and $\mathbf{b}_i \in \mathbb{R}^{Nx}$ are gains of the affine function that define the control action sequence. N_m is the number of critical regions.

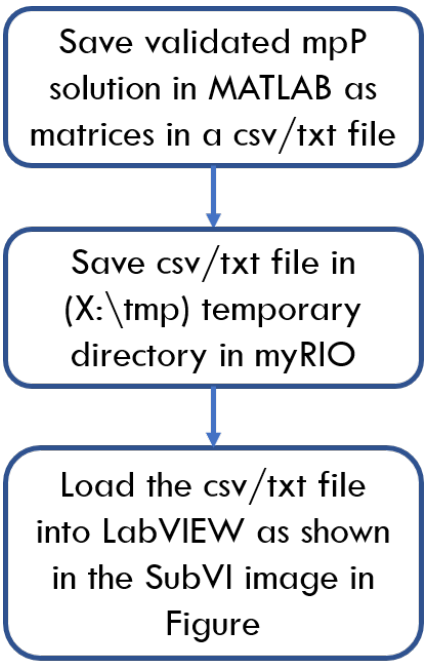

Figure 6.1: Flowchart for embedding the solution matrices into the myRIO Device

The following sets of matrices contained in the solution $\{\mathbf{Z}_i, \mathbf{z}_i, \mathbf{a}_i, \mathbf{b}_i\} \quad i = 1, ..., N_m$ are saved in a csv or text file format and the file is saved in the myRIO device. A LabVIEW VI is used to retrieve the data from the file and structure the data into matrices that LabVIEW mathscript can handle.

6.4 Real-Time mpMPC Implementation

When the controller is turned on, the implementation procedure for receding horizon policy follows the the flow chart in figure 6.2. At every sampling time, the parameter vector is realized and a search is conducted to identify the critical region where the parameter vector lies. When the critical region is identified, the affine function for the critical region is used to calculate the control actions. The control actions are sent to the actuators in the system to be implemented. This process repeats every sampling time. A more detailed description is given below.

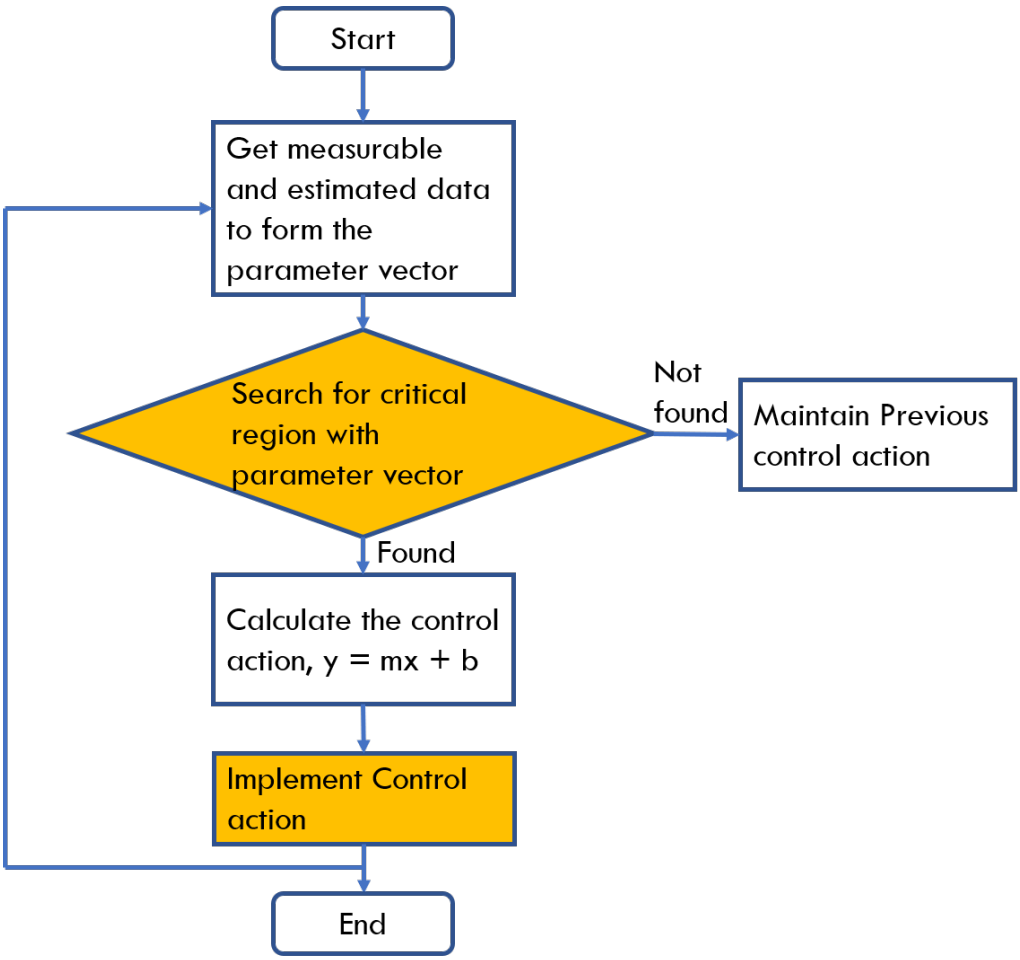

Figure 6.2: Flowchart for implementing real-time explicit MPC

6.4.1 Parameter vector

The parameters that make up the parameter vector are either measurable or unmeasurable variable. They include the pseudo-states, the output, the setpoint and the previous/initial input. Figure 6.3 shows the control configuration (in LabVIEW) for hydrogen storage in a metal hydride pod. The measurable variables are retrieved from the DAQ system during the sampling time and assigned to the networked variables as shown in Figure 6.3. The unmeasurable variables are estimated, either with a Kalman filter or a validated high fidelity model. The estimation step or procedure also requires sensor data from the DAQ system. As shown in Figure 6.3 all the variables that make the parameter vector are sent to the mpP solution subVI

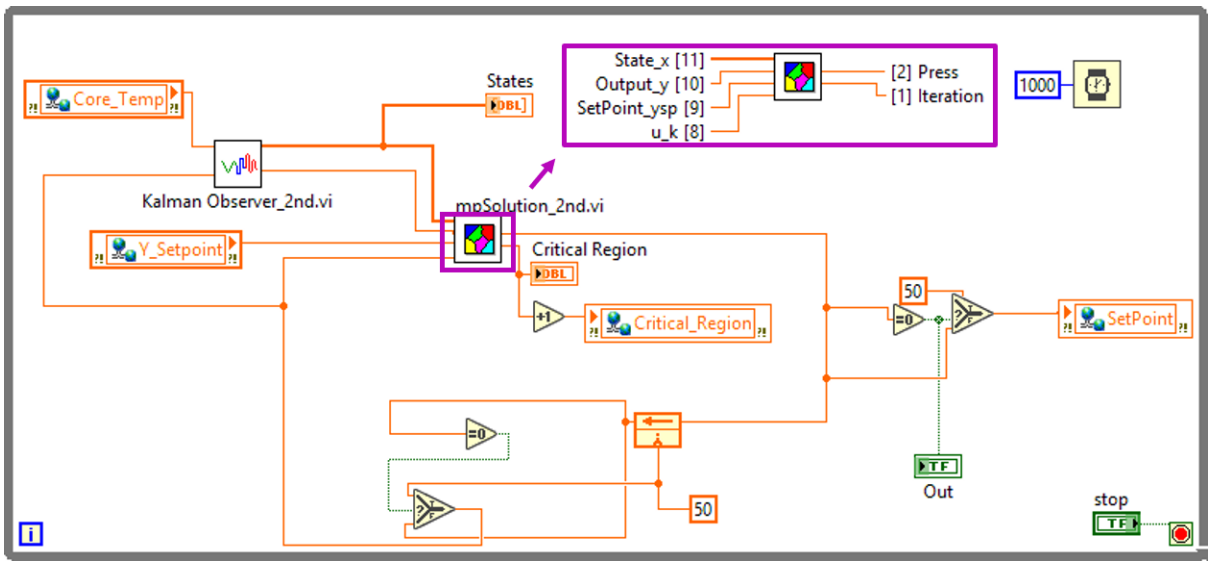

Figure 6.3: Control architecture for the real-time implementation of the control policy

6.4.2 Critical Region And Control Action

The next step is to search for the critical region where the parameter vector resides. The $\{\mathbf{Z} \in \mathbb{R}^{c \times d}$ and $\mathbf{z}_i \in \mathbb{R}^c$ matrices define a combination of critical regions or hyperplanes that spans the entire operating feasible space of the system. The search involves looping through all the critical regions to find the particular half-space where the parameter vector resides as described in algorithm in the figure 6.4. In LabVIEW, first, the matrices that describe the half-spaces or critical regions are retrieved from where they are stored in the myRIO directory as shown in figure 6.5. Then, using a while loop and a mathscript node the algorithm is setup to perform the search.

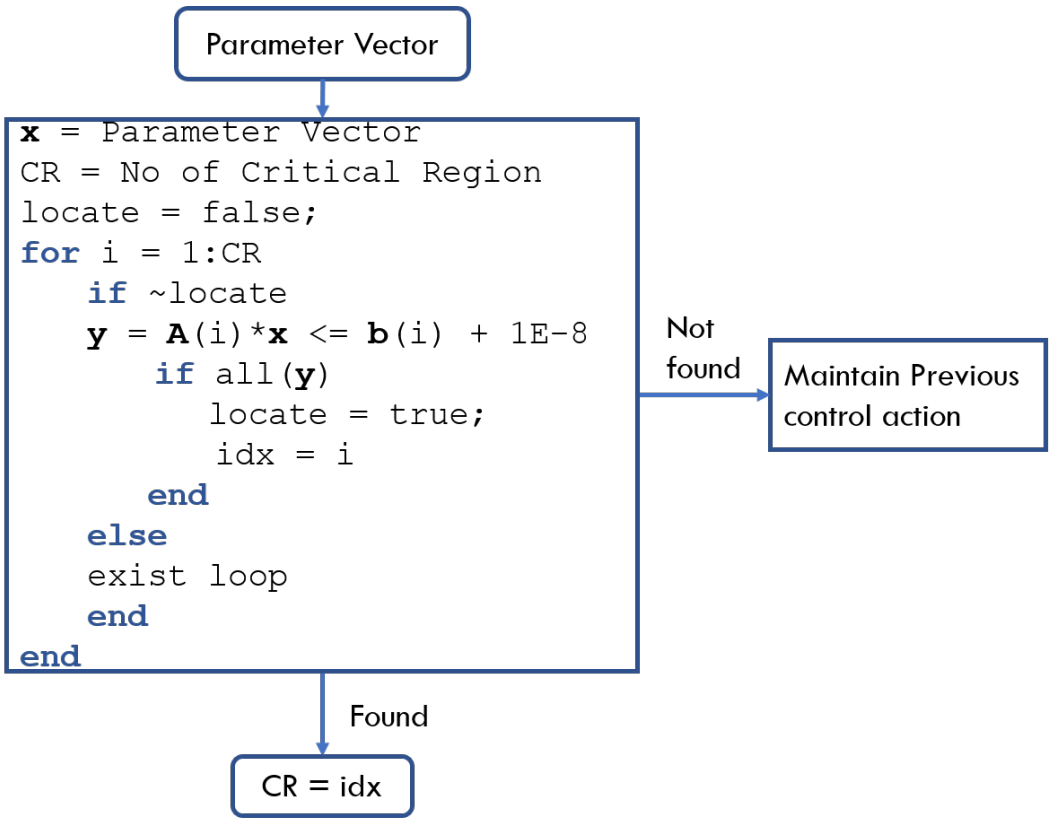

Figure 6.4: Flowchart diagram for the point location algorithm

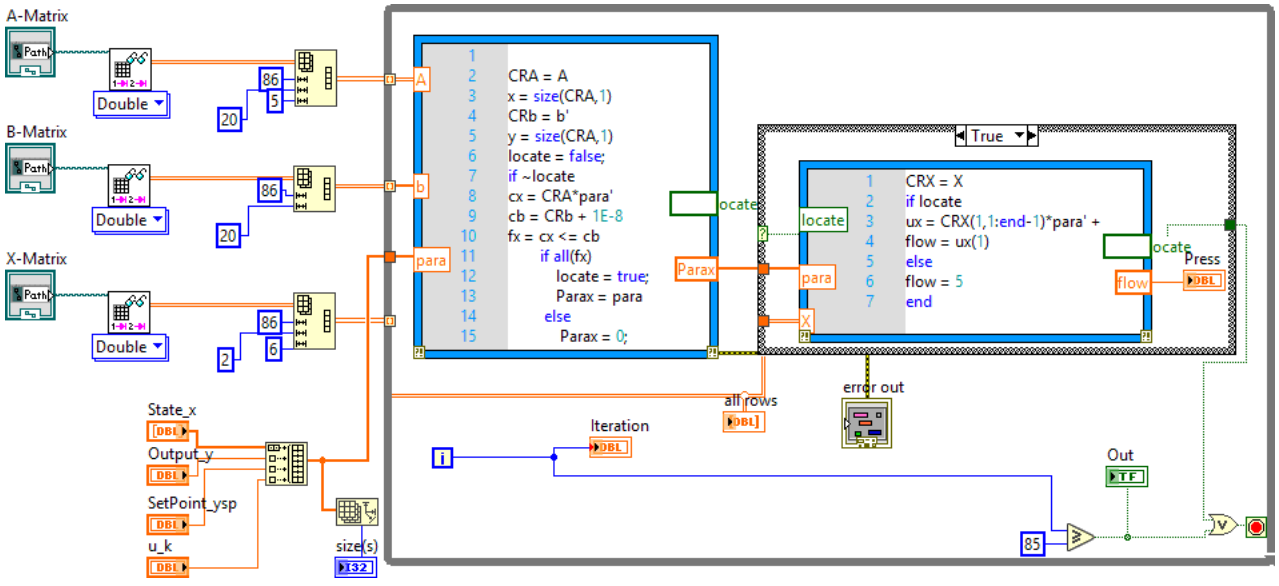

Figure 6.5: LabVIEW block diagram for implementing the point location algorithm

When the critical region is located, the affine function for the particular critical region is used to calculate the control action sequence which is sent to the networked variable and is written to an actuator. If the critical rgion is not found, the control configuration writes a default value or the previous control action sequence through the networked variable to the actuator.

6.4.3 Real-time Implementation in a Metal Hydride Refuel System Prototype

The actuator for the MHRS prototype is a pressure control device from Alicat. The pressure control device operating mechanism requires a control mechanism, thus a PID controller was built into it. The PID controller is used to maintain the pressure setpoint on the pressure control. Given the configuration of the pressure controller device, the explicit feedback control law we designed was implemented using a reference governor scheme. The control action generated at every sampling time is assigned as a new setpoint to the pressure controller. This setup is a typical setup in most chemical plants. Usually, the plant is built with variants of PID or basic legacy control (in most case, they are unaware of inherent constraints) and to optimize the plant operation, a retrofit predictive control is appended to the control system to manipulate the reference point (setpoints) such that the system is optimized.

Figure x shows a schematic of the control setup for the MHRS. A every sampling time, the sensor data for temperature and pressure is sent to the myRIO device and or a DAQ. The temperature and pressure data is used to estimate the hydrogen content of the metal hydride using a Kalman filter. The Kalman filter is also used to estimate the pseudo-states of the system. The estimated and measured data are used to form the parameter vector and the procedure described in Section 6.4 is used to determine the control action. The feedback law obtained from the off-line optimization has only 174 critical regions and looping through it takes less than 0.2 seconds. The number is very small compared to the *in silico* application which is 40 times larger. Also the combined size of the matrices (in a text file) is less than 75 KB.

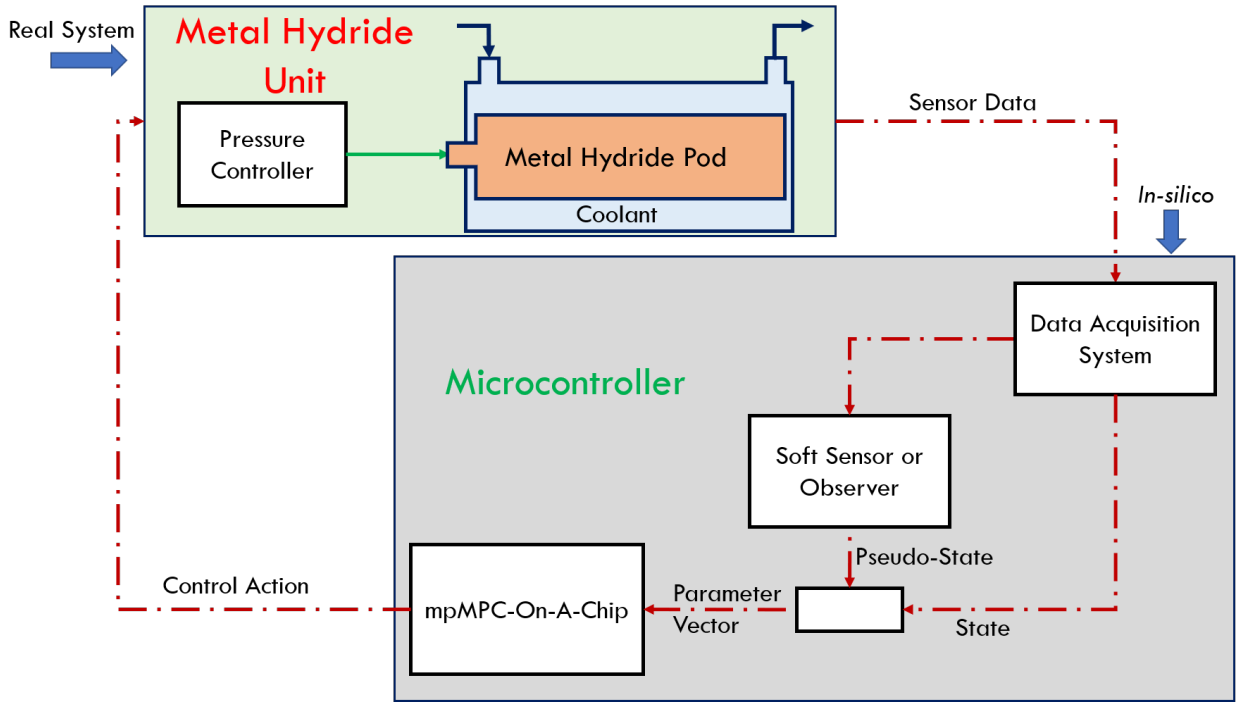

Figure 6.6: Control architecture for the real-time implementation of the control policy on the MHRS

The results of the refueling operation is recorded and Figure 6.7 shows the trajectories for temperature, state of charge of hydrogen and the filling pressure during the refueling operation when the controller is switched on. Also the results from the real-time applications in Figure 6.7 are similar to those of the *in silico* validation in Figure 6.7. The trajectory for the state of charge of the MH pod is smoother because it is estimated from the pressure and temperature data using the Kalman filter. As can be seen in Figure 6.7 the temperature maintained the setpoint keeping it well below the upper limit which 340 K. At the initial stage, the pressure increased in other to the filling the MH pod fast. However, as the temperature approached the setpoint, the pressure trajectory changes and continues in a slower increase to maintain the temperature at the set point. Given that the water flowrate was set to maximum and the hydriding the process is stabilizing, the temperature starts decreasing after a while. The main the control design to the shave the peak of the temperature curve or maintain the maximum temperature below the upper limit. The results

in Figure 6.7 shows how effective the explicit MPC controller is as regards its ability to meet the desired objectives.

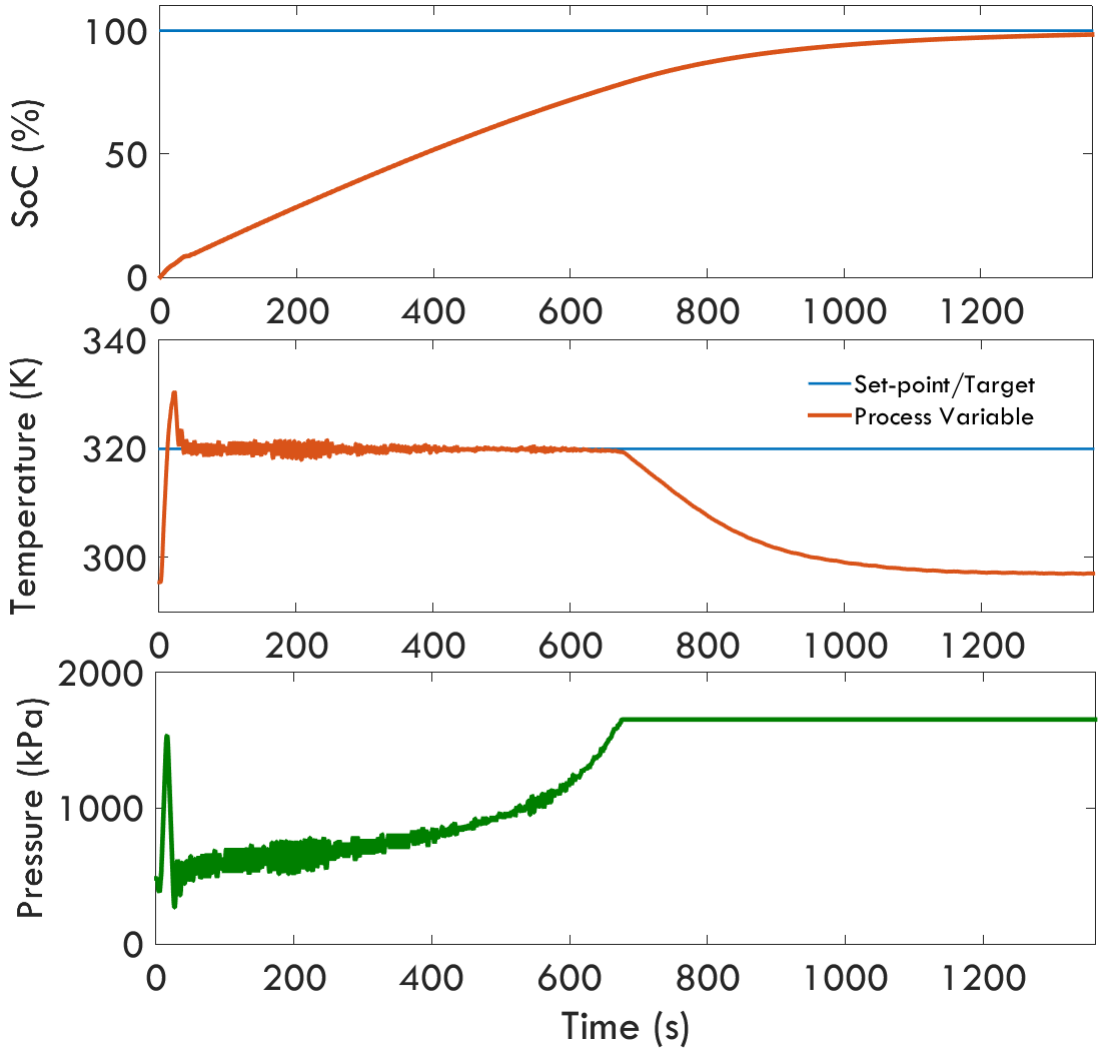

Figure 6.7: Real-time trajectory for the filling operation using the embedded mpMPC control policy - SoC of MH pod (top), MH core temperature (middle) and the filling pressure (bottom)

6.4.4 Real-time Implementation in a PEMWE Prototype

The PEMWE is a SISO system and the explicit feedback control law was applied directly to the system. The actuator is the PEMWE is the water pump, which is controlled by an L298N motor driver. The motor driver uses Pulse Width Modulation (PWM) input to regulate the voltage

supply to the pump which controls the flowrate of water. The control action is flowrate in grams per second and it is converted to PWN using equations 5.1 and 5.2 in LabVIEW. The LabVIEW is such that the flowrate of the water is the same calculated as the control action. The implementation in the PEMWE follows the procedures described in section and the resulted are recorded.

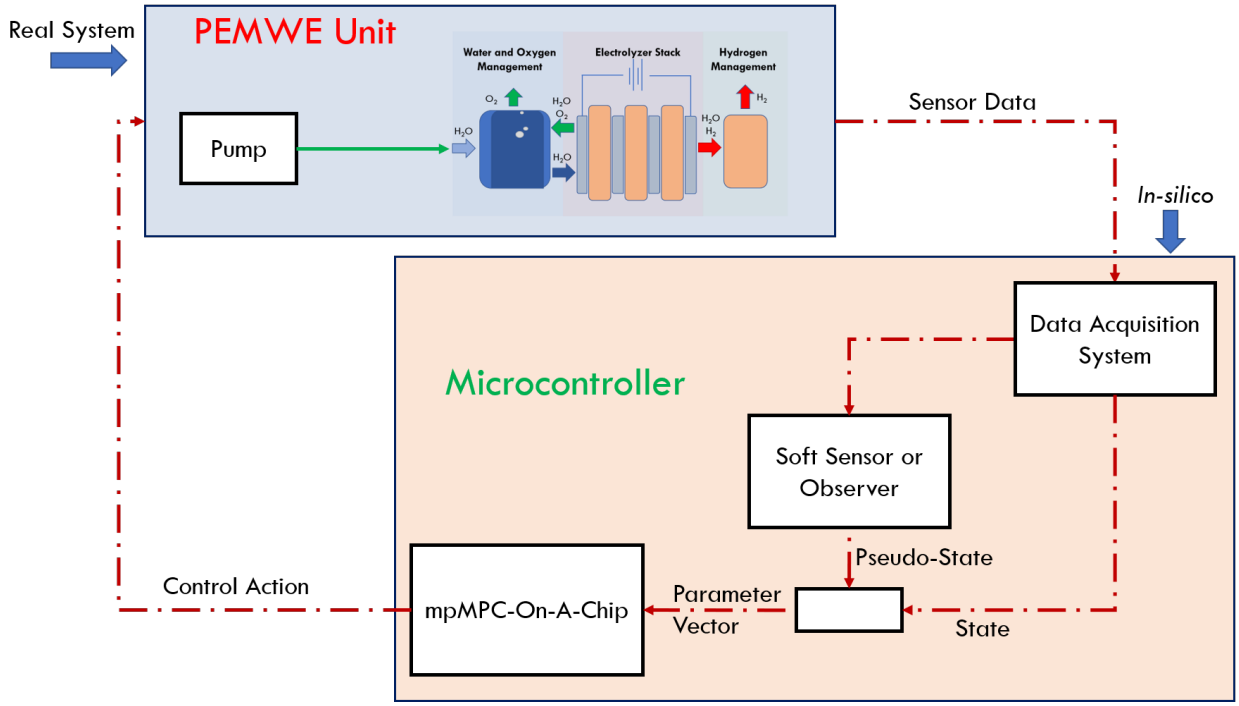

Figure 6.8: Control architecture for the real-time implementation of the control policy on the PEMWE

Figure 6.9 and 6.10 shows the trajectories for the ΔT, the flowrate and the the inlet and outlet temperature of the electrolyzer when hydrogen production rate is kept constant and when itis varied respectively. In figure 6.9 the current is fixed at 28 amperes and the control variable which is the ΔT tracks the setpoints well (figure 6.9a). Figure 6.9b shows the water flowrate profile which the manipulated variable and it is easy to notice that there is a reduced activity at higher ΔT setpoint. Figure 6.9c shows the inlet and output temperature profiles and they have an upward trend. As expected, operating temperature increases since the rate of heat generation is higher that the rate

of heat loss to the environment and mainly due to the fact that the water is recycled. Recycling the water maintains high resistivity in the water.

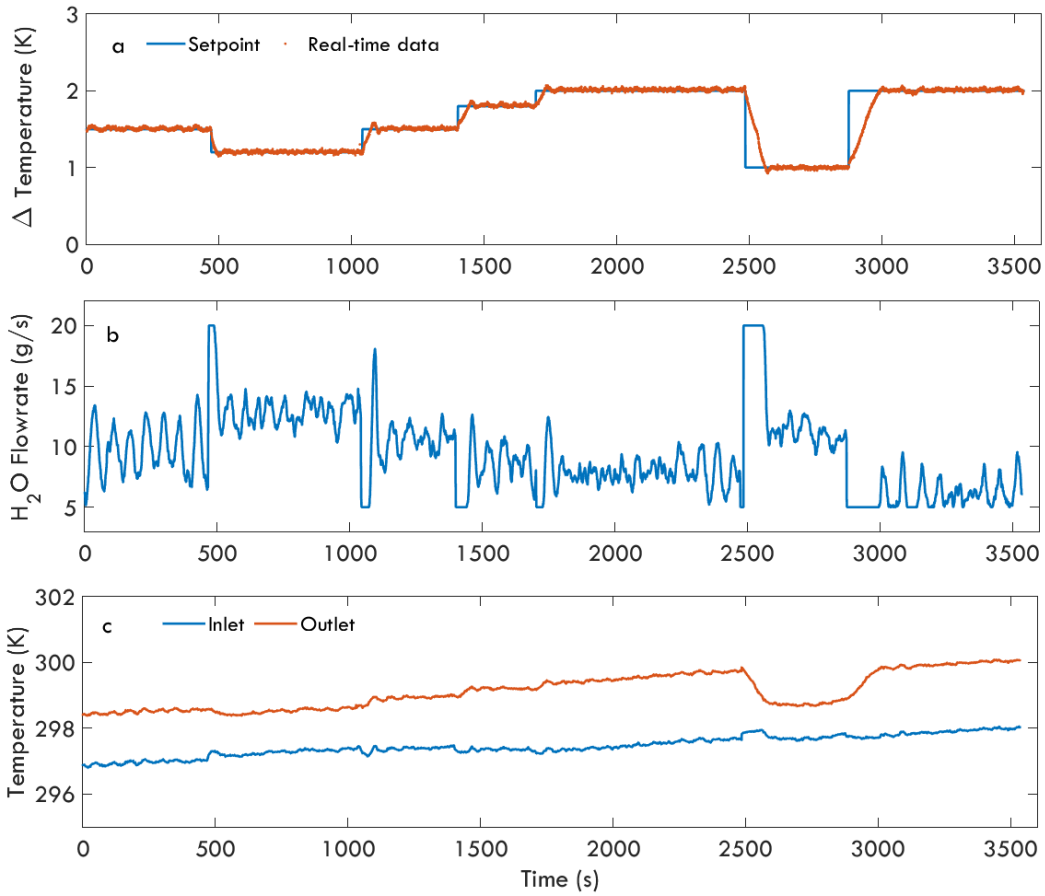

Figure 6.9: Real-time profiles of (a) ΔT, (b) water flowrate, (c) inlet and outlet temperature of electrolyzer.

Figure 6.10 is similar to 6.10 and even with the changes in the current (indirectly the hydrogen production rate) the ΔT still tracks the setpoint well. Figure 6.10 capture the startup phase of the operation since the controller was turned on at the beginning of the experiment when the outlet temperature was still below the inlet temperature and the ambient temperature below the outlet temperature (295 K).

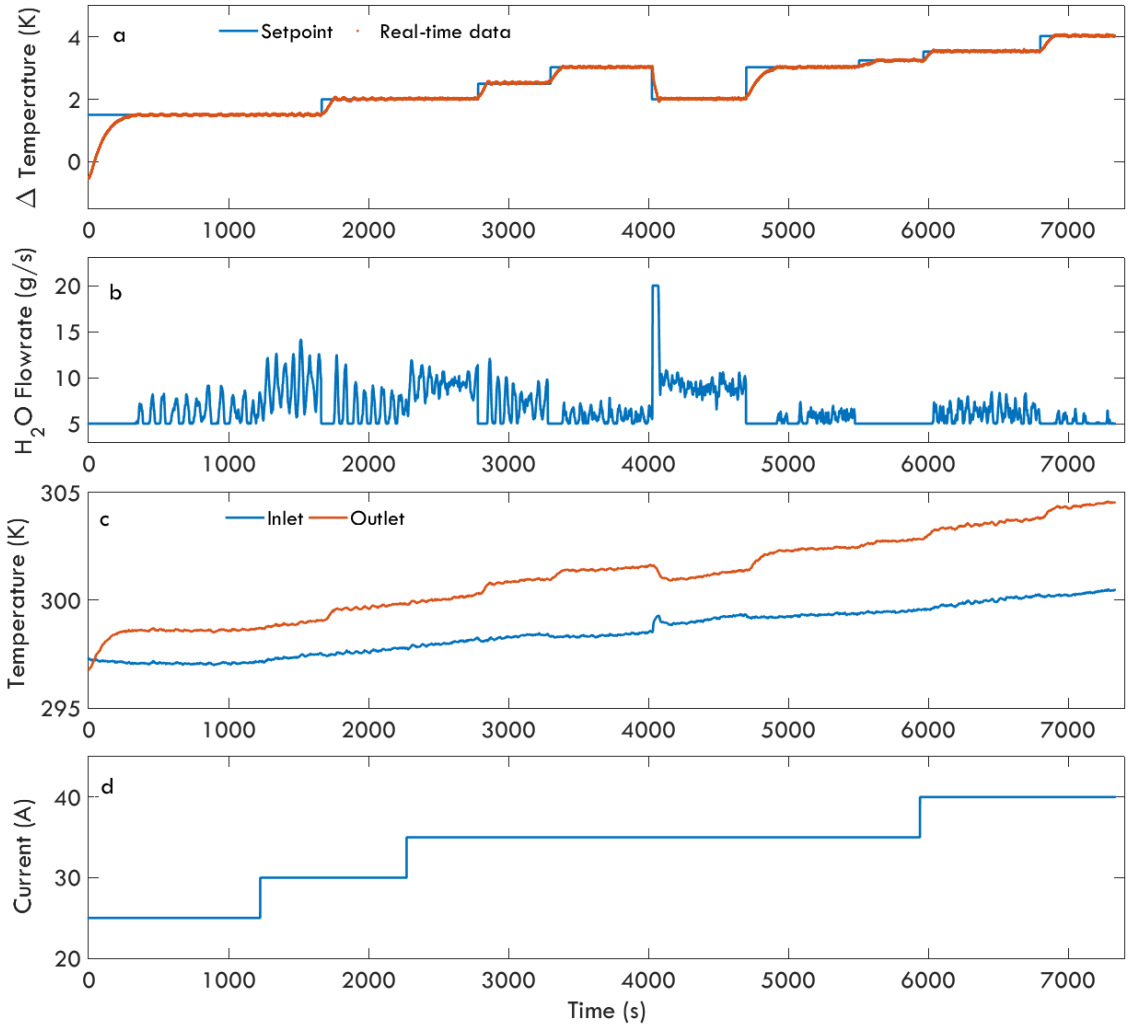

Figure 6.10: Real-time profiles of (a) ΔT, (b) water flowrate, (c) inlet and outlet temperature of electrolyzer, (d) current.

6.5 Conclusion

In this chapter we demonstrated the online implementation of the optimal receding horizon policy for a Metal hydride refueling process and the PEMWE process. The design of the receding horizon policy using the PAROC framework involves; the development and validation of a digital twin, the formulation of an MPC problem, the reformulation of the original MPC problem into a multi-parametric programming problem and solving it to get the feedback control policy, and the *in silico* validation of the feedback control policy with the digital twin. Lab-scale prototypes for

PEMWE and the metal hydride process was designed and built to not only validate the original high fidelity model but also demonstrate the real-time application of the controller. The receding horizon policy was deployed to a micro-controller and used in a real-time operation of the PEMWE process. we also illustrated the development and real-time application of an explicit control algorithm, embedded in a micro-controller and used on onboard metal hydride storage system prototype for a FCEV. The results from the real-time implementation of the explicit MPC demonstrates its potential to achieve DOE operation requirements for onboard hydrogen storage system in FCEV

7. CONCLUDING REMARKS AND FUTURE WORK

7.1 Conclusion

The primary aim of this thesis has been the development and demonstration of the application of explicit model predictive control feedback design strategy on hydrogen systems using the PARametric Optimization and Control framework. We started in chapter one with an introduction to smart manufacturing which is a terminology characterizing the intensified application of manufacturing intelligence in the manufacturing enterprise. The general goals of Smart manufacturing can be achieved by simultaneously developing the key elements of smart manufacturing; smart assets, workforce, products, network and data. While all the elements of manufacturing are important our focus was on developing smart assets for hydrogen energy. Chapter two details the development of a multi-objective hydrogen supply chain network formulated as an MINLP model to simultaneously (i) maximize the NPV and (ii) minimize the GHG emission. The MINLP model was linearized to an MILP for simplification and was adopted in the evaluation two scenarios: hydroge suppy in Texas and California. The results show that (i) SMR is cost effective when oxygen (by-product of hydrogen production from the electrolysis technologies) is vented into the atmosphere and (ii) when oxygen is collected, compressed and sold for revenue, the electrolysis technology becomes not just cost effective but also environmentally benign. Of the three kinds of water electrolysis technology, The PEM water electrolysis (PEMWE) has more operational advantage because of its high current density and compact design. Chapter three highlights various features of the PARCO framework deploys the framework in the development optimal operational strategy for the PEMWE. The framework was also used to develop optimal operating strategy for a hydrogen storage in a metal hydride system and a solid oxide fuel cell power generation system that combines natural gas reforming technology and fuel cell technology. The optimal operating strategies developed showed an improvement in the operational performance on the *in silico* model abstraction. With the knowledge of the system dynamics, Chapter four describes the development

of two lab-scale prototype system for the PEMWE and the Smart Metal Hydride Refueling System (SMHRS). The lab-scale prototypes are used to validate the high fidelity model used in chapter three for the explicit MPC. New explicit MPC are generated using the validated model. The explicit MPC generated with the validated models are used in the real-time application in chapter five. Chapter five details the online implementation of the optimal receding horizon policy for a SMHRS and the PEMWE process. The receding horizon policy is deployed to a micro-controller and used in a real-time operation of the PEMWE process. we also illustrated the development and real-time application of an explicit control algorithm, embedded in a micro-controller and used on onboard metal hydride storage system prototype for a FCEV. The results from the real-time implementation of the explicit MPC demonstrates its potential to achieve thermal operation requirements for both systems

7.2 Key Contributions

1 Development and testing of a multi period, multi-objective,MILP hydrogen supply chain model that (i) maximizes the NPV and (ii) minimizes the GHG emission considering renewable and fossil fuel based hydrogen production technologies.[20]

2 Development of a novel high-fidelity dynamic model for a Direct Internal Reformer Solid Oxide Fuel Cell (DIR SOFC) [121]

3 Design and fabrication of a lab-scale Metal hydride hydrogen refueling prototype and a PEM water electrolysis system prototype [146]

4 A novel integration of the explicit Model Predictive Control (eMPC) and a lab-scale prototype metal hydride storage system using the PAROC framework. Which involves the development and validation of a high-fidelity model, the design of an multi-parametric Model Predictive Control (mpMPC) and the real-time implementation of the mpMPC strategy on lab-scale prototype. The lab-scale prototype replicate the setup for refilling a Fuel Cell Electric Vehicle (FCEV) in a hydrogen gas station. [146]

5 A novel integration of the explicit Model Predictive Control (eMPC) and a lab-scale prototype PEM water electrolysis system using the PAROC framework. Which involves the development and validation of a high-fidelity model, the design of an multi-parametric Model Predictive Control (mpMPC) and the real-time implementation of the mpMPC strategy on lab-scale prototype.[105]

6 A demonstration of the mpMPC-on-a-chip concept using a novel simplified procedure in LabVIEW. The control strategy is embedded in a microcontroller and implemented in a standalone fashion using procedures outlined in the *in silico* demonstration of the PAROC framework [146] .

7.3 Future Work

7.3.1 Metal hydride State of Charge Estimation

At present, measuring the accurate amount of hydrogen in a metal hydride or the state of charge (SOC) is infeasible, it can only be estimated. In this thesis we used a Kalman observer to estimate the SOC. Though this is good enough, there are better estimation approaches that can be used. One approach in the using the moving horizon estimation with a variable storage capabilities which can be development using the PARCO framework. Another approach is deploying machine learning techniques in a deterministic fashion where the accuracy increases with increased number of refuel cycles.

7.3.2 Integration of Design Optimization and Control of Metal Hydride System

Effective heat removal in a Metal hydride hydrogen storage system is not just a control problem but also a design problem. A number of researchers have investigated design strategies that address this issue [131, 132, 133]. A plausible design approach is an integrated active cooling and heating strategy to improve Hydrogen uptake and discharge. This involves having conducting plates between thin layers of MH bed and running coolant. The thinner the MH bed the better the heat removal but given the weight ratio of hydrogen to metal hydride, the required amount of MH for a substantial amount of hydrogen, the size and weight of the MH storage system becomes a

major consideration. To address this, a distributed model can be optimized for heat removal given the size and weight constraints [134, 112]. An even better approach is an integration of design optimization and control with design parameters like the characteristic length which is the length to diameter ratio.The work by Burnak et al. [147] describes the methodology for implementing this approach. In the simultaneous design and control approach, the controller is aware of the design.

7.3.3 Comparative Analysis of the Robustification of Control Design

Chapter 6 discussed the implemetation of the control design strategy and also demonstrated that the control strategy effective meet the control objectives. However the control design have not been benchmarked against other control designs nor tested under uncertainty. A logical future direction will be to benchmark the control strategies developed in this thesis with (i) a regular MPC to determine which is faster (ii) a PID control to know how much effect a disturbance will have on the system. Another logical direction is to develop, deploy and test a robust multi-parametric Model Predictive Control (mpMPC) strategy of the prototypes developed to know how effective it is under uncertainty. It will be also interesting to know much a change in the boundaries of the any of the variables or parameters affect control strategy.

REFERENCES

[1] R. Martin, "Demand for hydrogen for fuel cells and other emerging markets will climb sharply through 2030," *Navigant Research*, 2014.

[2] E. F. Camacho and C. B. Alba, *Model predictive control*. Springer Science & Business Media, 2013.

[3] S. Schoenherr, "The Digital Revolution," in *Recording Technology History*, 2004.

[4] T. F. Edgar and E. N. Pistikopoulos, "Smart manufacturing and energy systems," *Computers & Chemical Engineering*, vol. 114, pp. 130–144, 2018.

[5] J. Davis, T. Edgar, J. Porter, J. Bernaden, and M. Sarli, "Smart manufacturing, manufacturing intelligence and demand-dynamic performance," *Computers & Chemical Engineering*, vol. 47, pp. 145–156, 2012.

[6] SMLC, "Implementing 21st Century Smart Manufacturing," tech. rep., 2011.

[7] P. Zakkour and G. Cook, "CCS Roadmap for Industry: High-purity CO2 sources," Tech. Rep. September, Carbon Counts Company (UK) Ltd, UK, 2010.

[8] J. A. Turner, "Sustainable Hydrogen Production," *Science*, vol. 305, pp. 972 LP – 974, aug 2004.

[9] G. W. Crabtree, M. S. Dresselhaus, and M. V. Buchanan, "The hydrogen economy," *Physics Today*, vol. 57, pp. 39–44, dec 2004.

[10] P. Liu, M. C. Georgiadis, and E. N. Pistikopoulos, "Advances in energy systems engineering," *Industrial & Engineering Chemistry Research*, vol. 50, no. 9, pp. 4915–4926, 2011.

[11] J. M. Ogden, M. M. Steinbugler, and T. G. Kreutz, "A comparison of hydrogen, methanol and gasoline as fuels for fuel cell vehicles: implications for vehicle design and infrastructure development," *Journal of Power Sources*, vol. 79, no. 2, pp. 143–168, 1999.

[12] C. Yang and J. Ogden, "Determining the lowest-cost hydrogen delivery mode," *International Journal of Hydrogen Energy*, vol. 32, no. 2, pp. 268–286, 2007.

[13] N. Johnson and J. Ogden, "A spatially-explicit optimization model for long-term hydrogen pipeline planning," *International Journal of Hydrogen Energy*, vol. 37, no. 6, pp. 5421–5433, 2012.

[14] A. Hugo and E. Pistikopoulos, "Environmentally conscious long-range planning and design of supply chain networks," *Journal of Cleaner Production*, vol. 13, no. 15, pp. 1471–1491, 2005.

[15] Z. Li, D. Gao, L. Chang, P. Liu, and E. N. Pistikopoulos, "Hydrogen infrastructure design and optimization: A case study of china," *International Journal of Hydrogen Energy*, vol. 33, no. 20, pp. 5275–5286, 2008.

[16] M. I. Ahmad, N. Zhang, and M. Jobson, "Modelling and optimisation for design of hydrogen networks for multi-period operation," *Journal of Cleaner Production*, vol. 18, no. 9, pp. 889–899, 2010.

[17] A. Almansoori and N. Shah, "Design and operation of a future hydrogen supply chain: Multi-period model," *International Journal of Hydrogen Energy*, vol. 34, no. 19, pp. 7883–7897, 2009.

[18] J. J. Brey, R. Brey, A. F. Carazo, I. Contreras, A. G. HernÃąndez-DÃ■az, and V. Gallardo, "Designing a gradual transition to a hydrogen economy in spain," *Journal of Power Sources*, vol. 159, no. 2, pp. 1231–1240, 2006.

[19] S. De-LeÃşn Almaraz, C. Azzaro-Pantel, L. Montastruc, and M. Boix, "Deployment of a hydrogen supply chain by multi-objective/multi-period optimisation at regional and national scales," *Chemical Engineering Research and Design*, vol. 104, pp. 11–31, 2015.

[20] G. S. Ogumerem, C. Kim, I. Kesisoglou, N. A. Diangelakis, and E. N. Pistikopoulos, "A multi-objective optimization for the design and operation of a hydrogen network for transportation fuel," *Chemical Engineering Research and Design*, vol. 131, pp. 279–292, 2018.

[21] Ø. Ulleberg, "Modeling of advanced alkaline electrolyzers: A system simulation approach," *International Journal of Hydrogen Energy*, vol. 28, no. 1, pp. 21–33, 2003.

[22] H. Kim, M. Park, and K. S. Lee, "One-dimensional dynamic modeling of a high-pressure water electrolysis system for hydrogen production," *International Journal of Hydrogen Energy*, vol. 38, no. 6, pp. 2596–2609, 2013.

[23] K. Aldas, "Application of a two-phase flow model for hydrogen evolution in an electrochemical cell," *Applied Mathematics and Computation*, vol. 154, no. 2, pp. 507–519, 2004.

[24] F. Marangio, M. Santarelli, and M. Calì, "Theoretical model and experimental analysis of a high pressure PEM water electrolyser for hydrogen production," *International Journal of Hydrogen Energy*, vol. 34, no. 3, pp. 1143–1158, 2009.

[25] A. Awasthi, K. Scott, and S. Basu, "Dynamic modeling and simulation of a proton exchange membrane electrolyzer for hydrogen production," *International Journal of Hydrogen Energy*, vol. 36, no. 22, pp. 14779–14786, 2011.

[26] H. Görgün, "Dynamic modelling of a proton exchange membrane (PEM) electrolyzer," *International Journal of Hydrogen Energy*, vol. 31, no. 1, pp. 29–38, 2006.

[27] T. Yigit and O. F. Selamet, "Mathematical modeling and dynamic Simulink simulation of high-pressure PEM electrolyzer system," *International Journal of Hydrogen Energy*, vol. 41, no. 32, pp. 13901–13914, 2016.

[28] T. Zhou and B. Francois, "Modeling and control design of hydrogen production process for an active hydrogen/wind hybrid power system," *International Journal of Hydrogen Energy*, vol. 34, pp. 21–30, 2009.

[29] S. A. Grigoriev, A. A. Kalinnikov, P. Millet, V. I. Porembsky, and V. N. Fateev, "Mathematical modeling of high-pressure PEM water electrolysis," *Journal of Applied Electrochemistry*, vol. 40, no. 5, pp. 921–932, 2010.

[30] K. Wipke, S. Sprik, J. Kurtz, T. Ramsden, C. Ainscough, and G. Saur, "National Fuel Cell Electric Vehicle Learning Demonstration: Final Report," Tech. Rep. July, National Renewable Energy Laboratory, 2012.

[31] S. A. Gadre, A. D. Ebner, S. A. Al-Muhtaseb, and J. A. Ritter, "Practical modeling of metal hydride hydrogen storage systems," *Industrial and Engineering Chemistry Research*, vol. 42, no. 8, pp. 1713–1722, 2003.

[32] S. J. Qin and T. A. Badgwell, "A survey of industrial model predictive control technology," *Control Engineering Practice*, vol. 11, no. 7, pp. 733–764, 2003.

[33] E. N. Pistikopoulos, N. A. Diangelakis, R. Oberdieck, M. M. Papathanasiou, I. Nascu, and M. Sun, "ParocâĂŤan integrated framework and software platform for the optimisation and advanced model-based control of process systems," *Chemical Engineering Science*, vol. 136, pp. 115–138, 2015.

[34] H. Lasi, P. Fettke, H.-G. Kemper, T. Feld, and M. Hoffmann, "Industry 4.0," *Business & Information Systems Engineering*, vol. 6, no. 4, pp. 239–242, 2014.

[35] L. Li, "China's manufacturing locus in 2025: With a comparison of âĂIJmade-in-china 2025âĂİ and âĂIJindustry 4.0âĂİ," *Technological Forecasting and Social Change*, vol. 135, pp. 66–74, 2018.

[36] US DOE, "FACT SHEET: President Obama Announces Winner of New Smart Manufacturing Innovation Institute and New Manufacturing Hub Competitions | Department of Energy," 2016.

[37] I. Chan, "Smart Manufacturing Innovation Institute: Overview, Goals and Activities," tech. rep., 2015.

[38] M. Georgiadis, A. Giovanoglou, E. Pistikopoulos, J. Palacin-Linan, and C. Pantelides, "gproms: An advanced tool for research and teaching on process modelling, simulation, design, control and optimisation," *Proceedings of PRES*, vol. 5, pp. 393–398, 2005.

[39] P. S. Enterprise, "gproms," 1997.

[40] A. Plus, "Aspen technology," *Inc., version*, vol. 11, 2009.

[41] B. Babu, *Process plant simulation*. Oxford University Press, USA, 2004.

[42] I. Grossmann, "Enterprise-wide optimization: A new frontier in process systems engineering," *AIChE Journal*, vol. 51, no. 7, pp. 1846–1857, 2005.

[43] D. Turner, "CESMII-Smart Manufacturing Accelerating Your Smart Manufacturing Transformation," tech. rep., 2018.

[44] K. Lepenioti, A. Bousdekis, D. Apostolou, and G. Mentzas, "Prescriptive analytics: Literature review and research challenges," *International Journal of Information Management*, vol. 50, pp. 57–70, 2020.

[45] R.-A. Paranay, "Investing in california's manufacturing and innovation," 12 2015.

[46] DOE, "Advanced Sensors, Control, Platforms, and Modeling for Manufacturing (Smart Manufacturing): Technology Assessment," tech. rep., 2015.

[47] T. Edgar and J. Davis, "NSF Workshop on Research needs in Advanced Sensors, Controls, Platforms, and Modeling (ASCPM) for Smart Manufacturing," pp. 1–66, 2015.

[48] L. Wang and G. Wang, "Big Data in Cyber-Physical Systems, Digital Manufacturing and Industry 4.0," *I.J. Engineering and Manufacturing*, vol. 4, pp. 1–8, 2016.

[49] Z. Yuan, B. Chen, G. Sin, and R. Gani, "State-of-the-art and progress in the optimization-based simultaneous design and control for chemical processes," *AIChE Journal*, vol. 58, no. 6, pp. 1640–1659, 2012.

[50] M. Luyben and C. Floudas, "Analyzing the interaction of design and controlâĂŤ1. a multiobjective framework and application to binary distillation synthesis," *Computers & Chemical Engineering*, vol. 18, no. 10, pp. 933–969, 1994.

[51] D. E. Shobrys and D. C. White, "Planning, scheduling and control systems: why cannot they work together," *Computers & Chemical Engineering*, vol. 26, no. 2, pp. 149–160, 2002.

[52] L. T. Biegler and V. M. Zavala, "Large-scale nonlinear programming using ipopt: An integrating framework for enterprise-wide dynamic optimization," *Computers & Chemical Engineering*, vol. 33, no. 3, pp. 575–582, 2009.

[53] J. H. Lee and Z. Yu, "Worst-case formulations of model predictive control for systems with bounded parameters," *Automatica*, vol. 33, no. 5, pp. 763–781, 1997.

[54] A. Bemporad, F. Borrelli, and M. Morari, "Min-max control of constrained uncertain discrete-time linear systems," *IEEE Transactions on Automatic Control*, vol. 48, no. 9, pp. 1600–1606, 2003.

[55] T. Gal, "The historical development of parametric programming," in *Parametric Optimization and Approximation*, pp. 148–165, Springer, 1984.

[56] N. A. Diangelakis, R. Oberdieck, and E. N. Pistikopoulos, "Explicit (offline) optimization for mpc," in *Handbook of Model Predictive Control*, pp. 359–385, Springer, 2019.

[57] V. Dua, N. A. Bozinis, and E. N. Pistikopoulos, "A multiparametric programming approach for mixed-integer quadratic engineering problems," *Computers & Chemical Engineering*, vol. 26, no. 4-5, pp. 715–733, 2002.

[58] P. TøNdel, T. A. Johansen, and A. Bemporad, "An algorithm for multi-parametric quadratic programming and explicit mpc solutions," *Automatica*, vol. 39, no. 3, pp. 489–497, 2003.

[59] R. Oberdieck, N. A. Diangelakis, and E. N. Pistikopoulos, "Explicit model predictive control: A connected-graph approach," *Automatica*, vol. 76, pp. 103–112, 2017.

[60] R. Oberdieck, N. A. Diangelakis, I. Nascu, M. M. Papathanasiou, M. Sun, S. Avraamidou, and E. N. Pistikopoulos, "On multi-parametric programming and its applications in process systems engineering," *Chemical Engineering Research and Design*, vol. 116, pp. 61 – 82, 2016. Process Systems Engineering - A Celebration in Professor Roger Sargent's 90th Year.

[61] Businesswire, "$16.2 Billion Fuel Cell Electric Vehicles Market - Global Outlook Report 2017-2026 - ResearchAndMarkets.com | Business Wire," 2018.

[62] S. W. Jorgensen, "Hydrogen storage tanks for vehicles: Recent progress and current status," *Current Opinion in Solid State and Materials Science*, vol. 15, no. 2, pp. 39–43, 2011.

[63] J. Zheng, H. Bie, P. Xu, H. Chen, P. Liu, X. Li, and Y. Liu, "Experimental and numerical studies on the bonfire test of high-pressure hydrogen storage vessels," *International Journal of Hydrogen Energy*, vol. 35, no. 15, pp. 8191–8198, 2010.

[64] B. Sakintuna, F. Lamari-Darkrim, and M. Hirscher, "Metal hydride materials for solid hydrogen storage: a review," *International Journal of Hydrogen Energy*, vol. 32, no. 9, pp. 1121–1140, 2007.

[65] DOE, "DOE Technical Targets for Onboard Hydrogen Storage for Light-Duty Vehicles | Department of Energy," 2012.

[66] F. Askri, M. B. Salah, A. Jemni, and S. B. Nasrallah, "Optimization of hydrogen storage in metal-hydride tanks," *International Journal of Hydrogen Energy*, vol. 34, no. 2, pp. 897–905, 2009.

[67] C. Panos, K. I. Kouramas, M. C. Georgiadis, and E. N. Pistikopoulos, "Dynamic optimization and robust explicit model predictive control of hydrogen storage tank," *Computers & chemical engineering*, vol. 34, no. 9, pp. 1341–1347, 2010.

[68] E. N. Pistikopoulos, N. A. Diangelakis, R. Oberdieck, M. M. Papathanasiou, I. Nascu, and M. Sun, "PAROC –an integrated framework and software platform for the optimisation and advanced model-based control of process systems," *Chemical Engineering Science*, vol. 136, pp. 115–138, 2015.

[69] M. Melnichuk, N. Silin, and H. Peretti, "Optimized heat transfer fin design for a metal-hydride hydrogen storage container," *International Journal of Hydrogen Energy*, vol. 34, no. 8, pp. 3417–3424, 2009.

[70] J. Nam, J. Ko, and H. Ju, "Three-dimensional modeling and simulation of hydrogen absorption in metal hydride hydrogen storage vessels," *Applied Energy*, vol. 89, no. 1, pp. 164–175, 2012.

[71] A. Bemporad, M. Morari, V. Dua, and E. N. Pistikopoulos, "The explicit linear quadratic regulator for constrained systems," *Automatica*, vol. 38, no. 1, pp. 3–20, 2002.

[72] G. GuillÃl'n-GosÃąlbez, F. D. Mele, and I. E. Grossmann, "A bi-criterion optimization approach for the design and planning of hydrogen supply chains for vehicle use," *AIChE Journal*, vol. 56, no. 3, pp. 650–667, 2010.

[73] J.-H. Han, J.-H. Ryu, and I.-B. Lee, "Multi-objective optimization design of hydrogen infrastructures simultaneously considering economic cost, safety and co2 emission," *Chemical Engineering Research and Design*, vol. 91, no. 8, pp. 1427–1439, 2013.

[74] J. Kim and I. Moon, "Strategic design of hydrogen infrastructure considering cost and safety using multiobjective optimization," *International Journal of Hydrogen Energy*, vol. 33, no. 21, pp. 5887–5896, 2008.

[75] N. Sabio, M. Gadalla, L. JimÃl'nez, and G. GuillÃl'n-GosÃąlbez, "Multi-objective optimization of a hydrogen supply chain for vehicle use including economic and financial risk metrics. a case study of spain," *Computer Aided Chemical Engineering*, vol. 28, pp. 121–126, 2010.

[76] A. Almansoori and N. Shah, "Design and operation of a stochastic hydrogen supply chain network under demand uncertainty," *International Journal of Hydrogen Energy*, vol. 37, no. 5, pp. 3965–3977, 2012.

[77] M. Dayhim, M. A. Jafari, and M. Mazurek, "Planning sustainable hydrogen supply chain infrastructure with uncertain demand," *International Journal of Hydrogen Energy*, vol. 39, no. 13, pp. 6789–6801, 2014.

[78] J. Kim, Y. Lee, and I. Moon, "Optimization of a hydrogen supply chain under demand uncertainty," *International Journal of Hydrogen Energy*, vol. 33, no. 18, pp. 4715–4729, 2008.

[79] T. Kato, M. Kubota, N. Kobayashi, and Y. Suzuoki, "Effective utilization of by-product oxygen from electrolysis hydrogen production," *Energy*, vol. 30, no. 14, pp. 2580 – 2595, 2005.

[80] P. Liu, A. Whitaker, E. N. Pistikopoulos, and Z. Li, "A mixed-integer programming approach to strategic planning of chemical centres: A case study in the uk," *Computers & Chemical Engineering*, vol. 35, no. 8, pp. 1359 – 1373, 2011.

[81] N. E. Koltsaklis, A. S. Dagoumas, G. M. Kopanos, E. N. Pistikopoulos, and M. C. Georgiadis, "A spatial multi-period long-term energy planning model: a case study of the greek power system," *Applied Energy*, vol. 115, pp. 456–482, 2014.

[82] B. Gaudernack and S. Lynum, "Hydrogen from natural gas without release of co2 to the atmosphere," *International Journal of Hydrogen Energy*, vol. 23, no. 12, pp. 1087–1093, 1998.

[83] J. Current, H. Min, and D. Schilling, "Multiobjective analysis of facility location decisions," *European Journal of Operational Research*, vol. 49, no. 3, pp. 295–307, 1990.

[84] EPA, "Emission factors for greenhouse gas inventories," 2014.

[85] H. Yeomans and I. E. Grossmann, "A systematic modeling framework of superstructure optimization in process synthesis," *Computers & Chemical Engineering*, vol. 23, no. 6, pp. 709 – 731, 1999.

[86] J. Brian and G. S. Daniel, DeSantis, "Final report: Hydrogen production pathways cost analysis," *DOE-StrategicAnalysis*, 2016.

[87] J. A. Elia, R. C. Baliban, X. Xiao, and C. A. Floudas, "Optimal energy supply network determination and life cycle analysis for hybrid coal, biomass, and natural gas to liquid (CBGTL) plants using carbon-based hydrogen production," *Computers & Chemical Engineering*, vol. 35, no. 8, pp. 1399 – 1430, 2011.

[88] A. Almansoori and N. Shah, "Design and operation of a future hydrogen supply chain," *Chemical Engineering Research and Design*, vol. 84, no. 6, pp. 423–438, 2006.

[89] P. Liu, D. I. Gerogiorgis, and E. N. Pistikopoulos, "Modeling and optimization of polygeneration energy systems," *Catalysis Today*, vol. 127, no. 1, pp. 347 – 359, 2007.

[90] M. R. Bussieck and A. Meeraus, "General algebraic modeling system (gams)," *Applied Optimization*, vol. 88, pp. 137–158, 2004.

[91] B. A. McCarl and T. H. Spreen, "Applied mathematical programming using algebraic systems," *Cambridge, MA*, 1997.

[92] U. E. I. Administration, "Energy-related carbon dioxide emissions at the state level,," 2014.

[93] U. E. I. Administration, "Annual energy outlook 2017," *Department of Energy*, 2017.

[94] C. Kim, *An Integrated Modelling and Optimization Approach For Hydrogen Energy Network*. thesis, 2017.

[95] D. Terlip, K. Hartmann, J. Martin, and C. Rivkin, "Adapted tube cleaning practices to reduce particulate contamination at hydrogen fueling stations," *International Journal of Hydrogen Energy*, vol. 44, no. 17, pp. 8692 – 8698, 2019. Special issue on The 7th International Conference on Hydrogen Safety (ICHS 2017), 11-13 September 2017, Hamburg, Germany.

[96] S. Moffitt, M. Lyddon, D. Morel, M. OâĂŹNeill, K. Smith, C. Willse, and D. K. Cohen, "State structures for instructional support in california," *Getting Down to Facts II*, 2018.

[97] J. Brian and G. S. Daniel, DeSantis, "Final report: Hydrogen production pathways cost analysis," *DOE-StrategicAnalysis*, 2016.

[98] E. N. Pistikopoulos and N. A. Diangelakis, "Towards the integration of process design, control and scheduling: Are we getting closer?," *Computers & Chemical Engineering*, vol. 91, pp. 85–92, 2016.

[99] J. Katz, N. A. Diangelakis, and E. N. Pistikopoulos, "Model approximation in multiparametric optimization and control–a computational study," in *Computer Aided Chemical Engineering*, vol. 44, pp. 655–660, Elsevier, 2018.

[100] L. Ljung, *System identification: theory for the user*. Prentice-hall, 1987.

[101] R. Oberdieck, N. A. Diangelakis, M. M. Papathanasiou, I. Nascu, and E. N. Pistikopoulos, "Pop–parametric optimization toolbox," *Industrial & Engineering Chemistry Research*, vol. 55, no. 33, pp. 8979–8991, 2016.

[102] A. Alessio and A. Bemporad, "A survey on explicit model predictive control," in *Nonlinear model predictive control*, pp. 345–369, Springer, 2009.

[103] M. Kvasnica, C. N. Jones, I. Pejcic, J. Holaza, M. Korda, and P. Bakaráč, "Real-time implementation of explicit model predictive control," in *Handbook of Model Predictive Control*, pp. 387–412, Springer, 2019.

[104] M. Klaučo, M. Kalúz, and M. Kvasnica, "Real-time implementation of an explicit mpc-based reference governor for control of a magnetic levitation system," *Control Engineering Practice*, vol. 60, pp. 99–105, 2017.

[105] G. S. Ogumerem and E. N. Pistikopoulos, "Dynamic modeling and explicit control of a pem water electrolysis process," *Smart and Sustainable Manufacturing Systems*, vol. 2, no. 2, pp. 25–43, 2018.

[106] T. A. Zawodzinski, "Water Uptake by and Transport Through Nafion® 117 Membranes," *Journal of The Electrochemical Society*, vol. 140, no. 4, p. 1041, 1993.

[107] T. E. Springer, T. A. Zawodzinski, and S. Gottesfeld, "Polymer Electrolyte Fuel Cell Model," *Journal of The Electrochemical Society*, vol. 138, p. 2334, aug 1991.

[108] F. Marangio, M. Santarelli, and M. Calì, "Theoretical model and experimental analysis of a high pressure PEM water electrolyser for hydrogen production," *International Journal of Hydrogen Energy*, vol. 34, no. 3, pp. 1143–1158, 2009.

[109] R. L. LeRoy, "The Thermodynamics of Aqueous Water Electrolysis," *Journal of The Electrochemical Society*, vol. 127, no. 9, p. 1954, 1980.

[110] R. García-Valverde, N. Espinosa, and A. Urbina, "Simple PEM water electrolyser model and experimental validation," *International Journal of Hydrogen Energy*, vol. 37, no. 2, pp. 1927–1938, 2012.

[111] G. Welch, G. Bishop, *et al.*, "An introduction to the kalman filter," *UNC at Chapel Hill*, pp. 41–95, 1995.

[112] C. Panos, "Modelling , Optimization and Control of Energy Systems," February 2012.

[113] E. S. Kikkinides, M. C. Georgiadis, and A. K. Stubos, "Dynamic modelling and optimization of hydrogen storage in metal hydride beds," *Energy*, vol. 31, pp. 2092–2110, may 2006.

[114] A. Jemni and S. B. Nasrallah, "Study of two-dimensional heat and mass transfer during absorption in a metal-hydrogen reactor," *International Journal of Hydrogen Energy*, vol. 20, no. 1, pp. 43–52, 1995.

[115] Y. Kaplan and T. N. Veziroglu, "Mathematical modelling of hydrogen storage in a LaNi5 hydride bed," *International Journal of Energy Research*, vol. 27, no. 11, pp. 1027–1038, 2003.

[116] X. Zhang, S. H. Chan, G. Li, H. K. Ho, J. Li, and Z. Feng, "A review of integration strategies for solid oxide fuel cells," *Journal of Power Sources*, vol. 195, no. 3, pp. 685–702, 2010.

[117] A. L. Dicks, "Advances in catalysts for internal reforming in high temperature fuel cells," *Journal of Power Sources*, vol. 71, no. 1, pp. 111–122, 1998.

[118] J. M. Klein, Y. Bultel, S. Georges, and M. Pons, "Modeling of a sofc fuelled by methane: From direct internal reforming to gradual internal reforming," *Chemical Engineering Science*, vol. 62, no. 6, pp. 1636–1649, 2007.

[119] K. Ahmed and K. Foger, "Kinetics of internal steam reforming of methane on ni/ysz-based anodes for solid oxide fuel cells," *Catalysis Today*, vol. 63, no. 2, pp. 479–487, 2000.

[120] S. KakaÃğ, A. Pramuanjaroenkij, and X. Y. Zhou, "A review of numerical modeling of solid oxide fuel cells," *International Journal of Hydrogen Energy*, vol. 32, no. 7, pp. 761–786, 2007.

[121] G. S. Ogumerem, N. A. Diangelakis, and E. N. Pistikopoulos, "Natural-gas-based sofc in distributed electricity generation: Modeling and control," *Natural Gas Processing from Midstream to Downstream*, pp. 509–525, 2018.

[122] J. Xu and G. F. Froment, "Methane steam reforming, methanation and water-gas shift: I. intrinsic kinetics," *AIChE Journal*, vol. 35, no. 1, pp. 88–96, 1989.

[123] A. Gebregergis, P. Pillay, D. Bhattacharyya, and R. Rengaswemy, "Solid oxide fuel cell modeling," *IEEE Transactions on Industrial Electronics*, vol. 56, no. 1, pp. 139–148, 2009.

[124] K. K. C. Yu, N. R. Watson, and J. Arrillaga, "An adaptive kalman filter for dynamic harmonic state estimation and harmonic injection tracking," *IEEE Transactions on Power Delivery*, vol. 20, pp. 1577–1584, April 2005.

[125] U. DOE, "Target Explanation Document: Onboard Hydrogen Storage for Light-Duty Fuel Cell Vehicles," tech. rep., U.S. Drive, 2017.

[126] K. Reddi, A. Elgowainy, N. Rustagi, and E. Gupta, "Impact of hydrogen sae j2601 fueling methods on fueling time of light-duty fuel cell electric vehicles," *International Journal of Hydrogen Energy*, vol. 42, no. 26, pp. 16675–16685, 2017.

[127] V. Strubel, "Hydrogen Storage System for Automotive Application," tech. rep., 2008.

[128] H. Kiyoshi and M. Steve, "Development of New H2 Refueling Method for FCV to Reduce Refueling Time | Research paper site of Honda R&D Co., Ltd.," *Honda R&D Technical Review*, vol. 27, no. 2, pp. 43 – 49, 2015.

[129] Q. Lai, M. Paskevicius, D. A. Sheppard, C. E. Buckley, A. W. Thornton, M. R. Hill, Q. Gu, J. Mao, Z. Huang, H. K. Liu, *et al.*, "Hydrogen storage materials for mobile and stationary applications: current state of the art," *ChemSusChem*, vol. 8, no. 17, pp. 2789–2825, 2015.

[130] E. I. Gkanas, "Metal hydrides: Modeling of metal hydrides to be operated in a fuel cell," in *Portable Hydrogen Energy Systems*, pp. 67–90, Elsevier, 2018.

[131] S. Mellouli, H. Dhaou, F. Askri, A. Jemni, and S. B. Nasrallah, "Hydrogen storage in metal hydride tanks equipped with metal foam heat exchanger," *International Journal of Hydrogen Energy*, vol. 34, no. 23, pp. 9393–9401, 2009.

[132] S. Shafiee and M. H. McCay, "Different reactor and heat exchanger configurations for metal hydride hydrogen storage systems–a review," *International Journal of Hydrogen Energy*, vol. 41, no. 22, pp. 9462–9470, 2016.

[133] F. Yang, G. Wang, Z. Zhang, X. Meng, and V. Rudolph, "Design of the metal hydride reactors–a review on the key technical issues," *International Journal of Hydrogen Energy*, vol. 35, no. 8, pp. 3832–3840, 2010.

[134] C. A. Krokos, D. Nikolic, E. S. Kikkinides, M. C. Georgiadis, and A. K. Stubos, "Modeling and optimization of multi-tubular metal hydride beds for efficient hydrogen storage," *International Journal of Hydrogen Energy*, vol. 34, no. 22, pp. 9128–9140, 2009.

[135] S. M. Nowee, A. Abbas, and J. A. Romagnoli, "Optimization in seeded cooling crystallization: A parameter estimation and dynamic optimization study," *Chemical Engineering and Processing: Process Intensification*, vol. 46, no. 11, pp. 1096–1106, 2007.

[136] M. Carmo, D. L. Fritz, J. Mergel, and D. Stolten, "A comprehensive review on pem water electrolysis," *International Journal of Hydrogen Energy*, vol. 38, no. 12, pp. 4901–4934, 2013.

[137] R. De Levie, "The electrolysis of water," *Journal of Electroanalytical Chemistry*, vol. 476, no. 1, pp. 92–93, 1999.

[138] W. Dönitz and E. Erdle, "High-temperature electrolysis of water vaporâĂŤstatus of development and perspectives for application," *International Journal of Hydrogen Energy*, vol. 10, no. 5, pp. 291–295, 1985.

[139] W. Grubb, "Ionic migration in ion-exchange membranes," *The Journal of Physical Chemistry*, vol. 63, no. 1, pp. 55–58, 1959.

[140] J. Russell, L. Nuttall, and A. Fickett, "Hydrogen generation by solid polymer electrolyte water electrolysis," *Am. Chem. Soc. Div. Fuel Chem. Prepr*, vol. 18, pp. 24–40, 1973.

[141] G. ELX, "G5 electrolyzer manual," *Giner ELX Electrolyzer Stack Operating Manual*, vol. 2.

[142] C. E. Garcia, D. M. Prett, and M. Morari, "Model predictive control: theory and practiceâĂŤa survey," *Automatica*, vol. 25, no. 3, pp. 335–348, 1989.

[143] P. TÃÿndel, T. Johansen, and A. Bemporad, "Evaluation of piecewise affine control via binary search tree," *Automatica*, vol. 39, no. 5, pp. 945 – 950, 2003.

[144] F. J. Christophersen, M. Kvasnica, C. Jones, and M. Morari, "Efficient evaluation of piecewise control laws defined over a large number of polyhedra," 07 2007.

[145] J. Drgoňa, M. Klaučo, F. Janeček, and M. Kvasnica, "Optimal control of a laboratory binary distillation column via regionless explicit mpc," *Computers & Chemical Engineering*, vol. 96, pp. 139–148, 2017.

[146] G. S. Ogumerem and E. N. Pistikopoulos, "Parametric optimization and control towards the design of a smart metal hydride refueling system," *AIChE Journal*, 2019.

[147] B. Burnak, J. Katz, N. A. Diangelakis, and E. N. Pistikopoulos, "Simultaneous process scheduling and control: A multiparametric programming-based approach," *Industrial & Engineering Chemistry Research*, vol. 57, no. 11, pp. 3963–3976, 2018.

[148] A. Hugo and E. Pistikopoulos, "Environmentally conscious long-range planning and design of supply chain networks," *Journal of Cleaner Production*, vol. 13, no. 15, pp. 1471–1491, 2005.

[149] R. E. Steuer, *Multiple criteria optimization: theory, computation, and applications*. Wiley, 1986.

APPENDIX A

HYDROGEN SUPPLY CHAIN MODEL

A.1 Set Definition and Nomenclature

We start outlining the compressed model formulation by defining the following set:

i: geographical locations or cell $i \in I : \{I_1, I_2, ..., I_{ni}, \}$

k: transportation mode $k \in K : \{K_1, K_2, ..., K_{nk}, \}$

l: plant of a given technology $l \in L : \{L_1, L_2, ..., L_{nl}, \}$

r: available primary energy resources $r \in R : \{R_1, R_2, ..., R_{nr}, \}$

p: products from the plants $p \in P : \{P_1, P_2, ..., P_{np}, \}$

w: waste from the plant $w \in W : \{W_1, W_2, ..., W_{nw}, \}$

t: time periods of the planning horizon $t \in T : \{T_1, T_2, ..., T_{nt}, \}$

b: available hydrogen production technologies $b \in B : \{B_1, B_2, ..., B_{nb}, \}$

m: a super set of all the materials $m \in M : \{P, R, W\}$

A.2 Material Balance

A.2.1 Material Balance of Products

Equ.A.1 represents the mass balance in the cell(geographical location). The product is related to the capacity of the plant by a capacity factor. In Equ.A.2 The amount of by-product produced is related to the product by a predetermined factor as shown in Equ.A.3.

$$\sum_{lb} P_{ilbt} + \sum_{j,k} Qp_{ijkt} = PD_{it} + \sum_{j,k} Qp_{jikt} \tag{A.1}$$

$$P_{ilbt} \leq Cf_b \,.\, Pcap_{ilbt} \tag{A.2}$$

$$Bp_{ilbt} = P_{ilbt} \,.\, \sigma_b \tag{A.3}$$

P_{ilbt} and PD_{it} denotes the amount of hydrogen produced and consumed in cell i respectively, Q_{ijkpt} and Q_{jikpt} represents the flow in and out of hydrogen in cell i respectively, $Pcap_{ilbt}$ is the capacity of plant and Bp_{ilbt} is the by-product produced at cell i during period t, σ_l is parameter representing the ratio of by-product per hydrogen produced, C_i is the capacity factor or availability of plant

A.2.2 Material Balance Resources Used as Feedstock

The sum of the primary feedstock required to make a product in a cell and the feedstock leaving the cell to other cells is equal to the sum of the amount of feedstock extracted in the cell, the amount of feedstock entering into the cell from other cell and the amount of feedstock imported into the cell from other states or country.

$$\sum_{lb} P_{ilbt} \,.\, \delta_{br} + \sum_{j,k} Q_{ijkrt} = Rxt_{irt} + \sum_{i,k} Q_{jikrt} + Imp_{irt} \tag{A.4}$$

δ_{br} is a parameter representing the ratio of feedstock require per hydrogen produced, Rxt_{irt} denotes the amount of feedstock extracted in cell i, Q_{ijkpt} and Q_{jikpt} represents the flow in and out of feedstock for producing hydrogen at cell i respectively Imp_{irt} is the amount of feedstock import into cell i.

A.2.3 Green House Gas Emissions in Carbon-dioxide Equivalent

A.2.3.1 Waste Generated from Equipment or Plant

The waste generated from the manufacturing of the equipment is dependent on its capital expenditure [89] which might change within the period as shown in Equ.A.5

$$ghge_t = \sum_{l} Capex_t \,.\, \xi_b \tag{A.5}$$

$ghge_t$ is the GHG from the production of the equipment used for each technology ξ is a param-

eter representing the ratio of carbon-dioxide equivalent waste produced.

A.2.4 Waste Generated from Feedstock Extraction

The amount of greenhouse gas emitted during the extraction or manufacturing and supply of the feed stock is given in Equ.A.6

$$ghgr_t = \sum_{irw} (Rxt_{irt} + Imp_{irt}) \ . \mu_{wr} \ . \tau_w \tag{A.6}$$

$ghgr_t$ is the GHG from the raw material extraction process μ_{wr} is a parameter representing the ratio of waste per raw material extracted, τ_w denotes the global warming potential of the waste generated.

A.2.4.1 Waste Generated From Production Process

The GHG emission generated during the production of the product is given by

$$ghgp_t = \sum_{ilbw} P_{ilbt} \ . \nu_{wb} \ . \tau_w \tag{A.7}$$

$ghgp_t$ is the GHG from the hydrogen production process ν_{wb} is a parameter representing the ratio of waste per hydrogen produced, τ_w is same as described above.

A.2.4.2 Waste Generated From Distributing The Product

The GHG emission generated during the transportation of the product is represented as

$$ghgt_t = \sum_{w} \tau_w \ . \ \sum_{k} \phi_w \sum_{ij} dist_{ij} \left(\sum_{r} N_{ijkrt} + \sum_{p} N_{ijkpt} \right) / mpg_k \tag{A.8}$$

$ghgt_t$ is the GHG from the transportation unit used in distributing the product and the raw materials ϕ_w is a parameter representing the amount of waste generated per gallon of transportation fuel used, mpg_k is a parameter denoting the mile per gallon of fuel used τ_w is same as described above.

A.3 Capacity Constraint

The capacity of the production plant and the transportation mode available in each period is equal to its value in the previous period plus any expansion or shrinkage during the previous period. This is represented in equations A.9 and B.4. Equation A.11 calculates the amount of transportation unit required to distribute the designated flows between cells.

$$Pcap_{ilbt+1} = Pcap_{ilbt} + Pext_{ilbt} + Psut_{ilbt} \tag{A.9}$$

$$\sum_{ij} N_{ijkmt+1} = \sum_{ij} N_{ijkmt} + Next_{kmt} + Nsut_{kmt} \tag{A.10}$$

$$N_{ijkmt} \,.\, Tcap_{km} \geq Q_{ijkmt} \tag{A.11}$$

$Pext_{ilbt}$ and $Next_{kmt}$ denotes the extension of plant and transportation mode respectively, $Psut_{ilbt}$ and $Nsut_{kmt}$ denotes the shrinkage or shutdown of plant and transportation mode respectively, $Tcap_{km}$ is the capacity of each transportation mode.

A.3.1 Variable Bounds

Here we put a bound on all the variables and introduce a binary variables to represent the existence or not of a component. It is one if the component exist and zero otherwise.

$$Lbound \,.\, ybin \leq Q_{ijkmt}, Rxt_{irt}, Imp_{irt}, Pext_{ilbt}, Psut_{ilbt}, Next_{ilbt}, Nsut_{ilbt} \leq Ubound \,.\, ybin \tag{A.12}$$

$Lbound$ and $Ubound$ represents the respective lower and upper bound of all the materials, plant extension, plant shrinkage transportation extension and shrinkage respectively. $ybin$ represents all the respective binary variable for the continuous variables

A.4 Cost Constraint

A.4.1 Capital And O&M Fixed Cost

The Capital investment cost as well as the operation and maintenance fixed cost are obtained using the respective cost and capacity of a reference plant (appendix) as shown in equations A.13 and A.14. Equ.A.15 represents all the capital expenditure on the plant and transportation mode expansion and shrinkage. Profit is given by the difference between the revenue generated from the products (and by-products) and the operating cost (Equ.A.16) as shown in Equ.A.17. The net present value is represented in Equ.A.18 and the total GHG emission in Equ.A.19

$$Cpcst_t = \sum_{i,l,b} Refpcst_l \; . \; \left(\frac{Pext_{ilbt}}{Refcap_l}\right)^{sf} \tag{A.13}$$

$$OMcst_t = \sum_{i,l,b} Refomcst_l \; . \; \left(\frac{Pcap_{ilbt}}{Refcap_l}\right)^{sf} \tag{A.14}$$

$$\begin{aligned} Capex_t = \sum_{km} Next_{kmt} \; . \; TCst_{km} + \sum_{km} Nsut_{kmt} \; . \; TDst_{km} \\ + \sum_{ilb} Psut_{ilbt} \; . \; PDst_l + Cpcst_t \end{aligned} \tag{A.15}$$

$$\begin{aligned} Opex_t = OMcst_t + \sum_{ilb} P_{ilbt}.Vst_l + \sum_{ijkm} Q_{ijkmt}.dist_{ij}.Topst_{km} \\ + Rxt_{irt}.Rcst_{km} + Imp_{irt}.Imcst_{km} \end{aligned} \tag{A.16}$$

$$Profit_t = \sum_{il} P_{ilbt} \; . \; Pzh_t + \sum_{il} Bp_{ilbt} \; . \; Pzb_t - Opex_t \tag{A.17}$$

$$NPV = \sum_{t,a} \frac{Profit_t}{(1+dr)^{cad(ord_t-1)+ord_a-1}} - \sum_{t} \frac{Capex_t}{(1+dr)^{cad(ord_t-1)}} \tag{A.18}$$

$$GHG = \sum_{t} ghge_t + 365 \; . \; 5 \; . \; (ghgr_t + ghgp_t + ghgt_t) \tag{A.19}$$

A.5 Multi-objective Technique

Problems that are posed with more than one objective are common in real situations. In most cases the objective functions have conflicting criteria; where optimizing one of the objective undermines the optimum of other objective(s). Multi-objective optimization is the optimization of a multi-objective problem A.20 with two or more (conflicting) criteria subject to certain constraints.

$$\begin{aligned} \min_{x,y} z &= U\{\ f_1(x,y), f_2(x,y), ..., f_k(x,y)\} \\ st &: h(x,y) = 0 \\ & g(x,y) \leq 0 \\ & x \in R^n, y \in Y = \{1,0\} \end{aligned} \tag{A.20}$$

where U is the utility function and x and y represent the vectors of continuous and discrete variables respectively belonging to the feasible region of equality and inequality constraints. In principle the reformulated problem can then be solved using developed algorithms for parametric optimization [148]. However as explained by Steuer in [149] the ϵ-constraint method can neither guarantee feasibility nor efficiency and both conditions need to be verified once the complete set of solutions has been obtained.

A.6 Variables and Parameters

Table A.1: Binary variables

$PXbin_{iblt}$	1 if technology b expands for plant l in cell i period t, 0 if not
$SHbin_{iblt}$	1 if technology b shrinks for plant l in cell i period t, 0 if not
$Rxbin_{irt}$	1 if resource r is extracted in cell i at period t, 0 if not
$Qpbin_{ijkpt}$	1 if product p flows from cell i to j by mode tr period t, 0 if not
$Qrbin_{ijkrt}$	1 if raw material r flows from cell i to j through tr @ period t, 0 if not
$TXbinp_{kpt}$	1 if transport units tr for product p expands in period t, 0 if not
$TXbinr_{krt}$	1 if transport units tr for raw material r expands in period t, 0 if not
$Tsbinp_{kpt}$	1 if transport units tr for product p shrinks in period t, 0 if not
$Tsbinr_{krt}$	1 if transport units tr for raw material r shrinks in period t, 0 if not

Table A.2: Non binary variables

Nxp_{kpt}	Transport units of mode tr for product p purchased in period t
Nxr_{krt}	Transport units of mode tr for raw material r purchased in period t
Np_{ijkpt}	Transport units of mode tr for product p from cell i to cell j in period t
Nr_{ijkrt}	Transport units of mode tr for raw material r from cell i to cell j in period t
Nsp_{kpt}	Transport units of mode tr for product p sold in period t
Nsr_{krt}	Transport units of mode tr for raw material r sold in period t

Table A.3: Continuous variables

$Capex_t$	Capital expenditure in period t
NPV	Net present value of the entire time horizon
$Opex_t$	Operation expenditure in period t
P_{ilt}	Mass of product produced per day in cell i period t
Pb_{ilt}	Mass of by-product produced per day in cell i period t
$CPcst_t$	Plant capital cost period t
$OMcst_t$	Plant fixed O&M period t
PDC_t	Plant decommissioning cost period t
$Sales_t$	Product income per day period t
$TCst_t$	Transport capital cost for product period t
$TDst_t$	Transport decommissioning cost for product period t
$Profit_t$	Difference between $Sales_t$ and $Opex_t$ period t
$Pcap_{iblt}$	Available capacity of technology b in plant l in cell i period t
$Pext_{iblt}$	Capacity expansion of technology b in plant l in cell i in period t
$Psut_{iblt}$	Capacity shrinkage of technology b in plant l in cell i in period t
Rxt_{irt}	Mass of resource r extracted per day from cell i period t
RE_{ibet}	Electricity e used per day by technology b in cell i in period t

Table A.4: Continuous variables contd.

Qr_{ijkrt}	Mass of product p flow from cell i to cell j by mode tr in period t
Qp_{ijkpt}	Mass of raw material r flow from cell i to cell j by mode tr in period t
Imp_{irt}	Mass of raw material imported from a different state or country
GHG	Mass of waste w dumped of the entire time horizon
$ghge_t$	Waste generated during the manufacturing of the equipment
$ghgr_t$	Waste generated during the extraction of raw material
$ghgp_t$	Waste generated during the production of the primary product
$ghgt_t$	Waste generated from Distributing the Product and raw material

Table A.5: Model parameters

$Rmax_{ir}$	Maximum mass per day of raw material r that can be extracted from cell i
$Rmin_{ir}$	Minimum mass per day of raw material r that can be extracted from cell i
$Nmax$	Maximum number of transport units that can be bought per period
$Nmin$	Minimum number of transport units that can be bought per period
$Qmax_{ijk}$	Maximum mass that can flow between cell i and cell j by mode k
$Qmin_{ijk}$	Minimum mass that can flow between cell i and cell j by mode k
$Qtmax_b$	Maximum capacity expansion or shrinking for technology b per period
$Qtmin_b$	Minimum capacity expansion or shrinking for technology b per period
σ_b	Ratio of by-products produced from each technology
δ_{br}	Raw material r required by technology b to produce a unit of product
ξ_b	The ratio of CO_2 equivalent GHG emitted per capital of plant or equipment
μ_{wr}	The ratio of waste per raw material extracted
τ_w	The global warming potential of the GHG emissions
ν_{bw}	The ratio of waste per hydrogen produced
ϕ_w	Ratio of waste generated per gallon of transportation fuel used
mpg_k	The average mile per gallon of rating of the transportation unit
$Ordpy_{py}$	The order of period year py within its set
$Ordtp_t$	The order of period t within its set
sf	Plant size factor
$Speed_{tr}$	Transportation speed by mode tr
$Tcap_{tr}$	Maximum capacity of one transport unit of mode tr

Table A.6: List of model constants

Cf_b	Proportion of time for which technology b is available for production
Pzh_t	Cost per unit mass of product p of the entire time horizon
Pzb_t	Cost per unit mass of by-product p of the entire time horizon
$Rcst_t$	Cost per unit mass of raw material r extracted of the entire time horizon
$Reflantcost_b$	Cost of the reference plant for technology b
$Reflantcap_b$	Capacity of the reference plant for technology b
$RefixedOM_b$	Fixed operations and maintenance costs of the reference plant for technology b
$Fuelprice_k$	Fuel price by mode tr
$Demand_{it}$	Mass per day of total products demanded in cell i period t
$dist_{ij}$	Distance between cell i and cell j
dr	Discount rate
$EPOT_{ie,t}$	Maximum amount of electricity from source e in cell i period t
$Fuel_k$	Fuel mileage by mode tr

Table A.7: Projected population of each region over time

Region	2015	2020	2025	2030	2035	2040
i1	861,081	942,285	999,906	1,060,766	1,122,212	1,184,026
i2	558,838	579,760	593,434	605,376	614,386	620,354
i3	7,922,450	8,262,583	9,223,446	10,350,467	11,652,101	13,142,957
i4	1,175,101	1,237,949	1,307,615	1,380,440	1,454,396	1,531,382
i5	779,391	836,526	873,647	911,083	946,905	981,402
i6	6,895,132	7,591,647	8,483,669	9,466,708	10,540,101	11,712,202
i7	3,283,634	3,758,358	4,222,430	4,722,791	5,270,225	5,883,251
i8	2,765,627	3,149,310	3,443,804	3,743,990	4,028,264	4,307,984
i9	566,784	642,563	679,719	717,040	752,739	786,097
i10	845,333	980,456	1,063,374	1,142,673	1,215,074	1,281,526
i11	2,362,179	2,560,541	2,808,263	3,053,750	3,295,852	3,524,715

Table A.8: Distance between two regions (in miles) - Texas

City	Wayside	Albany	Colleyville	Big Sandy	Woodville	Houston	Rogers	San Antonio	Big Lake	Fort Davis	Falfurrias
Wayside	60	264	349	471	598	601	443	486	298	424	653
Albany	264	60	137	263	372	364	206	270	213	372	437
Colleyville	349	137	60	139	249	275	151	281	322	496	446
Big Sandy	471	263	139	60	153	228	204	332	448	623	499
Woodville	598	372	249	153	60	110	195	291	478	725	381
Houston	601	364	275	228	110	60	155	196	437	614	273
Rogers	443	206	151	204	195	155	60	152	294	483	310
San Antonio	486	270	281	332	291	196	152	60	259	423	171
Big Lake	298	213	322	448	478	437	294	259	60	210	426
Fort Davis	424	372	496	623	725	614	483	423	210	60	533
Falfurrias	653	437	446	499	381	273	310	171	426	533	60

Table A.9: Distance between two regions (in miles) - California

City	Mendocino	Shasta	Nevada	Solano	San Benito	Calaveras	Fresno	Kern	Imperial	Inyo	Los Angeles
Mendocino	50	246	176	180	278	233	329	438	724	540	524
Shasta	246	50	182	203	366	263	405	488	782	482	582
Nevada	176	182	30	90	224	93	259	342	640	375	440
Solano	180	203	90	30	171	82	215	298	589	404	389
San Benito	278	366	224	171	30	152	141	187	474	345	274
Calaveras	233	263	93	82	152	30	161	253	551	304	351
Fresno	329	405	259	215	141	161	40	157	454	315	254
Kern	438	488	342	298	187	253	157	40	316	170	135
Imperial	724	782	640	589	474	551	454	316	30	354	201
Inyo	540	482	375	404	345	304	315	170	354	30	226
Los Angeles	524	582	440	389	274	351	254	135	201	226	20

Table A.10: Material costs

Materials	$\$/kg$ or $\$/kwh$
Biomass	0.0858
Coal	0.0413
Natural Gas	0.2320
Process Water	0.0005
Hydro Electricity	0.0594
Solar Electricity	0.0599
Wind Electricity	0.0469

Table A.11: Reference plant data for hydrogen production methods

Technology	Reference Plant Capital Cost (MM $)	Reference Plant Capacity (kg /day)	Fixed O&M Cost ($/kg /day)
SMR	225.433	341448	21203
Coal Gasification	452.433	255447	63208
Biomass Gasification	189.124	139712	30064
Alkaline/PEM Electrolyzer	24.446	48500	19546
Solid Oxide Electrolyzer	22.117	41220	14824

The values in Table A.12 is gotten from Almansoori et al. [88]

Table A.12: Transportation parameters

Cost type	Tube Trailer	Truck Trailer
Fuel economy (miles/gal)	9.997	
Fuel price ($/gal)	1.06	
Speed (miles/hr)	27.962	
Load/Unload (hr)	12	
Driver wage ($/hr)	23	
Unit price ($M/unit)	0.1	
Unit capacity (kg/unit)	720	2372

APPENDIX B

MULTI-PARAMETRIC MODEL PREDICTIVE CONTROL SETUP

B.1 Linear Discrete-time Model To Multi-parametric Solution

As an example, given a discrete-time, linear, time invariant system of the form presented in equation B.1

$$\begin{aligned} x_{k+1} &= Ax_k + Bu_k \\ y_k &= Cx_k \end{aligned} \tag{B.1}$$

bounded by $\quad u_{min} \leq u_k \leq u_{max}, \quad x_{min} \leq x_k \leq x_{max}, \quad y_{min} \leq y_k \leq y_{max}$

The MPC problem for setpoint tracking in the discrete-time, linear, time invariant system is presented in Equation B.2 for the case of a quadratic performance index

$$\begin{aligned} \min_u J = & \sum_{k=1}^{N-1} \left(\left(y_k - y_k^R\right)^T QR \left(y_k - y_k^R\right) \right) + \sum_{k=0}^{M-1} \left(\Delta u_k^T R \Delta u_k\right) \\ \textbf{s.t.} \quad & x_{k+1} = Ax_k + Bu_k \\ & y_k = Cx_k \\ & u_{min} \leq u_k \leq u_{max} \qquad k = 0, ..., M-1 \\ & \Delta u_{min} \leq \Delta u_k \leq \Delta u_{max} \qquad k = 0, ..., M-1 \\ & x_{min} \leq x_k \leq x_{max} \qquad k = 0, ..., N \\ & y_{min} \leq y_k \leq y_{max} \qquad k = 0, ..., N \end{aligned} \tag{B.2}$$

where x_k are the state variables; u_k is the control variables; Δu_k denotes the difference between two consecutive control actions; y_k and y_k^R are the outputs and their respective set points; R and QR are the corresponding weights in the quadratic objective function; N and M are the prediction horizon and control horizon, respectively; k is the time step; A, B, and C are the matrices of the

discrete linear state-space model.

Using the following substitution, $x_k = A_o x_o + \sum_{i=0}^{M} B_{o,i} u_i, \forall i \in [0, M-1]$, the MPC problem in B.2 can be reformulated to the quadratic problem in equation B.3

$$\begin{aligned} z(x) = \min_{u,\theta} \quad & \mathbf{u}^T \mathbf{H} \mathbf{u} + \theta^T \mathbf{F} \mathbf{u} \\ \text{s.t.} \quad & \mathbf{G}\mathbf{u} \leq \mathbf{W} + \mathbf{S}\theta \\ & \mathbf{u} \in U \\ & \theta \in \Theta = \{\theta \in \mathbb{R}^q | \mathbf{CR}_A \theta \leq \mathbf{CR}_b\} \end{aligned} \tag{B.3}$$

where $\mathbf{H} \in \mathbb{R}^{n \times n}$, $\mathbf{F} \in \mathbb{R}^{n \times q}$, $\mathbf{G} \in \mathbb{R}^{n \times m}$, $\mathbf{W} \in \mathbb{R}^q$, and $\mathbf{S} \in \mathbb{R}^{m \times q}$ are matrices. $\mathbf{u}$ is a vector that contain a sequence of control actions, n and q is the size of the control and parameter vector respectively, and consequently the size of the parametric solution and parametric space of the problem. The uncertain parameters or parameter realized at every sampling time are denoted by θ and they include the initial states x_0, the output y_k the set points y_k^R, and previous control actions u_{-1} for evaluating Δu_k.

The bounds on the output variable u, x and y have been set according to the model in equation B.1. The multi-parametric model predictive controller problem (equation B.3) is solved using POP toolbox in MATLAB® [101]. The solution obtained is of the form $\mathbf{u} = f(\theta)$ mapping the parameters θ to a sequence of control actions $\mathbf{u}$. $f(\theta)$ is a piece-wise affine function of the uncertain parameters as shown below .

$$f(\theta) = \begin{cases} a_1\theta + b_1 & \text{if } \theta \in \mathbf{CR}_1; \\ \dots & \dots \\ a_m\theta + b_m & \text{if } \theta \in \mathbf{CR}_m. \end{cases} \tag{B.4}$$

where $\mathbf{CR}_i = \{\theta \in \mathbb{R}^q | \mathbf{X}_i \theta \leq \mathbf{x}_i\}, \quad i = 1, ..., N_m$ are polyhedral critical regions defined

by active sets Thus, at every sampling time, the parameter vector is realized from measurements of the state and outputs and its used as inputs to evaluate the PWA function to obtain the sequence of control action.

APPENDIX C

KALMAN OBSERVER

Given a system or plant that can be described with a mathematical model (Linear in this case) as shown in Figure C.1 and has immeasurable states (x), a Kalman Filter can be employed to estimate the immeasurable states ($\hat{x}$) using measurements of other related variables or output.

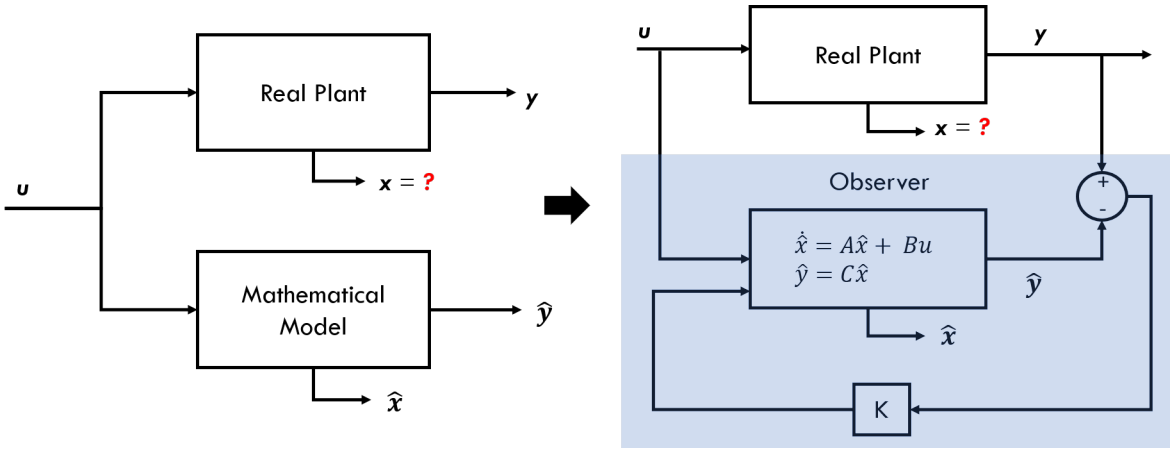

Figure C.1: Kalman Observer Schematic

In setting up the state observer, the goal is to reduce the error ($Er_{obs} = x - \hat{x}$). After substitution error can be reformulated as $\dot{Er} = (A - KC)\, Er_{obs}$ and then solved to get $Er_{obs}(t) = \exp^{(A-KC)t}\, Er_{obs}(0)$. If $(A - KC) < 0$ then $Er \to 0$ as $t \to \infty$ thus $\hat{x} \to x$.

A Kalman filter is a type of state observer for stochastic system. It involves a two stage estimation: (1) a priori estimate or predicted, which is calculated before obtaining the value of the measurable variable and (2) the a posteriori estimate or update which is used to update the estimate. Equation C.1 describes the plant with measurement and process noise

$$\begin{aligned} \dot{x}_k &= Ax_{k-1} + Bu_k + w_k \\ y_k &= Cx_k + v_k \end{aligned} \tag{C.1}$$

where $v \sim N(0, R)$ and $w \sim N(0, Q)$. R and Q represents the covariance matrix for the output measurement and process noise.

The a priori and a posteriori are given below

Prediction

$$\begin{aligned} \hat{x}_k^o &= A\hat{x}_{k-1} + Bu_k \\ P_k^o &= AP_{k-1}A^T + Q \end{aligned} \tag{C.2}$$

Update

$$\begin{aligned} K_k &= \frac{P_k^o C^T}{CP_k^o C^T + R} \\ \hat{x}_k &= \hat{x}_k^o + K_k\left(y_k - C\hat{x}_k^o\right) \\ P_k &= \left(1 - K_k C\right) P_k^o \end{aligned} \tag{C.3}$$

The kalman filter algorithm is set up in an iterative fashion. The prediction equations C.2 uses the model of the system to predict the a priori estimate $\hat{x}_k^o$ and the error covariance matrix P_k^o. The update equations C.3 updates the a priori estimate the error covariance matrix obtained from equation C.2 using the calculated K matrix

APPENDIX D

FUTURE WORK - BENCHMARKING CONTROL SCHEMES

This Appendix document compares the control scheme adopted for this thesis to other standard control scheme. This material is not included in the main document because it is outside the scope.

D.1 mpMPC vs MPC

The multi-parameteric Model Predictive control (mpMPC) adopted in the development of the thermal management strategy of the Metal hydride system is derived for the classical MPC formulation. Unlike the classical MPC, the optimization in the mpMPC strategy is done ones and offline thus the online application of the control strategy is reduced to a function evaluation of an affine function. However, the results from the MPC and mpMPC are similar.

D.2 mpMPC vs PID

When compared with the PID the mpMPC is more suitable because of the reasons discussed below. The main purpose of the thermal management strategy is to maintain the temperature within a safe threshold while filling the metal hydride pod with hydrogen. It is common knowledge that MPC is more suitable for MIMO system with constrained variables . Figure D.1 compares the mpMPC strategy to a PID control strategy of the metal hydride hydrogen storage system. The output variables are the state of charge (SOC) and the temperature (bounded between $260°C$ and $333°C$) of the metal hydride pod, while the input variables are the water flowrate (bounded between 10 and 450 g/s) and the pressure (bounded between 10 and 250 psi). The PID is developed such that the pressure is used to control the SOC and the water flowrate is used to control temperature. From the figure D.1, its clear that though the metal hydride fills up faster with the PID controller, the temperature is not maintained within the limits. However the mpMPC is able to not just fill up the MH pod at a good time but also maintain the temperature within set limits. Also for the PID, the inputs variable are saturated at their upper limit.

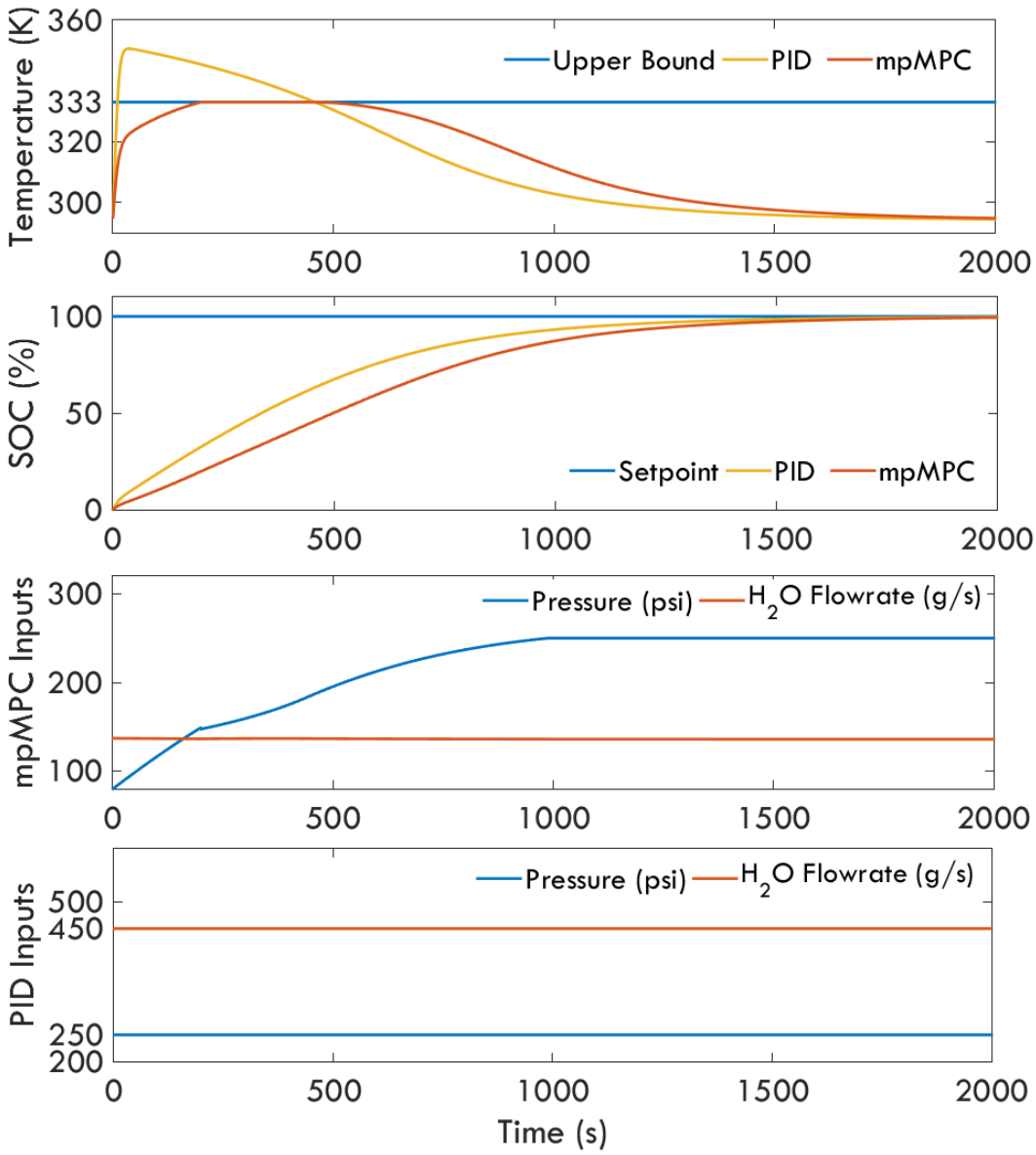

Figure D.1: *In silico* application of a mpMPC and PID controller to the metal hydride system with bounds on the temperature; The temperature profile (first), the SOC profile (second), the mpMPC control input profile (third), the PID control input profile (fourth)

When an time invariant trajectory is used as a temperature setpoint to for both the PID and the mpMPC, though the bounds on the variable are not systematically considered for the PID, the performance of the PID controller does not measure up with the mpMPC controller as shown in figure D.2. In Figure D.2 the MH pod fill up faster with the mpMPC than the PID. Also the temperature profile stays on the setpoint $320^{\circ}C$ below the upper limit $333^{\circ}C$.

Note: The refueling of the metal hydride system is a batch process and the inherent temperature profile of the batch operation (as shown in the result from the experiment) has the shape of a positively skewed distribution function. Thus irrespective of the control strategy used the temperature decays after it reaches the maximum temperature.

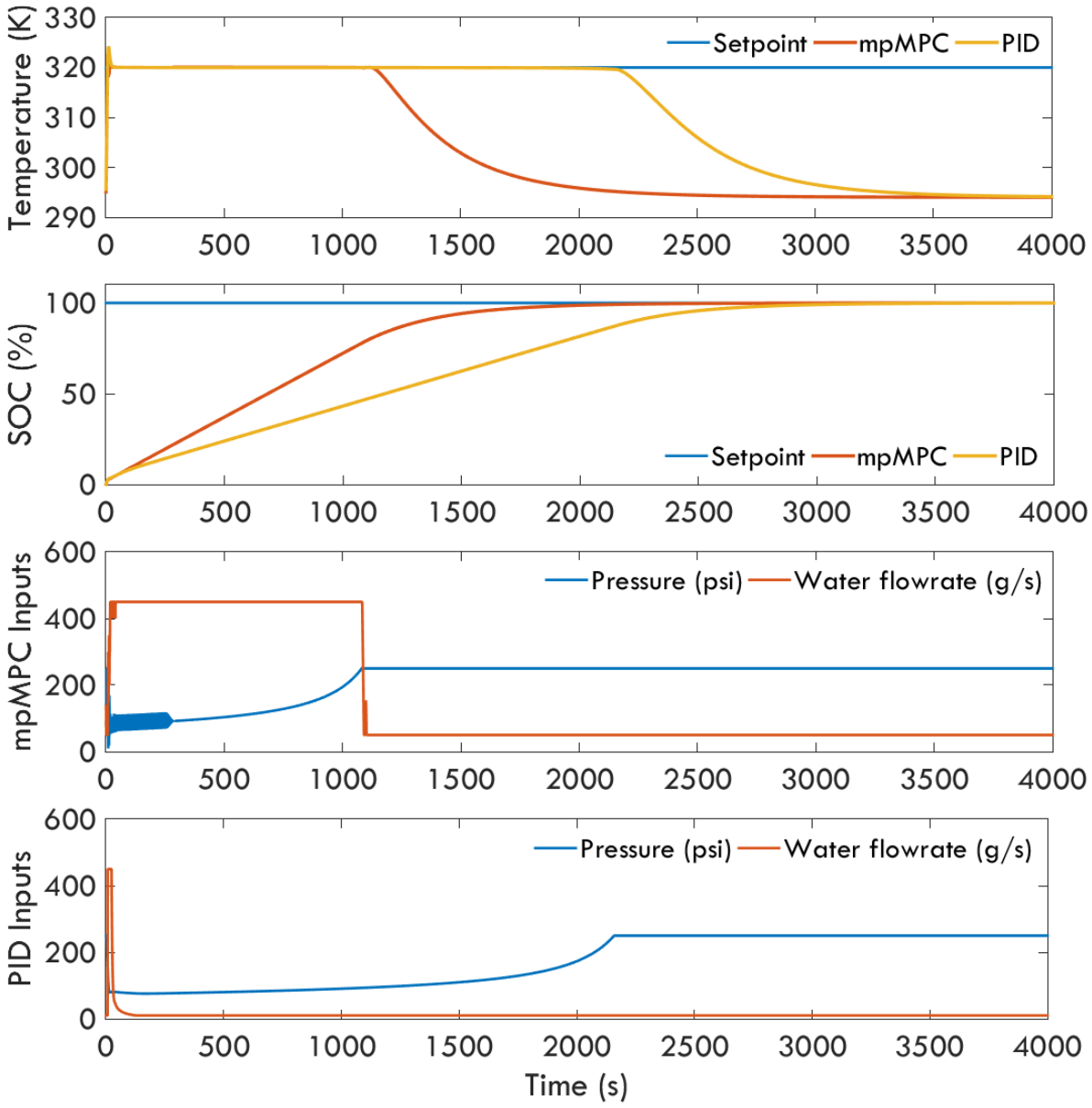

Figure D.2: *In silico* application of a mpMPC and PID controller to the metal hydride system with temperature setpoint; The temperature profile (first), the SOC profile (second), the mpMPC control input profile (third), the PID control input profile (fourth)